



School of
Engineering

Two-Dimensional Compressible Vortex Analysis

A thesis submitted by

Andrew Hubble

In partial fulfillment of the requirements

for the degree of

Masters of Science

in

Mechanical Engineering

Department of Mechanical Engineering

Tufts University

Medford, Massachusetts, USA

April 2015

Abstract

With the introduction of bivelocity in 2004, new models for the prediction of Maxwellian, compressible micro-channel flows have recently been developed. This thesis utilizes a non-kinetic method to explore an analytic prediction of two-dimensional velocity profiles of steady and transient, unbounded, compressible vortex flows. This bivelocity hydrodynamic model is compared to the traditional analytical solutions of the Navier-Stokes Fourier (NSF), Boltzmann, and Burnett equations, as well as to Mandella's 1987 experiments in compressible vortices, highlighting the stark contrasts between these models. While definitive convergence has yet to be obtained, the bivelocity approach has shown promise in resolving these issues. The importance of these bivelocity addition provides a clean explanation for the poor analytic correlations to experimental data previously attempted. While further investigation is required, bivelocity definitively improves upon the current models.

Contents

Abstract	ii
Acknowledgments	vi
Nomenclature	vii
1 Introduction	1
1.1 Mach Number	4
1.2 The Knudsen Number	4
1.3 The Navier-Stokes Equations	5
1.4 Boltzmann Equation	5
1.5 Burnett Equation	6
2 Compressible Free Vortex	7
2.1 Structure	7
2.2 The Dissipation of Eddies	8
2.3 Mandella's Experimental Analysis	9
2.4 Analytic Solutions	10
2.4.1 Colonius, Lele, and Moin	10
2.4.2 Ellenrieder and Cantwell	12
2.4.3 Aboelkassem, Vatistas and Esmail	12
2.5 Rotor Driven Flow	13
3 Bivelocity Hydrodynamics	14
3.1 Introduction and Formation	14
3.2 Volume and Momentum Transport	14
3.3 Continuum Phoretic Motions	15
3.4 Incompleteness of Navier-Stokes-Fourier	15
3.5 Bivelocity and Navier-Stokes-Fourier	16
3.6 Bivelocity Shock Waves	16
3.7 Micro-Channel Couette Flow	17

3.8	Bivelocity Derivation	18
3.8.1	Continuity	18
3.8.2	Conservation of Momentum	19
3.8.3	Conservation of Energy	19
3.8.4	Ideal Gas	20
3.8.5	Dimensionless Forms	21
3.9	Bivelocity Significance	25
3.9.1	Absolute Significance	25
3.9.2	Relative Significance	27
4	The Singularity	32
5	Steady-State and ODEs	33
5.1	Steady Equation Set	33
5.2	Steady Compressible Results	34
6	Transience and PDEs	37
6.1	Initial and Boundary Conditions	38
7	Discussion	54
7.1	Knudsen Number	54
7.2	Convergence	54
7.3	Experimental Validation	55
8	Concluding Remarks	55
9	Appendix A	57
9.1	Mass Equation	57
9.2	Momentum Equation	58
9.3	Energy Equation	63
9.4	Ideal Gas	68
9.5	Nondimensionalization	68
9.5.1	Mass	68

9.5.2	Radial Momentum	70
9.5.3	Angular Momentum	72
9.5.4	Energy	73
9.5.5	Ideal Gas	78
10	Bibliography	79

Acknowledgments

I would like to thank Tufts University for giving me the opportunity to further my academic career, and for the financial support to make this possible. I am grateful for the support of the entire department, as well as the office space and access to the cluster computer, without which this work could not have been accomplished.

Although the work contained in this thesis is designed to highlight my efforts, this project as a whole was a collaborative effort between myself and Dr. Behrouz Abedian, without whom none of this would have even been conceived. It was his relentless drive and sleepless nights that led us to many of our breakthroughs. Apart from his direct contributions, Dr. Abedian was an excellent mentor who always kept me pointed in the right direction, and whose passion for fluid mechanics is truly infectious. Thanks to Dr. Abedian what I learned far exceeds the scope of this paper, and I am confident his imparted knowledge will serve me well throughout my career.

Finally, I would like to thank my family and friends for all their support throughout this process. In particular, the energy and work culture of everyone in the TA office provided the lighthearted humor and Folgers necessary to stay both on track and in good spirits.

Nomenclature

The terms used in this text are defined below:

Latin:

C = Compressibility Constant
 \hat{e} = Energy (of the System)
 e_r = Radial Rate of Deformation
 e_θ = Angular Rate of Deformation
 i_r = Radial Unit vector
 i_θ = Angular Unit Vector
 \mathbf{I} = Identity Matrix
 J_e = Energy Flux
 J_u = Diffusive Internal Energy Flux
 J_v = Diffuse Volume Flux
 k = Thermal Conductivity Coefficient
 k' = Thermal Conductivity Specific Ratio
 Kn = Knudson Number
 Ma = Mach Number
 M_o = Net Moment Constant
 p = Equilibrium Pressure
 \mathbf{P} = Pressure Tensor
 Pr = Prandtl Number
 r = Radius
 R = Ideal Gas Constant
 Re = Reynolds Number
 \mathbf{T} = Viscous Stress Tensor
 T = Temperature
 $tr()$ = Trace of a Tensor
 u_r = r -Component of Velocity
 u_θ = θ -Component of Velocity
 \mathbf{U} = Internal Energy
 V = Representative velocity
 \mathbf{V} = Magnitude of Mass Velocity
 \mathbf{v}_m = Mass Velocity
 \mathbf{v}_v = Volume Velocity

Greek:

α = Thermal Diffusivity
 γ = Heat Capacity Ratio (c_p / c_v)
 Γ_∞ = Circulation (strength of vortex)
 ∇ = Del Operator
 ζ = Non-dimensional quantity
 η = Refractive Index
 θ = Angle
 μ = Dynamic Viscosity
 ν = Momentum Diffusivity or Kinematic Viscosity
 π_v = Volume Production Rate
 ρ = Density
 ψ = Generic Variable

Other Notation:

Superscript T = Transpose
 Subscript o = Reference parameter
 Tilde \sim = Nondimensionalized parameter

1 Introduction

Vortex flows represent an important branch of fluid dynamics. Vortices can be observed from spinning electron charges to revolving galaxy clusters, covering 38 orders of magnitude [2]. More well known are the vortices found in sinks and bathtubs, or hurricanes and tornadoes. The two major areas where the traditional approach begins to fail for compressible flows are at high Mach numbers and high Knudsen numbers. A particularly important instance of compressible vortices are found in both fixed wing and rotary aircraft. Specifically, rotary aircraft blade tip velocities reach into the transonic range [3]. Once the flow has been identified as compressible, describing it mathematically can become challenging. This paper attempts to help fill the gaps in our collective understanding of fluid mechanics.

Research in compressible vortex flows has stagnated in recent years. Previously, analytical studies like those done by Colonius, Lele and Moin utilized the Navier-Stokes equations to model two-dimensional axisymmetric vortices [4]. While certain calculations are in agreement with numerical solutions, much of the prediction correlates poorly with the experiments done by Mandella, Moon and Bershader [4, 5]. Mandella explored the interactions of a single, quasi-uniform, two-dimensional compressible vortex with an airfoil by a traveling shock. Below in Figure 1, distinct density contours can be seen in great detail.

In effect, this thesis - as well as the previous work discussed herein - endeavors to improve upon the Navier-Stokes-Fourier model by adding the bivelocity assumption to derive a set of mathematical expressions which can be used to accurately predict these compressible vortices, which are so predominant in our universe. Fortunately, thanks to the dedicated work of others before, there exists an understanding of what the structure should look like. Mandella's holographic interferograms produced a number of excellent photos showing the density distribution, and has proven to be instrumental in the hunt to find a generic compressible vortex solution.



Figure 1: (Mandella Figure 1.3): Vortex Structure Interferogram [2]

This interferogram marks variation in density, just as a topographical map indicates variation in elevation. Here, the darkened lines represent changes in density of approximately $1/20^{th}$ of sea-level atmospheric density between contours [2]. Additionally, while directionality is not implied by the interferogram, it is known that the density is decreasing towards the center of the vortex where the fluid becomes increasingly rarefied and further susceptible to decompression.

In general, we can simplify the interferogram by splitting it into three distinct parts. Long-understood vortex structure has determined that the major regions include the core, viscous layer, and inviscid periferi - as seen below in Figure 2. This specific vortex structure is known as a Rankine vortex [2].

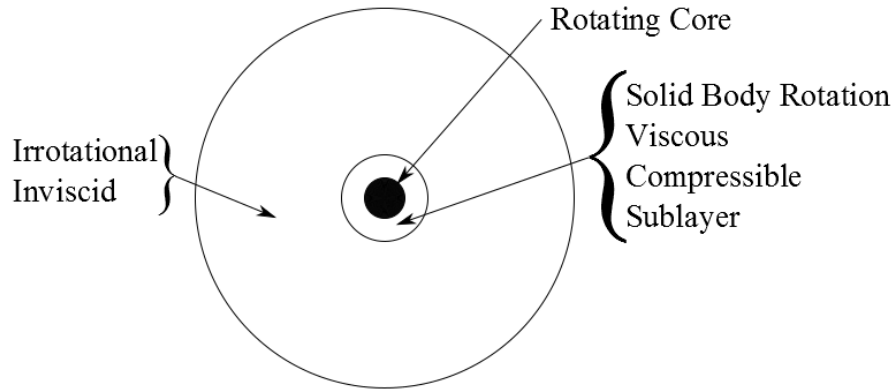


Figure 2: Diagram of Vortex zones

Rather than model a free vortex - to avoid singularity issues - the solid core at the center of the matrix drives the flow. Immediately adjacent to the rotating core, a viscous layer develops. This corresponds to the darkened concentric rings in the interferogram above in Figure 1. In order to have a rotational vortex flow, velocity must increase as radius increases. Farther away from the core, the viscous layer breaks down, and the flow becomes irrotational, where tangential velocity begins to decrease with increasing radius. The velocity profile can be seen below in Figure 3.

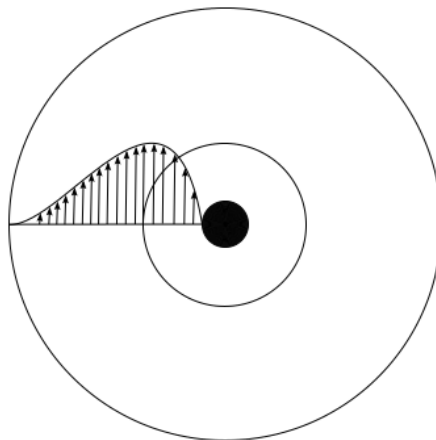


Figure 3: Rotational-Irrotational Velocity Field

As discussed previously, the tangential velocity increases from the core, to a maximum

at the edge of the viscous layer, where it begins to drop to zero.

1.1 Mach Number

It is generally accepted that a Mach number of at least 0.3 is required before effects of compressibility must be considered [6]. The Mach number, defined as

$$Ma = \frac{v_f}{v_s}, \quad (1)$$

where v_f is the speed of the flow and v_s is the localized speed of sound in that medium. The Mach number is affected by the medium of the flow. Still, the Mach number is not necessarily constant throughout a single medium. The effects of temperature and density can vary the Mach number greatly.

It's important to note that in high-speed flows, the conservation of mass flow rate becomes counter intuitive. Under subsonic flows, a narrowing of the flow channel causes an increase in velocity - to compensate for the reduced cross-sectional area. However, once the flow transitions to supersonic speeds, a narrowing of the flow channel will result in a decrease velocity.

1.2 The Knudsen Number

Application of the bivelocity equations (which have yet to be defined in this paper) is independent of whether the flow falls under continuum or statistical mechanics. However, in statistical mechanical approaches where the Boltzmann equation is used to describe particle interaction, it's important to define the difference between the continuum and non-continuum flows. A typical indicator is the Knudsen number Kn where the Knudsen number is defined as

$$Kn = \frac{\lambda}{L}, \quad (2)$$

where λ is the mean free path and L is the representative length scale. The mean free path is defined as the average distance a particle travels in between collisions. A

representative length scale for a micro-poiseuille flow would be the tube diameter. Free vortex flows have no geometric length scale, and it would be difficult to define a characteristic length scale. In this paper, the Knudsen number represents a reference Knudsen number where the flow is in local thermal equilibrium. When $Kn \ll 1$ the flow behaves according to continuum mechanics, and when $Kn \gg 1$ the flow can be analyzed according to statistical mechanics.

As the representative length scale approaches the mean free path, the collisions between particles decrease to the point where thermal energy and momentum are not effectively exchanged. Once this happens, the flow can no longer be treated as continuous, and must be observed as discrete particles. Similar to turbulent and laminar flows, there does not exist a specific transition from continuum to statistical mechanics. However, the generally accepted transition at $Kn = 0.01$ [7] is used in this paper.

1.3 The Navier-Stokes Equations

The Navier-Stokes equations are used to describe a wide variety of fluids behavior, and are an application of Newton's second law to fluid mechanics. The Navier-Stokes equations are well adapted to incompressible flows [1, 8] and flows with a known analytical relationship between ρ and p [8]. It remains, however, that a full complement of equations which include density, pressure, as well as temperature exists. Additionally, Navier-Stokes assumes the flow is a continuum ($Kn \ll 1$) and requires different method for non-continuum flows (discussed below).

1.4 Boltzmann Equation

The Boltzmann Transport Equation (BTE) can be applied to flows identified as non-continuum, where Navier-Stokes no longer applies ($Kn \gg 1$). The BTE does not consider the position (\hat{p}) and momentum (\hat{M}) of every particle in the flow, but rather uses the probability that a certain number of particles will have particular properties at a given moment. This is accomplished by defining a phase space, which

is a domain of possible positions and momenta. If all three spatial dimensions are considered, the resulting position/momentum points will be 6-dimensional [9]. The resulting particle density function $f(\hat{p}, \hat{M}, t)$ is defined as

$$dN = f(\hat{p}, \hat{M}, t) d^3\hat{p} d^3\hat{M} \quad (3)$$

Integrating over the position and momentum spaces gives

$$\begin{aligned} N &= \int_{\text{positions}} d^3\hat{p} \int_{\text{momenta}} d^3\hat{M} f(\hat{p}, \hat{M}, t) \\ &= \int \int \int_{\text{positions}} \int \int \int_{\text{momenta}} f(\hat{p}_x, \hat{p}_y, \hat{p}_z, \hat{M}_x, \hat{M}_y, \hat{M}_z, t) d\hat{p}_x d\hat{p}_y d\hat{p}_z d\hat{M}_x d\hat{M}_y d\hat{M}_z \end{aligned} \quad (4)$$

It is important to note that this method assumes a set of uniform particles i.e. a uniform composition medium. There still exists an issue with BTE solutions and their uniqueness which are not fully understood. Additionally, there are issues with fitting the BTE to experimental data [10]

1.5 Burnett Equation

The Navier-Stokes Equations were derived from the first order Knudsen number, and the Burnett Equation was derived from the second order Knudsen number using the Chapman-Enskog expansion of the Boltzmann equation in 1935 [11]. By 1991 linearized third-order terms were added to the Burnett equation to help compensate for its inherent instability, however, this was not entirely successful. The linear stability analysis was not adequate in justifying the instability in flows with high Knudsen numbers, and it was realized that the Burnett equations could violate the second law of thermodynamics at high Knudsen numbers [12]. The nonlinear collision integral was redefined with the Bhatnagar-Gross-Krook (BGK) operator. Despite the difficulties with the Burnett equations, they have remained a major focus. The scientific community continues to develop Burnett Regime derivations

of the Boltzmann equation in hopes of creating a simplified and more accurate set of equations [12, 13]. In general, the Burnett Regime - also called the Transition Regime - refers to flows with Knudsen numbers in the range of $0.01 < Kn < 10$.

2 Compressible Free Vortex

2.1 Structure

The structure of a compressible free vortex model contains multiple important regions, touched on in the previous section. Figure 4 below overlays the velocity profile over the two vortex structures.

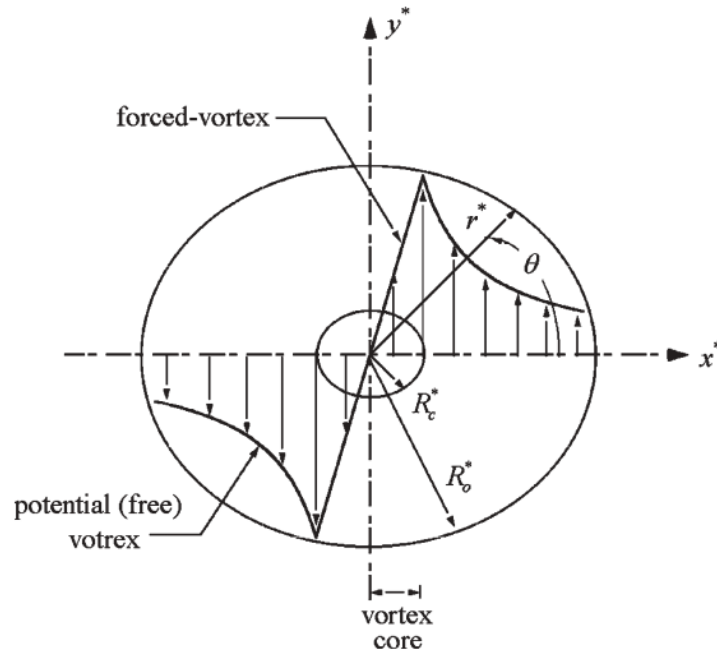


Figure 4: Rotational-Irrotational Velocity Field [14]

A compressible vortex will develop a viscous layer towards the core. This layer displays different behavior than its free vortex counterpart; most notably, the viscous layer will in fact be rotational. Vorticity is used to determine whether a flow is rotational or irrotational, and is defined as

$$\omega \equiv \nabla \times \vec{u} \quad (5)$$

where ω is the vorticity and \vec{u} is the flow field. For the vortex to be rotational - as the core of the compressible vortex is - the velocity must increase proportionally with increasing radius. This allows the relative position of two points at different radii to remain constant. Once the viscous layer is breached, the vortex begins to behave as a free vortex where velocity decreases with increasing radius. This rather unique and elusive velocity profile has become one of the major performance benchmarks when determining the effectiveness of the bivelocity equations.

2.2 The Dissipation of Eddies

One of the first to tackle the problem of viscous vortex flows was Sir Geoffrey Ingram Taylor. In 1918 Taylor published on the effects of dissipating eddies in response to the effects of drag on airships [15]. Taylor noted that the effects on these airships from eddies appeared to die away above a distance of seven feet, but it was not well understood what caused this effect. However, Taylor proposed a number of causes such as the viscous effects of adjacent rotating vortices, as well as the inward radial flow, which in the two dimensional plane builds mass towards the center, which is then translated into the third dimension, effectively growing the core of the vortex until the vortex's death. Taylor described the two-dimensional angular velocity as

$$\omega = \frac{B e^{\frac{-r^2}{4\nu t}}}{t^2 \sqrt{4\nu}} \quad (6)$$

Taylor discovered this solution which has become the backbone of viscous vortex flow. He went on to model vortices where angular velocity is at a maximum in the center and decreases outward. He discovered a nonlinear decrease in radial velocity, but found that in the viscous layer region, the tangential velocity increased before decreasing in the free vortex region.

Taylor recognized the importance of the vortex time dependency, and related an equation for the time taken for a vortex of initial radius a to die down to 1/ n th of its original velocity, which could be expressed as

$$t - t_0 = t_0(n^{2/3} - 1) = \frac{a^2}{2\nu}(n^{2/3} - 1) \quad (7)$$

This result was highly significant, considering he was able to verify this approximation with a series of experiments performed previously and independently [15]. But an interesting phenomenon occurred. Taylor observed experimentally that the vortex had a degradation period of one-half of what was expected. Vortices behind grating of quarter-inch diameter vertical rods died down to half at a distance of 4 feet. Given the velocity in the channel was 40 feet per second, the expected degradation time was 1/5th of a second. In actuality, the vortices degraded in 1/10th of a second. Because of the similar order of magnitude, Taylor concluded that while the viscosity was not the only driving factor, its contribution was incredibly significant to the overall degradation. Taylor's suggestion was to repeat the experiment with different channel velocities and grating sizes and spacing. Once performed, a curve fit could be created to solve for the complete dissipation of vortices.

2.3 Mandella's Experimental Analysis

Michael Mandella's work is in large part the motivation for this paper. In his 1987 experiments, Michael Mandella utilized holographic interferograms to analyze quasi-uniform vortex stream flow [2]. Mandella was able to derive a general mathematical expression to predict density, which was combined with pressure to solve for the radial momentum equation which yielded fluid velocities. However, he was unable to derive a predictive expression from first principals.

In order to gather vortex data, Mandella utilized holographic interferograms. The shock tube setup contains a vortex generator at one end, and an open-ended tube at the other. The generator created a pseudo-two dimensional compressible vortex, which traveled along the shock tube where it passed in front of measuring windows [2]. Measurements are made using an electronically timed double-pulsed laser, and when assessed, density can be extracted. In order to stem errors, pressure measurements

were taken separately with a pressure transducer.

As Mandella's experiments were transient, his density profiles reflected both vortex location and age. Once the measurements had been taken, Mandella performed curve fitting on pressure and density to generalize these relationships, and derive equations of motion. The resulting curve resembled a Cauchy distribution, expressed as [2]

$$\rho(r, t) = \rho_{\infty}(t) - \frac{\Delta\rho(t)}{1 + \left(\frac{r}{\Delta r(t)}\right)^2} \quad (8)$$

where ρ , P , and r represent density, pressure and radius respectively, the subscript ∞ refers to the far-field reference parameter, and $\Delta\rho$ and Δr refer to the well depth, and half-width at half-maximum respectively. To correlate the experimental pressure readings to a curve fit, Mandella again utilized a modified Cauchy distribution expressed as

$$P(r, t) = P_{\infty}(t) - \frac{\Delta P}{1 + \left(\frac{r}{\Delta r_p}\right)^2} \quad (9)$$

In this case the pressure and density curve fits pertain specifically to the vortices generated by Mandella's setup. While Mandella's Cauchy curves fit the data quite well, they are not derived from continuity or conservation equations. The purpose of this thesis is to develop a set of expressions to numerically solve for any general nondimensionalized vortex given certain criteria such as Mach and Knudsen number.

2.4 Analytic Solutions

2.4.1 Colonius, Lele, and Moin

Following Mandella's experiments, Colonius, Lele, and Moin's expanded on his work in 1991, which again attempted to take into account the compressible effects of the high Mach, low Knudsen number vortex flows. Colonius et al were unable to develop an equation set which accurately matched Mandella's findings. The prevailing theory

was the experimental-analytic transition from two dimensions to three dimensions was the cause of the discrepancy [4].

To model the two-dimensional axisymmetric flow, Colonius et al utilized continuity, conservation of momentum and energy, and the perfect gas equation. Their predictors are similar to this paper, but lacking the bivelocity terms. Colonius et al solved for the full compressible equations utilizing a grid of 151 mesh points extending ten times the core radii in each direction. Spatial derivatives are computed with a sixth-order modified Padé scheme, and the derivatives are advanced with a fourth-order Runge-Kutta scheme [4].

Ultimately, the derived solution did not match Mandella's experiments as was expected. While this error was attributed to the discrepancy between the two-dimensional model and three-dimensional experiments, a grave error went unnoticed by Colonius and his team. To simplify the equation determining the ambient speed of sound - which changes as fluid density changes - both viscosity and thermal conductivity were held constant [4, p. 48], however, This assumption cannot be made with a non-isothermal compressible fluid. The proportionality between viscosity and temperature has long been accepted [16], and is expected to play a role in Colonius et al's results. Additionally, Colonius et al performed their analytics by taking the ambient speed of sound into consideration, since the local Mach number is dependent the speed of sound, and speed of sound is dependent on the velocities. As will be discussed in the bivelocity section, this paper uses a representative Knudsen number to account for these effects.

Finally, the discrepancies between Mandella's experiments and Colonius et al's analytics were greater than they had hoped. Certain aspects, like much of pressure and low radial values of tangential velocity seem to correlate well. However, with radial velocity containing large discrepancies, the equation set cannot be said to accurately predict the vortex flow. The major contributors to this deviation are the

constant viscosity assumption and the lack of bivelocity.

2.4.2 Ellenrieder and Cantwell

Ellenrieder and Cantwell took a similar approach to Colonius, Lele, and Moin. Assuming a constant viscous fluid, Ellenrieder and Cantwell analyzed the transient compressible solution [17]. To model the two dimensional free vortex, Ellenrieder and Cantwell used slightly modified versions of Colonius, Lele, and Moin's equations; Ellenrieder and Cantwell lump the time and Reynolds dependency into a single variable τ .

Ultimately, Ellenrieder and Cantwell's solutions were close to Mandella's experiments, but did not match them exactly - similar to Colonius, Lele, and Moin's. Without providing a direct comparison to Mandella's data, Ellenrieder and Cantwell proved that the amount of local compression strongly influences the local magnitude of the radial velocity. Ellenrieder and Cantwell discuss the use of non-constant-viscosity, and speak to its importance, but end by incorporating it into the Reynolds and Prandtl numbers [17].

2.4.3 Aboelkassem, Vatistas and Esmail

Most recently, Yasser Aboelkassem, Georgios Vatistas, and Nabil Esmail published in 2005 on analytical solutions for a time-decaying Rankine vortex [14]. Aboelkassem et al consider a pure swirling, incompressible, and axisymmetric vortex whose behavior is modeled according to continuity, angular and radial momentum, and vorticity.

While promising, Aboelkassem et al's results are somewhat restrictive. These solutions work only for zero-meridional flow (flow whose radial velocity is zero), which is not the case.

Having reviewed the analytic attempts to describe generic compressible vortex flows, this paper joins those before it in attempting to solve this elusive sect of fluid

mechanics. What sets this paper apart from those before it is the introduction of bivelocity, discussed in the next section.

2.5 Rotor Driven Flow

In 1993 Ashish Bagai and J. Gordon Leishman performed an analytic analysis on compressible vortex flows with respect to rotary-wing devices such as propellers and helicopter blades [18]. Like Colonius, Lele, and Moin, Bagai and Leishman were concerned with the models for acoustics and hoped to develop a general solution to compressible vortices.

Bagai and Leishman were aware of the experimental problems in vortex modeling. Mostly with respect to intrusive measurement systems such as hot-wire anemometry and multi-hole pressure probes, which are controversial as the probes themselves could interfere with the vortex structure. Similarly, non-intrusive methods such as laser velocimetry - Such as those used by Mandella and Bershader - are also unreliable, due to the poor readability with high tangential velocities. Regardless, shadowgraphy was used to create flow visualizations of propeller wakes.

To perform these analytic predictions, Bagai and Leishman utilized the local light refractive effects produced by density variations. Through their derivations, Bagai and Leishman developed the following velocity profile predictor

$$v_{\theta}(r) = \frac{\Gamma_{\infty} r}{2 \pi (r_c^{2n} + r^{2n})^{1/n}} \quad (10)$$

Utilizing different integers of n , Bagai and Leishman were able to generate a number of vortices (such as the Rankine free vortex), but the goal was to predict a specific subset of vortices, not create an overarching theory. While some of the evaluative techniques were useful, this solution could not be applied to this paper.

3 Bivelocity Hydrodynamics

3.1 Introduction and Formation

Bivelocity theory is named for its consideration of two independent velocities, which is in contrast with traditional theories. Bivelocity also applies to compressible flows in general, without being bound to either continuum or non-continuum cases, which is again in contrast with traditional methods. In this paper \mathbf{v}_m and \mathbf{v}_v represent the mass and volume velocities respectively, where volume velocity is defined as the sum of the mass velocity and the diffusive flux density,

$$\mathbf{v}_v = \mathbf{v}_m + \mathbf{j}_v \quad (11)$$

Essentially, the mass velocity accounts for the bulk fluid movement through the system, where the volume velocity accounts for the expansion (or contraction) of the fluid due to the non-constant density [1, 19]. So far, bivelocity theory has been successful in describing experimental data in both continuum and statistical flows [22]. Recently, bivelocity has been successfully applied to micro-Couette flows [13, 23].

3.2 Volume and Momentum Transport

It is well understood that volume cannot always be considered a conserved quantity. An example where this holds true is when one mixes quantities of hot and cold water (adiabatically and isobarically). It can be observed that once allowed to reach thermal equilibrium, the resultant fluid volume will not be the sum of the initial hot and cold volumes [13, 24].

Brenner derived the “volume continuity equation” seen below [24]

$$\nabla \cdot n_v = \pi_v, \quad (12)$$

where n_v is the Eulerian flux density of volume, and π_v is the volume production rate. There is no Newtonian mechanics counterpart to π_v , making this continuity

equation fundamentally different from other transport quantities. Every particle in a continuum flow contains no volume, whereas in non-continuum flows every point-size particle carries mass, momentum, and energy.

Since momentum production in bivelocity is unchanged from the NSF case, it is the accounting of volume that separates bivelocity and Navier-Stokes-Fourier (NSF).

3.3 Continuum Approach to Phoretic Motions

While they had not yet coined the name bivelocity, Brenner and Bielenberg proposed the idea in 2005 of accounting for two separate but dependent velocities in continuum fluid mechanics [22]. This came about from studying the motion of particles by thermophoresis when it was discovered that aerosol particle motion near heated surfaces was not driven thermally, but rather by a resulting pressure gradient. This pressure - not temperature - gradient caused a discrepancy between barycentric velocity (\mathbf{v}_m) and volume velocity (\mathbf{v}_v), and would ultimately become the focal point of numerous publications on the subject, including this paper.

3.4 Incompleteness of Navier-Stokes-Fourier

After proposing his bivelocity theory in 2010, Howard Brenner followed up with a proof exemplifying the incompleteness of the Navier-Stokes-Fourier (NSF) with relation to compressible flows [21]. Brenner began with the widely accepted transport phenomena energy equation where the velocity is largely defined by its task in altering the pressure tensor. The belief was the velocity term was defined solely as the barycentric velocity, and not in any part as the volume velocity.

It was demonstrated that in order for the NSF equations to maintain their complete general form, a single flux term would not be sufficient. While in most continuum cases both terms may not have equal significance, both must be present to maintain completeness. This was obtained through an importantly simple counterexample of

steady quiescent flow where linear irreversible thermodynamic principals show the volume velocity is non-zero.

These series of examples and stark realizations of Navier-Stokes-Fourier's inadequacies have become the backbone for a multi-velocity comprehensive general fluid theory.

3.5 Bivelocity and Navier-Stokes-Fourier Heat Conduction

To further his point, Brenner illustrated a surprising comparison between bivelocity and compressible Navier-Stokes-Fourier [20]. It has been known that NSF is unsatisfactory in rarefied gas flows (non-small Knudsen numbers), but has not been confirmed for gaseous continua - as was commonly believed. Brenner offered a simulation to test the viability of NSF in this region.

To determine the validity, Brenner considered an annulus between concentric solid cylinders; the space between was filled with various noble gasses. Both cylinders would rotate at constant angular velocity, and would be bound with the same temperature. The NSF scheme predicts that the gas - moving as a rigid body - would have a uniform temperature distribution. The gasses did in fact not contain a uniform temperature gradient, and under these specific tests, varied as much as 15°C [20], bringing the validity of NSF into question. This was a stark realization, with Navier-Stokes having been used in continuum mechanics for more than a century and a half. In contrast, bivelocity was evaluated to determine the magnitude of the expected temperature change, which were also shown to be large enough to be measured with relatively primitive thermometers.

3.6 Bivelocity Shock Waves

Bounding off of Brenner's determination of bivelocity, Greenshields and Reese tested the robustness of bivelocity utilizing shock waves [25]. Since the bivelocity modifications are most important in flows with high density gradients, shock waves make an

excellent evaluation tool.

Initial results suggested that bivelocity was inadequate, and nonsensical physical relationships developed. This was attributed to the instances when kinematic viscosity was less than the volume diffusion coefficient. Once these two properties were equated, bivelocity began to outperform Navier-Stokes [25].

3.7 Micro-Channel Couette Flow

In addition to Mandella's experimental results, previous success with bivelocity in micro-channel couette flow [13, 23] has led to the adoption of this theory to vortex flows. Walls et al utilized Brenner's bivelocity equations governing mass, momentum and energy transport for a steady, ideal body force free gas [23]. Integral to the Couette solution was the proper application of boundary conditions, since Couette flow is shear driven, and not gradient driven. Following Brenner's lead, Walls used a no-slip boundary condition at the walls - contrary to traditional micro-channel flows with Knudsen numbers near 1 [26].

Ultimately, while Walls' adaptation of bivelocity accurately predicted temperature, density, and pressure profiles, it proved difficult to draw definitive conclusions given the very limited and aging experimental data sets existing for micro-channel Couette flow. However, Walls demonstrated the functionality of bivelocity over a range of Knudsen numbers, affecting the density distribution and temperature.

3.8 Governing Equations and Bivelocity Derivation

For the full step-by-step derivation of the governing equations and their bivelocity terms, see attached Appendix A. Below is an abbreviated expansion for the purposes of illustrating bivelocity's place in the governing equations.

3.8.1 Continuity

The conservation of mass - or continuity - for this compressible system can be defined in totality as seen in numerous previous works [2]. However, for the sake of completeness, continuity will begin with the bivelocity equation governing transport of mass [1].

$$\frac{\partial \rho}{\partial t} + \nabla \cdot (\rho \mathbf{v}) = 0 \quad (13)$$

Separating the velocity vector and carrying density through, as well as accounting for the system's two-dimensional and axisymmetric nature, the final continuity equation becomes

$$\frac{\partial \rho}{\partial t} + \frac{1}{r} \frac{\partial}{\partial r} (r \rho v_r) = 0 \quad (14)$$

The axisymmetric assumption is seen in previous work, and this equation is no different than the equations used by Mandella [2], Colonius et al [4], or Ellenrider and Cantwell [17], as there is no continuity bivelocity term to account for. One of the motivations behind the axisymmetric assumption stems from Mandella's interferograms and velocity data. As seen previously in Figure 1, the inner density variations can be seen as concentric circles, and thus support the axisymmetric notion. Additionally, Mandella's tangential velocity values dwarf the radial velocity terms by three orders of magnitude. This disparity would allow for an introduced particle to circumnavigate the vortex with negligible change in radial distance.

3.8.2 Conservation of Momentum

Similar to continuity, the launching point for the momentum equations is Brenner's bivelocity [1]

$$\rho \frac{D\mathbf{v}_m}{Dt} + \rho \mathbf{v}_m \cdot (\nabla \cdot \mathbf{v}_m) = -\nabla \cdot \mathbf{P} \quad (15)$$

The pressure tensor \mathbf{P} can be rewritten and substituted back into the momentum equation before it is split into its radial and tangential components.

$$\begin{aligned} \rho \frac{\partial u_r}{\partial t} + \rho (\mathbf{v}_m \cdot \nabla) u_r - \rho \frac{u_\theta^2}{r} &= -\frac{\partial p}{\partial r} + \nabla \cdot \mathbf{T}|_{rr} \\ \rho \frac{\partial u_\theta}{\partial t} + \rho (\mathbf{v}_m \cdot \nabla) u_\theta - \rho \frac{u_r u_\theta}{r} &= \nabla \cdot \mathbf{T}|_{r\theta} \end{aligned} \quad (16)$$

Furthermore, evaluating the viscous stress tensor, the volume velocity, and taking into account the axial symmetry and lack of a third spatial dimension, the system ultimately yields

$$\begin{aligned} \rho \frac{\partial u_r}{\partial t} + \rho u_r \frac{\partial u_r}{\partial r} - \left(\rho \frac{u_\theta^2}{r} \right) &= -\frac{\partial p}{\partial r} + \frac{1}{r} \frac{\partial}{\partial r} \left(r \mu \frac{\partial u_r}{\partial r} \right) - \frac{\mu u_r}{r^2} + \frac{1}{r} \frac{\partial}{\partial r} \left(r \mu \frac{\partial}{\partial r} \left(\frac{C}{Pr} \frac{\mu}{\rho^2} \frac{\partial \rho}{\partial r} \right) \right) \\ \rho \frac{\partial u_\theta}{\partial t} + \rho u_r \frac{\partial u_\theta}{\partial r} + \left(\rho \frac{u_r u_\theta}{r} \right) &= \frac{1}{r} \frac{\partial}{\partial r} \left(r \mu \frac{\partial u_\theta}{\partial r} \right) - \frac{\mu u_\theta}{r^2} \end{aligned} \quad (17)$$

3.8.3 Conservation of Energy

Conservation of energy can again be derived from Brenner's bivelocity [1]

$$\rho \frac{D\hat{u}}{Dt} + \rho \mathbf{v}_m \cdot \nabla \hat{e} = -\nabla \cdot \mathbf{J}_e \quad (18)$$

Evaluating all fluxes, substituting thermal conductivities and specific heats, redefining temperature gradients and pressure tensors, the energy equation takes on a whole new form

$$J_e = J_u + \mathbf{P} \cdot \mathbf{v}_v \quad (19)$$

$$J_u = -k' \nabla T \quad (20)$$

$$\nabla T = \left(\frac{\partial T}{\partial r}\right) i_r + \left(\frac{1}{r} \frac{\partial T}{\partial \theta}\right) i_\theta \quad (21)$$

$$(\mathbf{P} \cdot \mathbf{v}) = \mathbf{P}_{ij} \mathbf{v}_j \quad (22)$$

Where the substitutions now result in

$$\rho \frac{D\hat{u}}{Dt} + \rho \mathbf{v} \cdot \nabla \hat{e} = \frac{1}{r} \frac{\partial}{\partial r} (k' r \frac{\partial T}{\partial r}) - \frac{1}{r} \frac{\partial}{\partial r} (r (\mathbf{P}_{rr} u_r + \mathbf{P}_{r\theta} u_\theta)) - \frac{1}{r} \frac{\partial}{\partial r} (r (\mathbf{P}_{rr} J_v^r)) \quad (23)$$

\hat{u} in this case represents the internal energy, which can be modeled as temperature. Remaining pressure tensors can be unfolded into each appropriate direction, and the flux term can be evaluated as

$$J_v^r = \frac{C}{Pr} \gamma \frac{1}{\rho} \frac{d\rho}{dr} \quad (24)$$

Producing a final result of

$$\begin{aligned} \rho R \frac{\partial T}{\partial t} + \rho u_r \frac{\partial}{\partial r} \left(\frac{3}{2} R T + \frac{\mathbf{V}^2}{2} \right) &= \frac{1}{r} \frac{\partial}{\partial r} (k' r \frac{\partial T}{\partial r}) - \frac{1}{r} \frac{\partial}{\partial r} \left(r \left((p - 2\mu \frac{\partial u_r}{\partial r}) u_r \right. \right. \\ &\quad \left. \left. + (p - r\mu \frac{\partial}{\partial r} \left(\frac{u_\theta}{r} \right)) u_\theta \right) \right) - \frac{1}{r} \frac{\partial}{\partial r} \left(r \left((p - 2\mu \frac{\partial u_r}{\partial r}) \left(\frac{C}{Pr} \frac{\mu}{\rho^2} \frac{\partial \rho}{\partial r} \right) \right) \right) \end{aligned} \quad (25)$$

3.8.4 Ideal Gas

At this point, there exists four fundamental equations: continuity, conservation of angular and radial momentum, and conservation of energy. However, the unknowns include radial and tangential velocity, pressure, density, and temperature. Fortunately,

the remaining equation can be taken from Ideal gas.

$$p = \rho R T \quad (26)$$

3.8.5 Dimensionless Forms

The full nondimensionalization of the above equations can be found in Appendix A. Found here are the reduced steps involved in the nondimensionalizing process.

Before the governing equations can be made dimensionless, each parameter must be defined with respect to a reference. In some instances this is very straight forward. Temperature, pressure, viscosity, radius, and density can be referred to by a far-field value. This designs the system to return all these properties to a value of one as radius tends to infinity. The velocities are nondimensionalized in a manner similar to Walls and Xue [13, 27]

$$\begin{aligned} \tilde{u}_r &= \frac{u_r}{\sqrt{R T_o}} & \tilde{u}_\theta &= \frac{u_\theta}{\sqrt{R T_o}} & \tilde{T} &= \frac{T}{T_o} \\ \tilde{r} &= \frac{r}{r_o} & \tilde{p} &= \frac{p}{p_o} & \tilde{\mu} &= \frac{\mu}{\mu_o} \\ \tilde{\rho} &= \frac{\rho}{\rho_o} & \tilde{k} &= \frac{k}{\mu_o \hat{c}_p} & \tilde{t} &= \frac{t}{r_o^2 \rho_o 10^{-2} \mu_o^{-1}} \end{aligned}$$

The last parameter listed, time, is nondimensionalized in a different fashion than the rest. With the axisymmetric and two-dimensional flow assumptions, quantities are convected by radial velocity alone; and with $u_r \ll u_\theta$, convection is of secondary importance. Colonius, Lele, and Moin expanded the timescale to be able to observe the evolution of the vortex on both the fast acoustic time, and the slow viscous time [4].

Since the fluid is modeled as Maxwellian and monatomic, thermal conductivity

and dynamic viscosity are proportional to temperature such that

$$\tilde{\mu} = \tilde{T} \qquad \tilde{k} = \frac{3}{2} \tilde{T}$$

The goal is to either cancel out dimensional terms, or substitute them out for dimensionless parameters such as the Knudsen or Prandtl numbers, shown below.

$$Kn_o = \frac{\mu_o}{\rho_o r_o \sqrt{RT_o}} \qquad Pr = \hat{c}_p \frac{\tilde{\mu} \mu_o}{\tilde{k} \mu_o \hat{c}_p} = \frac{\tilde{\mu}}{\tilde{k}} = \frac{2}{3}$$

Beginning with the continuity equation (14) rewritten below, the substitutions of the above nondimensional factors can be done quickly.

$$\frac{\partial \rho}{\partial t} + \frac{1}{r} \frac{\partial}{\partial r} (r \rho v_r) = 0 \qquad (27)$$

Expanding the derivatives and collecting all the initial parameters on one side yields

$$100 \frac{\partial \tilde{\rho}}{\partial \tilde{t}} + \frac{\rho_o r_o \sqrt{RT_o}}{\mu_o} \left[\tilde{u}_r \frac{\partial \tilde{\rho}}{\partial \tilde{r}} + \tilde{\rho} \frac{\partial \tilde{u}_r}{\partial \tilde{r}} + \frac{\tilde{\rho}}{\tilde{r}} \tilde{u}_r \right] = 0 \qquad (28)$$

Immediately apparent is the inverse of the Knudsen number remaining in front of the second term. The final solution can be written as

$$100 \frac{\partial \tilde{\rho}}{\partial \tilde{t}} + \frac{1}{Kn_o} \left[\tilde{u}_r \frac{\partial \tilde{\rho}}{\partial \tilde{r}} + \tilde{\rho} \frac{\partial \tilde{u}_r}{\partial \tilde{r}} + \frac{\tilde{\rho}}{\tilde{r}} \tilde{u}_r \right] = 0 \qquad (29)$$

With radial and angular momentum respectively (equation 17) things become slightly more complex.

$$\begin{aligned} \rho \frac{\partial u_r}{\partial t} + \rho u_r \frac{\partial u_r}{\partial r} - \left(\rho \frac{u_\theta^2}{r} \right) &= -\frac{dp}{dr} + \frac{1}{r} \frac{\partial}{\partial r} (r \mu \frac{\partial u_r}{\partial r}) - \frac{\mu u_r}{r^2} + \frac{1}{r} \frac{\partial}{\partial r} (r \mu \frac{\partial}{\partial r} (\frac{C}{Pr} \frac{\mu}{\rho^2} \frac{d\rho}{dr})) \\ \rho \frac{\partial u_\theta}{\partial t} + \rho u_r \frac{\partial u_\theta}{\partial r} + \left(\rho \frac{u_r u_\theta}{r} \right) &= \frac{1}{r} \frac{\partial}{\partial r} (r \mu \frac{\partial u_\theta}{\partial r}) - \frac{\mu u_\theta}{r^2} \end{aligned} \qquad (30)$$

Again, substituting all the dimensionless quantities in, the equations transform to
Radial:

$$\begin{aligned}
& \left(\frac{100 \mu_o \sqrt{RT_o}}{r_o^2} \right) \tilde{\rho} \frac{\partial \tilde{u}_r}{\partial \tilde{t}} + \left(\frac{\rho_o RT_o}{r_o} \right) \tilde{\rho} \tilde{u}_r \frac{\partial \tilde{u}_r}{\partial \tilde{r}} - \left(\frac{\rho_o RT_o}{r_o} \right) \frac{\tilde{\rho} \tilde{u}_\theta^2}{\tilde{r}} = \left(\frac{-p_o}{r_o} \right) \frac{\partial \tilde{p}}{\partial \tilde{r}} \\
& + \left(\frac{\mu_o \sqrt{RT_o}}{r_o^2} \right) \frac{1}{\tilde{r}} \frac{\partial}{\partial \tilde{r}} \left[\tilde{r} \tilde{\mu} \frac{\partial \tilde{u}_r}{\partial \tilde{r}} \right] - \left(\frac{\mu_o \sqrt{RT_o}}{r_o^2} \right) \frac{\tilde{\mu} \tilde{u}_r}{\tilde{r}^2} \\
& + \left(\frac{C \mu_o^2}{Pr \rho_o r_o^3} \right) \frac{1}{\tilde{r}} \frac{\partial}{\partial \tilde{r}} \left[\tilde{r} \tilde{\mu} \frac{\partial}{\partial \tilde{r}} \left(\frac{\tilde{\mu}}{\tilde{\rho}^2} \frac{\partial \tilde{\rho}}{\partial \tilde{r}} \right) \right]
\end{aligned} \tag{31}$$

Angular:

$$\begin{aligned}
& \left(\frac{100 \mu_o \sqrt{RT_o}}{r_o^2} \right) \tilde{\rho} \frac{\partial \tilde{u}_\theta}{\partial \tilde{t}} + \left(\frac{\rho_o RT_o}{r_o} \right) \tilde{\rho} \tilde{u}_r \frac{\partial \tilde{u}_\theta}{\partial \tilde{r}} + \left(\frac{\rho_o RT_o}{r_o} \right) \frac{\tilde{\rho} \tilde{u}_\theta \tilde{u}_r}{\tilde{r}} = \\
& \left(\frac{\mu_o \sqrt{RT_o}}{r_o^2} \right) \frac{1}{\tilde{r}} \frac{\partial}{\partial \tilde{r}} \left[\tilde{r} \tilde{\mu} \frac{\partial \tilde{u}_\theta}{\partial \tilde{r}} \right] - \left(\frac{\mu_o \sqrt{RT_o}}{r_o^2} \right) \frac{\tilde{\mu} \tilde{u}_\theta}{\tilde{r}^2}
\end{aligned} \tag{32}$$

Canceling and collecting terms, and recognizing the Knudsen and Prandtl numbers, radial and angular momentum respectively become

$$\begin{aligned}
100 Kn_o \tilde{\rho} \frac{\partial \tilde{u}_r}{\partial \tilde{t}} + \tilde{\rho} \tilde{u}_r \frac{\partial \tilde{u}_r}{\partial \tilde{r}} - \frac{\tilde{\rho} \tilde{u}_\theta^2}{\tilde{r}} = -\frac{\partial \tilde{p}}{\partial \tilde{r}} + Kn_o \frac{1}{\tilde{r}} \frac{\partial}{\partial \tilde{r}} \left[\tilde{r} \tilde{\mu} \frac{\partial \tilde{u}_r}{\partial \tilde{r}} \right] \\
- Kn_o \frac{\tilde{\mu} \tilde{u}_r}{\tilde{r}^2} + \left(\frac{3C Kn_o^2}{2} \right) \frac{1}{\tilde{r}} \frac{\partial}{\partial \tilde{r}} \left[\tilde{r} \tilde{\mu} \frac{\partial}{\partial \tilde{r}} \left(\frac{\tilde{\mu}}{\tilde{\rho}^2} \frac{\partial \tilde{\rho}}{\partial \tilde{r}} \right) \right]
\end{aligned} \tag{33}$$

$$100 Kn_o \tilde{\rho} \frac{\partial \tilde{u}_\theta}{\partial \tilde{t}} + \tilde{\rho} \tilde{u}_r \frac{\partial \tilde{u}_\theta}{\partial \tilde{r}} + \frac{\tilde{\rho} \tilde{u}_\theta \tilde{u}_r}{\tilde{r}} = \frac{Kn_o}{\tilde{r}} \frac{\partial}{\partial \tilde{r}} \left[\tilde{r} \tilde{\mu} \frac{\partial \tilde{u}_\theta}{\partial \tilde{r}} \right] - Kn_o \frac{\tilde{\mu} \tilde{u}_\theta}{\tilde{r}^2} \tag{34}$$

Energy starts as equation 25

$$\begin{aligned}
\rho R \frac{\partial T}{\partial t} + \rho u_r \frac{\partial}{\partial r} \left(\frac{3}{2} RT + \frac{\mathbf{V}^2}{2} \right) = \frac{1}{r} \frac{\partial}{\partial r} \left(k' r \frac{\partial T}{\partial r} \right) - \frac{1}{r} \frac{\partial}{\partial r} \left(r \left((p - 2\mu \frac{\partial u_r}{\partial r}) u_r \right. \right. \\
\left. \left. + (p - r\mu \frac{\partial}{\partial r} \left(\frac{u_\theta}{r} \right)) u_\theta \right) \right) - \frac{1}{r} \frac{\partial}{\partial r} \left(r \left((p - 2\mu \frac{\partial u_r}{\partial r}) \left(\frac{C}{Pr} \frac{\mu}{\rho^2} \frac{d\rho}{dr} \right) \right) \right)
\end{aligned} \tag{35}$$

An expansion of the derivatives and dimensionless substitutions yield

$$\begin{aligned}
& \frac{100 \mu_o R T_o}{r_o^2} \left(\tilde{\rho} \frac{\partial \tilde{T}}{\partial \tilde{t}} \right) + \frac{1}{2} \frac{\tilde{\rho} \rho_o \tilde{u}_r}{r_o} (R T_o)^{3/2} \left[3 \frac{\partial \tilde{T}}{\partial \tilde{r}} + \frac{\partial \tilde{u}_r^2}{\partial \tilde{r}} + \frac{\partial \tilde{u}_\theta^2}{\partial \tilde{r}} \right] = \\
& \frac{1}{\tilde{r} r_o^2} \frac{\partial}{\partial \tilde{r}} \left(\frac{3}{5} \tilde{k} \mu_o \hat{c}_p \tilde{r} r_o \frac{T_o}{r_o} \frac{\partial \tilde{T}}{\partial \tilde{r}} \right) - \frac{1}{\tilde{r} r_o^2} \frac{\partial}{\partial \tilde{r}} \left[\tilde{r} r_o \tilde{p} p_o \sqrt{R T_o} (\tilde{u}_r + \tilde{u}_\theta) \right] \\
& + \frac{1}{\tilde{r} r_o^2} \frac{\partial}{\partial \tilde{r}} \left[2 \tilde{r} r_o \tilde{\mu} \mu_o \tilde{u}_r \frac{R T_o}{r_o} \frac{\partial \tilde{u}_r}{\partial \tilde{r}} + \tilde{r}^2 r_o^2 \tilde{\mu} \mu_o \tilde{u}_\theta \frac{R T_o}{r_o^2} \frac{\partial}{\partial \tilde{r}} \left(\frac{\tilde{u}_\theta}{\tilde{r}} \right) \right] \\
& - \frac{C}{\tilde{r} r_o^2 Pr} \frac{\partial}{\partial \tilde{r}} \left[\frac{\tilde{r} r_o \tilde{\mu} \mu_o \tilde{p} p_o}{\tilde{\rho}^2 \rho_o^2} \frac{\rho_o}{r_o} \frac{\partial \tilde{\rho}}{\partial \tilde{r}} \right] + \frac{2C}{\tilde{r} r_o^2 Pr} \frac{\partial}{\partial \tilde{r}} \left[\frac{\tilde{r} r_o \tilde{\mu}^2 \mu_o^2}{\tilde{\rho}^2 \rho_o^2} \frac{\rho_o \sqrt{R T_o}}{r_o^2} \frac{\partial \tilde{\rho}}{\partial \tilde{r}} \frac{\partial \tilde{u}_r}{\partial \tilde{r}} \right]
\end{aligned} \tag{36}$$

Canceling and collecting terms leads to the final form of

$$\begin{aligned}
100 K n_o \tilde{\rho} \frac{\partial \tilde{T}}{\partial \tilde{t}} + \frac{1}{2} (\tilde{\rho} \tilde{u}_r) \left[3 \frac{\partial \tilde{T}}{\partial \tilde{r}} + \frac{\partial \tilde{u}_r^2}{\partial \tilde{r}} + \frac{\partial \tilde{u}_\theta^2}{\partial \tilde{r}} \right] &= \left(\frac{45}{20} K n_o \right) \frac{1}{\tilde{r}} \frac{\partial}{\partial \tilde{r}} \left[\tilde{r} \tilde{T} \frac{\partial \tilde{T}}{\partial \tilde{r}} \right] \\
- \frac{1}{\tilde{r}} \frac{\partial}{\partial \tilde{r}} \left[\tilde{r} \tilde{p} (\tilde{u}_r + \tilde{u}_\theta) \right] + (K n_o) \frac{1}{\tilde{r}} \frac{\partial}{\partial \tilde{r}} \left[2 \tilde{r} \tilde{\mu} \tilde{u}_r \frac{\partial \tilde{u}_r}{\partial \tilde{r}} + \tilde{r}^2 \tilde{\mu} \tilde{u}_\theta \frac{\partial}{\partial \tilde{r}} \left(\frac{\tilde{u}_\theta}{\tilde{r}} \right) \right] & \\
- \left(\frac{3C}{2} K n_o \right) \frac{1}{\tilde{r}} \frac{\partial}{\partial \tilde{r}} \left[\frac{\tilde{r} \tilde{\mu} \tilde{p}}{\tilde{\rho}^2} \frac{\partial \tilde{\rho}}{\partial \tilde{r}} \right] + (3C K n_o^2) \frac{1}{\tilde{r}} \frac{\partial}{\partial \tilde{r}} \left[\frac{\tilde{r} \tilde{\mu}^2}{\tilde{\rho}^2} \frac{\partial \tilde{\rho}}{\partial \tilde{r}} \frac{\partial \tilde{u}_r}{\partial \tilde{r}} \right] &
\end{aligned} \tag{37}$$

Lastly, ideal gas is the simplest. Beginning with equation 26

$$p = \rho R T \tag{38}$$

A quick substitution yields the form

$$\tilde{p} = \tilde{\rho} \tilde{T} \tag{39}$$

3.9 Bivelocity Significance

3.9.1 Absolute Significance

Before delving into the application of bivelocity to all governing equations, its significance can be determined by evaluating the bivelocity term (as seen below in the second line of the radial momentum conservation equation derived in Appendix A as equation 154)

$$100 Kn_o \tilde{\rho} \frac{\partial \tilde{u}_r}{\partial \tilde{t}} + \tilde{\rho} \tilde{u}_r \frac{d\tilde{u}_r}{d\tilde{r}} - \frac{\tilde{\rho} \tilde{u}_\theta^2}{\tilde{r}} = -\frac{d\tilde{p}}{d\tilde{r}} + \left(Kn_o \right) \frac{1}{\tilde{r}} \frac{d}{d\tilde{r}} \left[\tilde{r} \tilde{\mu} \frac{d\tilde{u}_r}{d\tilde{r}} \right] - \left(Kn_o \right) \frac{\tilde{\mu} \tilde{u}_r}{\tilde{r}^2} + \left(\frac{C Kn_o^2}{Pr} \right) \frac{1}{\tilde{r}} \frac{d}{d\tilde{r}} \left[\tilde{r} \tilde{\mu} \frac{d}{d\tilde{r}} \left(\frac{\tilde{\mu}}{\tilde{\rho}^2} \frac{d\tilde{\rho}}{d\tilde{r}} \right) \right] \quad (40)$$

While Mandella's curve-fits are not derived from the governing equations, their accuracy in describing the vortex behavior is useful. Before attempting to solve the bivelocity equation set, bivelocity's significance can be determined by substituting in Mandella's values for a comparison. If we utilize Mandella's equations for density and pressure (equations 8 and 9 respectively) with temperature below.

$$T = \frac{p}{R\rho} \quad (41)$$

Since the radial momentum equation has been nondimensionalized - and this is generally a more compact form - Mandella's equations can be quickly nondimensionalized, and become

$$\tilde{\rho} = 1 - \frac{\Delta\rho/\rho_\infty}{1 + \left(\frac{\tilde{r}}{\Delta r}\right)^2} \quad (42)$$

$$\tilde{p} = 1 - \frac{\Delta p/p_\infty}{1 + \left(\frac{\tilde{r}}{\Delta r p}\right)^2} \quad (43)$$

$$\tilde{T} = \frac{\tilde{p}}{R\tilde{\rho}T_\infty} \quad (44)$$

With these terms, the bivelocity term can be calculated directly. Assuming $Kn_o = 0.1$, $C = 1$, and $Pr = 2/3$, with Mathematica we find a bivelocity correction profile shown below. Since all parameters have been nondimensionalized (including the radius), it is only the power of the term that is being observed.

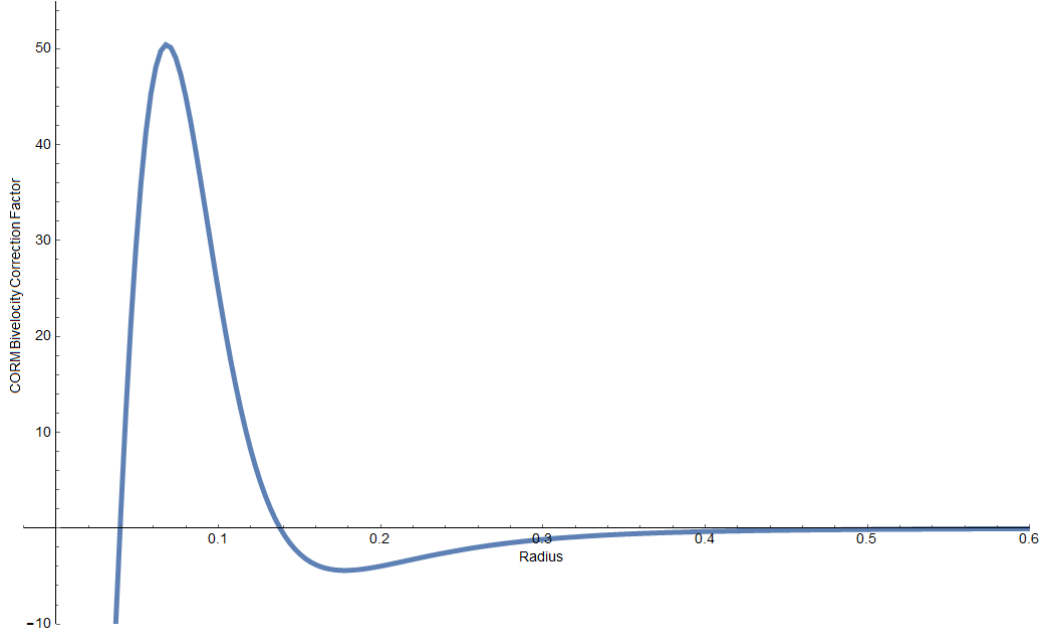


Figure 5: Evaluation of bivelocity component $\left(\frac{C Kn_o^2}{Pr}\right) \frac{1}{\tilde{r}} \frac{d}{d\tilde{r}} \left[\tilde{r} \tilde{\mu} \frac{d}{d\tilde{r}} \left(\frac{\tilde{\mu}}{\tilde{\rho}^2} \frac{d\tilde{\rho}}{d\tilde{r}} \right) \right]$ utilizing Mandella's temperature and density

Similarly, the bivelocity component of the energy equation can be evaluated (Third line seen below and derived from equation 177 in Appendix A)

$$\begin{aligned}
100 Kn_o \tilde{\rho} \frac{\partial \tilde{T}}{\partial \tilde{t}} + \frac{1}{2} (\tilde{\rho} \tilde{u}_r) \left[3 \frac{d\tilde{T}}{d\tilde{r}} + \frac{d\tilde{u}_r^2}{d\tilde{r}} + \frac{d\tilde{u}_\theta^2}{d\tilde{r}} \right] &= \left(\frac{45}{20} Kn_o \right) \frac{1}{\tilde{r}} \frac{d}{d\tilde{r}} \left[\tilde{r} \tilde{T} \frac{d\tilde{T}}{d\tilde{r}} \right] \\
- \frac{1}{\tilde{r}} \frac{d}{d\tilde{r}} \left[\tilde{r} \tilde{p} (\tilde{u}_r + \tilde{u}_\theta) \right] + (Kn_o) \frac{1}{\tilde{r}} \frac{d}{d\tilde{r}} \left[2 \tilde{r} \tilde{\mu} \tilde{u}_r \frac{d\tilde{u}_r}{d\tilde{r}} + \tilde{r}^2 \tilde{\mu} \tilde{u}_\theta \frac{d}{d\tilde{r}} \left(\frac{\tilde{u}_\theta}{\tilde{r}} \right) \right] & \quad (45) \\
- \left(\frac{C}{Pr} Kn_o \right) \frac{1}{\tilde{r}} \frac{d}{d\tilde{r}} \left[\frac{\tilde{r} \tilde{\mu} \tilde{p}}{\tilde{\rho}^2} \frac{d\tilde{\rho}}{d\tilde{r}} \right] + \left(\frac{2C}{Pr} Kn_o^2 \right) \frac{1}{\tilde{r}} \frac{d}{d\tilde{r}} \left[\frac{\tilde{r} \tilde{\mu}^2}{\tilde{\rho}^2} \frac{d\tilde{\rho}}{d\tilde{r}} \frac{d\tilde{u}_r}{d\tilde{r}} \right] &
\end{aligned}$$

Which will develop in a similar fashion seen below.

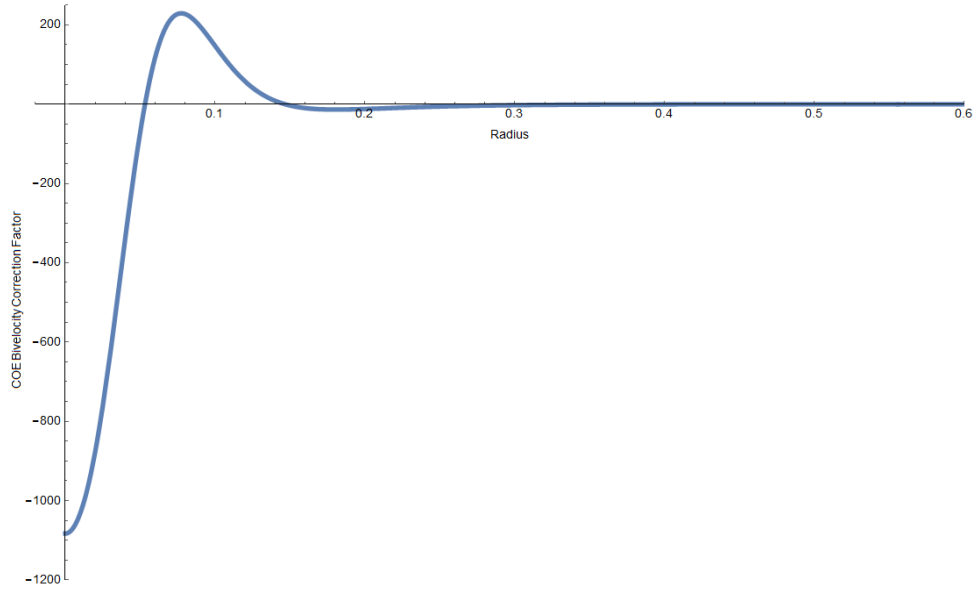


Figure 6: Evaluation of bivelocity component

$$\left(\frac{-C}{Pr} Kn_o \right) \frac{1}{\tilde{r}} \frac{d}{d\tilde{r}} \left[\frac{\tilde{r} \tilde{\mu} \tilde{p}}{\tilde{\rho}^2} \frac{d\tilde{p}}{d\tilde{r}} \right] + \left(\frac{2C}{Pr} Kn_o^2 \right) \frac{1}{\tilde{r}} \frac{d}{d\tilde{r}} \left[\frac{\tilde{r} \tilde{\mu}^2}{\tilde{\rho}^2} \frac{d\tilde{p}}{d\tilde{r}} \frac{d\tilde{u}_r}{d\tilde{r}} \right]$$

utilizing Mandella's temperature, pressure, density, and velocity

These curves illustrate bivelocity's importance to the equation set by showing a relative bump in generic value (Whether it's velocity or temperature), as is expected in the developed viscous layer. Additionally, both tend to zero at far-field radii, as there should be little to no contribution of these compressibility effects far from the center. Both also show some destabilization below $\tilde{r} = 0.1$, which correlates to the singularity issues encountered and discussed later in this paper.

3.9.2 Relative Significance

While the significance of the bivelocity term is important, it is only useful to talk about bivelocity significance with respect to the power of the remaining terms. The energy equation's bivelocity component may contribute up to a factor of 10, but if the remaining terms contribute a factor of 1000, the bivelocity term would be quite insignificant. Below is the rewritten form of the radial momentum (31) equation developed previously

$$\begin{aligned}
100 Kn_o \tilde{\rho} \frac{\partial \tilde{u}_r}{\partial \tilde{t}} + \tilde{\rho} \tilde{u}_r \frac{\partial \tilde{u}_r}{\partial \tilde{r}} - \frac{\tilde{\rho} \tilde{u}_\theta^2}{\tilde{r}} = & -\frac{d\tilde{p}}{\partial \tilde{r}} + Kn_o \frac{1}{\tilde{r}} \frac{\partial}{\partial \tilde{r}} \left[\tilde{r} \tilde{\mu} \frac{\partial \tilde{u}_r}{\partial \tilde{r}} \right] \\
& - Kn_o \frac{\tilde{\mu} \tilde{u}_r}{\tilde{r}^2} + \left(\frac{3C Kn_o^2}{2} \right) \frac{1}{\tilde{r}} \frac{\partial}{\partial \tilde{r}} \left[\tilde{r} \tilde{\mu} \frac{\partial}{\partial \tilde{r}} \left(\frac{\tilde{\mu}}{\tilde{\rho}^2} \frac{\partial \tilde{\rho}}{\partial \tilde{r}} \right) \right]
\end{aligned} \tag{46}$$

Looking at the rest of the factors

$$\begin{aligned}
100 Kn_o \tilde{\rho} \frac{\partial \tilde{u}_r}{\partial \tilde{t}} + \tilde{\rho} \tilde{u}_r \frac{\partial \tilde{u}_r}{\partial \tilde{r}} - \frac{\tilde{\rho} \tilde{u}_\theta^2}{\tilde{r}} + \frac{d\tilde{p}}{\partial \tilde{r}} \\
- Kn_o \frac{1}{\tilde{r}} \frac{\partial}{\partial \tilde{r}} \left[\tilde{r} \tilde{\mu} \frac{\partial \tilde{u}_r}{\partial \tilde{r}} \right] + Kn_o \frac{\tilde{\mu} \tilde{u}_r}{\tilde{r}^2} = 0
\end{aligned} \tag{47}$$

Since every parameter is dimensionless, their additive properties should yield a meaningful comparison. Below in Figure 7 the radial momentum bivelocity term can again be seen (blue), but is compared to the viscous term (yellow). The bivelocity term is about a quarter of the strength of the viscous term, and while not an incredibly powerful contribution, it should not be ignored either.

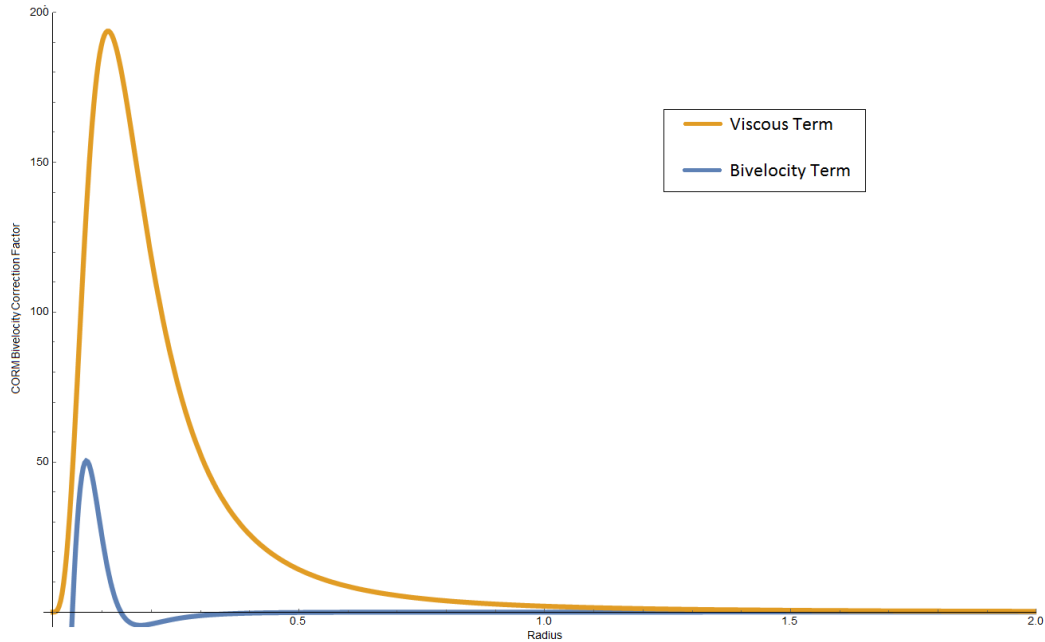


Figure 7: Conservation of Radial Momentum Bivelocity term compared to the Viscous term utilizing Mandella's curve-fits

It should be mentioned that the above viscous term excludes the transient parameter. This was done because each property was computed utilizing Mandella's curve fitting equations. Because Mandella evaluated at specific times (these values come from approximately $500\mu s$), a transient term could not be employed. Below in Figure 8 the same comparison can be seen with bivelocity and the viscous term for the energy equation.

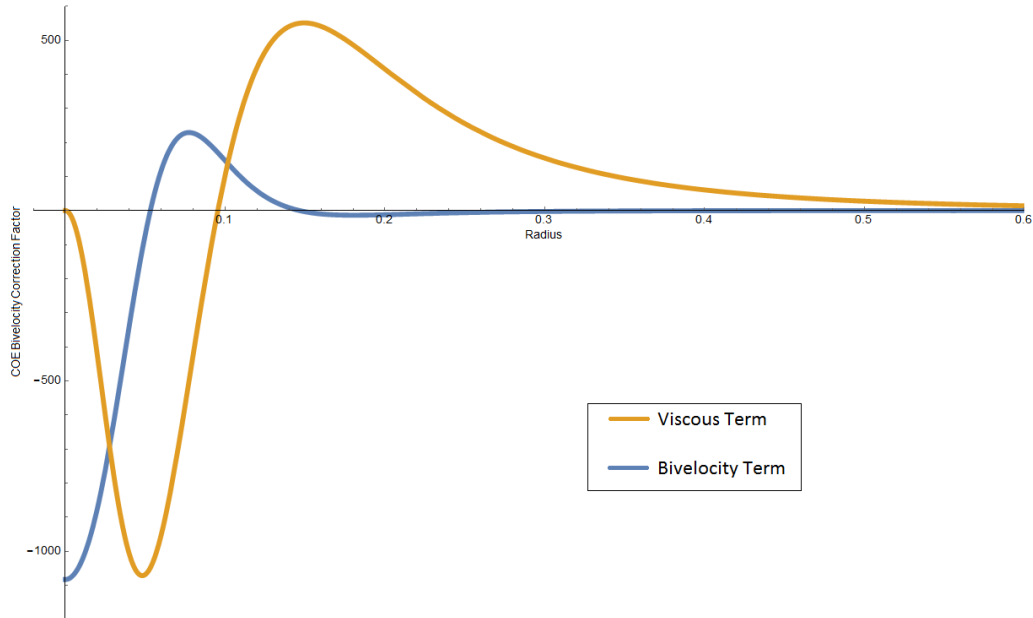


Figure 8: Conservation of Energy Bivelocity term compared to the Viscous term utilizing Mandella's curve-fits

As with radial momentum, the property values come from Mandella's curve-fit equations, and thus exclude transience. In this case however, the comparative power of bivelocity is about half of the viscous term, and affects the system much closer to the viscous layer.

Attention can be turned towards the effect of varied Knudsen numbers on the strength of the bivelocity term. Below those effects can be seen for radial momentum and energy.

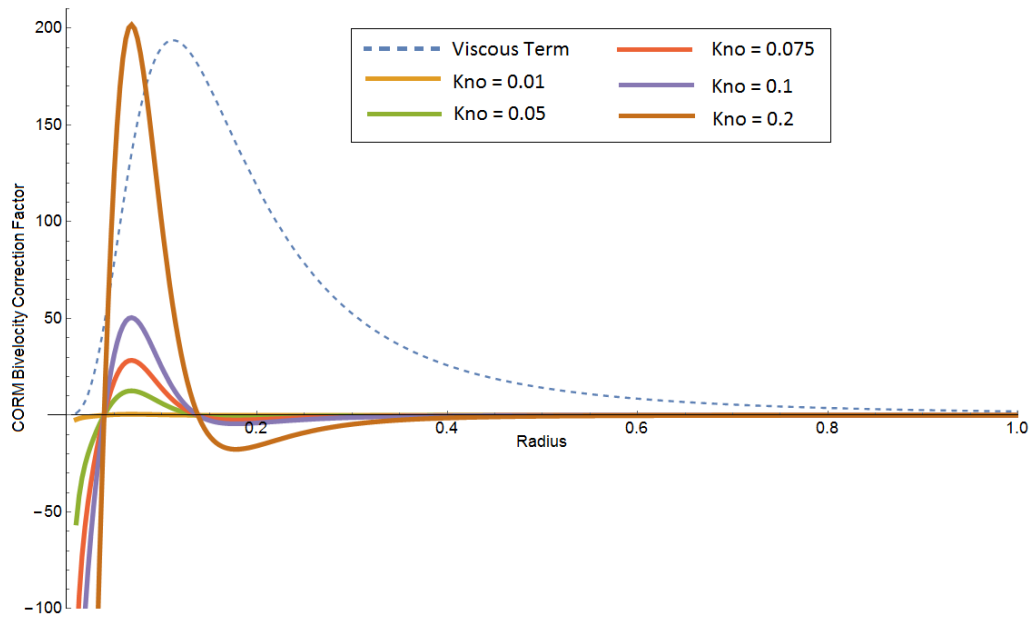


Figure 9: Effects of Knudsen number on radial momentum bivelocity

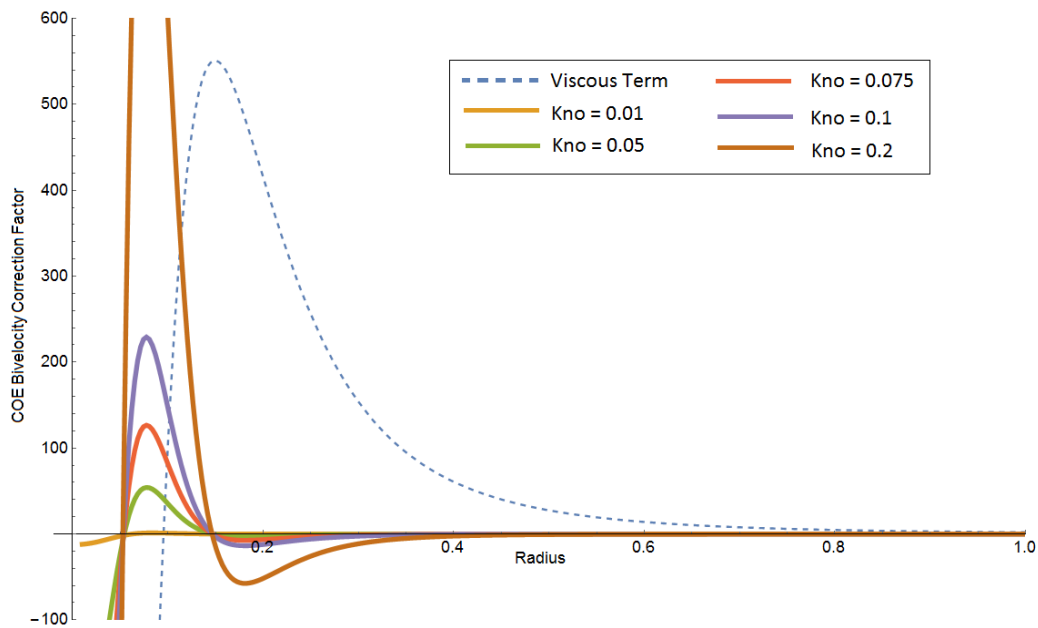


Figure 10: Effects of Knudsen number on energy bivelocity

Small perturbations in Knudsen number have a profound effect on the strength of the bivelocity term. For both radial momentum and energy, the effects of the bivelocity term when compared to the viscous term are negligible with $Kn_o = 0.01$.

At approximately $Kn_o = 0.2$ the bivelocity term for radial momentum matches the viscous effects, and surpasses them for energy.

Clearly, when a density gradient is present, this bivelocity term cannot be ignored. The following sections develop a method to generically solve for the compressible free vortex.

4 The Singularity

It is important to note that the lower bound of the radius for this paper was set to $\tilde{r} = 0.01$. This was done to simulate a solid cylinder at the center of the vortex (with a nondimensional radius of 0.01) to avoid the problem of a singularity. If we consider for a moment the problem of a three-dimensional vortex, as the fluid approaches the center, it is dumped into the third dimension - say, the z -direction - as opposed to the radial and angular directions. When this three-dimensional problem is solved in two dimensions, the singularity cannot be evaluated easily, and causes complications that propagate throughout the entire solution. The cylinder - with some predefined rotation rate - prevents the singularity from becoming a problem.

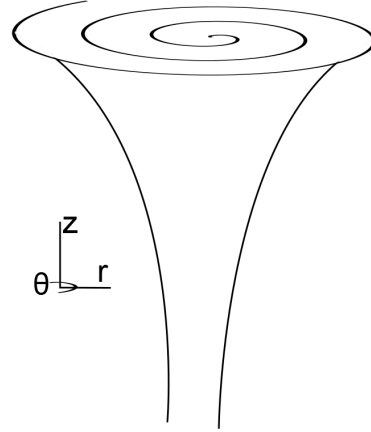


Figure 11: 3-D Singularity Dump

5 Steady-State and ODEs

In this section the steady case is briefly explored. The first step was to create a working set of equations to model incompressible isothermal flow - and then steady, compressible, non-isothermal - in order to set a convergence benchmark. Primary derivations begin with Radial and Angular Momentum equations which were derived in the fully compressible and time-dependent case (see Appendix A). The following sections show how the desired equations are formed, and how they are used in MatLab to simulate steady vortex flows.

5.1 Steady Equation Set

The bivelocity terms have been removed from these equations to bring the equation set back to the starting point similar to others' equations who have worked on this problem before. Utilizing the derivations in Appendix A, the steady-state equation set can be represented by:

$$\tilde{\rho} \tilde{u}_r \frac{\partial \tilde{u}_\theta}{\partial \tilde{r}} + \frac{\tilde{\rho} \tilde{u}_\theta \tilde{u}_r}{\tilde{r}} = \frac{Kn_o}{\tilde{r}} \frac{\partial}{\partial \tilde{r}} \left[\tilde{r} \tilde{\mu} \frac{\partial \tilde{u}_\theta}{\partial \tilde{r}} \right] - Kn_o \frac{\tilde{\mu} \tilde{u}_\theta}{\tilde{r}^2} \quad (48)$$

$$\begin{aligned} \tilde{\rho} \tilde{u}_r \frac{\partial \tilde{u}_r}{\partial \tilde{r}} - \frac{\tilde{\rho} \tilde{u}_\theta^2}{\tilde{r}} = & - \frac{d\tilde{p}}{d\tilde{r}} + Kn_o \frac{1}{\tilde{r}} \frac{\partial}{\partial \tilde{r}} \left[\tilde{r} \tilde{\mu} \frac{\partial \tilde{u}_r}{\partial \tilde{r}} \right] \\ & - Kn_o \frac{\tilde{\mu} \tilde{u}_r}{\tilde{r}^2} + \left(\frac{3C Kn_o^2}{2} \right) \frac{1}{\tilde{r}} \frac{\partial}{\partial \tilde{r}} \left[\tilde{r} \tilde{\mu} \frac{\partial}{\partial \tilde{r}} \left(\frac{\tilde{\mu}}{\tilde{\rho}^2} \frac{\partial \tilde{\rho}}{\partial \tilde{r}} \right) \right] \end{aligned} \quad (49)$$

$$\begin{aligned} \frac{1}{2} (\tilde{\rho} \tilde{u}_r) \left[3 \frac{d\tilde{T}}{d\tilde{r}} + \frac{d\tilde{u}_r^2}{d\tilde{r}} + \frac{d\tilde{u}_\theta^2}{d\tilde{r}} \right] = & \left(\frac{45}{20} Kn_o \right) \frac{1}{\tilde{r}} \frac{d}{d\tilde{r}} \left[\tilde{r} \tilde{T} \frac{d\tilde{T}}{d\tilde{r}} \right] \\ & - \frac{1}{\tilde{r}} \frac{d}{d\tilde{r}} \left[\tilde{r} \tilde{p} (\tilde{u}_r + \tilde{u}_\theta) \right] + (Kn_o) \frac{1}{\tilde{r}} \frac{d}{d\tilde{r}} \left[2 \tilde{r} \tilde{\mu} \tilde{u}_r \frac{d\tilde{u}_r}{d\tilde{r}} + \tilde{r}^2 \tilde{\mu} \tilde{u}_\theta \frac{d}{d\tilde{r}} \left(\frac{\tilde{u}_\theta}{\tilde{r}} \right) \right] \end{aligned} \quad (50)$$

$$\tilde{u}_r = \frac{Ma}{2\pi \tilde{r} \tilde{\rho}} \quad (51) \quad \tilde{p} = \tilde{\rho} \tilde{T} \quad (52)$$

The boundary conditions for this equation set play an incredibly vital role and as such, are chosen carefully. Before bivelocity is even added to the equation set, the

goal is to match Mandella's findings as closely as possible. Because Mandella fit curves to his data, this gives a launching point to determine the boundary conditions.

5.2 Steady Compressible Results

Ultimately, the steady compressible solution converges either poorly or not at all - depending on the method chosen. After further investigation, the problem lies not with the compressibility, but rather the steady-state assumption. Having used the viscous layer as the benchmark for convergence, it can be stated with complete certainty that it is in fact the time-dependency that allows the solution to form the layer. A steady-state solution containing the viscous layer would in reality require an infinite amount of input energy. This is, however, for the two dimensional case. Figure 14 below illustrates the issue with these assumptions.

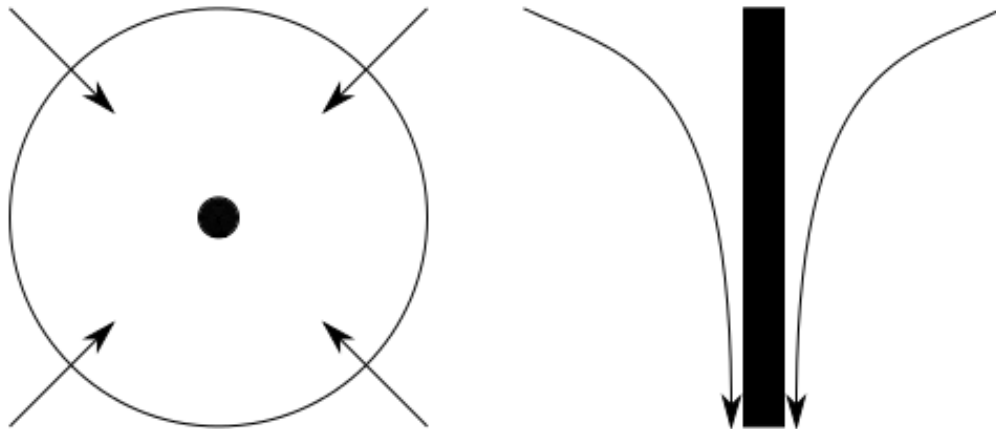


Figure 12: Two-Dimensional (left) vs. Three-Dimensional (right) Radial Flow

The problem arises because radial velocity is drawn inwards, but ultimately has nowhere to go (unless a third dimension, or time dependency is introduced). The past few sections have demonstrated with complete certainty that the steady-state solution for a two-dimensional, compressible, axisymmetric vortex containing both the forced vortex core and the free vortex far-field does not exist.

Final convergence for the steady solution can be seen below. While properties like temperature, pressure, and density displayed expected characteristics, the velocities match the expected inviscid solution where no viscous layer is formed.

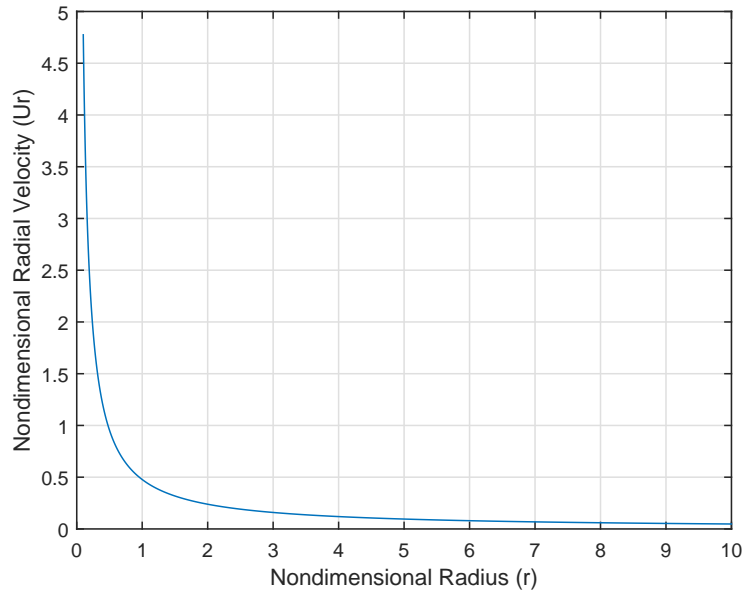


Figure 13: Steady radial velocity displaying inviscid characteristics

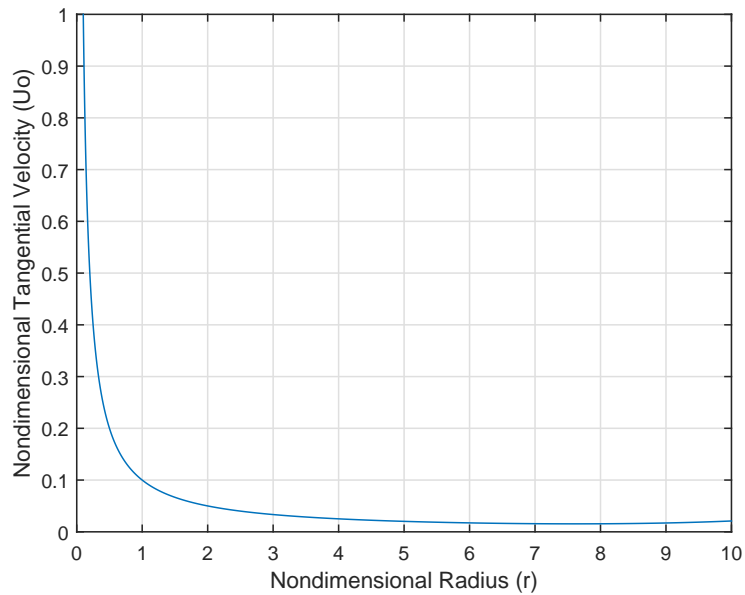


Figure 14: Steady tangential velocity displaying inviscid characteristics

With all options exhausted for this time-independent scenario, attention must be

turned towards the transient solution. Only the transient solution derivative terms can account for the stored energy, as the viscous layer develops. This is an important conclusion, considering that Walls - a bivelocity predecessor - successfully solved the steady solution for micro-channel Couette flow.

6 Transience and PDEs

With the importance of bivelocity already shown, the challenge is in the convergence of the equation set with bivelocity terms added. The previous section has shown the importance of transience, but adding time dependency moves this problem from a set of ordinary differential equations (ODEs) - whose only dependency was radius - to partial differential equations (PDEs) - with both radius and time.

The alterations to the equations (seen in Appendix A) required minimal effort, but great care must be taken to maintain nondimensionality. Previously, with the ODE scheme, two of the fundamental equations - continuity and ideal gas - could be written explicitly. With the new time dependency, a new density term appears in the continuity equation which renders it a differential equation. The remaining ideal gas equation, however, can be substituted inside the remaining conservation of momentum and conservation of energy. The fundamental equations for this section are listed below:

Continuity:

$$100 \frac{\partial \tilde{\rho}}{\partial \tilde{t}} + \frac{1}{Kn_o} \left[\tilde{u}_r \frac{\partial \tilde{\rho}}{\partial \tilde{r}} + \tilde{\rho} \frac{\partial \tilde{u}_r}{\partial \tilde{r}} + \frac{\tilde{\rho}}{\tilde{r}} \tilde{u}_r \right] = 0 \quad (53)$$

Conservation of Angular Momentum:

$$100 Kn_o \tilde{\rho} \frac{\partial \tilde{u}_\theta}{\partial \tilde{t}} + \tilde{\rho} \tilde{u}_r \frac{\partial \tilde{u}_\theta}{\partial \tilde{r}} + \frac{\tilde{\rho} \tilde{u}_\theta \tilde{u}_r}{\tilde{r}} = \frac{Kn_o}{\tilde{r}} \frac{\partial}{\partial \tilde{r}} \left[\tilde{r} \tilde{\mu} \frac{\partial \tilde{u}_\theta}{\partial \tilde{r}} \right] - Kn_o \frac{\tilde{\mu} \tilde{u}_\theta}{\tilde{r}^2} \quad (54)$$

Conservation of Radial Momentum:

$$100 Kn_o \tilde{\rho} \frac{\partial \tilde{u}_r}{\partial \tilde{t}} + \tilde{\rho} \tilde{u}_r \frac{\partial \tilde{u}_r}{\partial \tilde{r}} - \frac{\tilde{\rho} \tilde{u}_\theta^2}{\tilde{r}} = -\frac{d\tilde{p}}{d\tilde{r}} + Kn_o \frac{1}{\tilde{r}} \frac{\partial}{\partial \tilde{r}} \left[\tilde{r} \tilde{\mu} \frac{\partial \tilde{u}_r}{\partial \tilde{r}} \right] - Kn_o \frac{\tilde{\mu} \tilde{u}_r}{\tilde{r}^2} + \left(\frac{3C Kn_o^2}{2} \right) \frac{1}{\tilde{r}} \frac{\partial}{\partial \tilde{r}} \left[\tilde{r} \tilde{\mu} \frac{\partial}{\partial \tilde{r}} \left(\frac{\tilde{\mu}}{\tilde{\rho}^2} \frac{\partial \tilde{\rho}}{\partial \tilde{r}} \right) \right] \quad (55)$$

Conservation of Energy:

$$\begin{aligned}
100 K n_o \tilde{\rho} \frac{\partial \tilde{T}}{\partial \tilde{t}} + \frac{1}{2} (\tilde{\rho} \tilde{u}_r) \left[3 \frac{d\tilde{T}}{d\tilde{r}} + \frac{d\tilde{u}_r^2}{d\tilde{r}} + \frac{d\tilde{u}_\theta^2}{d\tilde{r}} \right] &= \left(\frac{45}{20} K n_o \right) \frac{1}{\tilde{r}} \frac{d}{d\tilde{r}} \left[\tilde{r} \tilde{T} \frac{d\tilde{T}}{d\tilde{r}} \right] \\
- \frac{1}{\tilde{r}} \frac{d}{d\tilde{r}} \left[\tilde{r} \tilde{p} (\tilde{u}_r + \tilde{u}_\theta) \right] + (K n_o) \frac{1}{\tilde{r}} \frac{d}{d\tilde{r}} \left[2 \tilde{r} \tilde{\mu} \tilde{u}_r \frac{d\tilde{u}_r}{d\tilde{r}} + \tilde{r}^2 \tilde{\mu} \tilde{u}_\theta \frac{d}{d\tilde{r}} \left(\frac{\tilde{u}_\theta}{\tilde{r}} \right) \right] & \quad (56) \\
- \left(\frac{3C}{2} K n_o \right) \frac{1}{\tilde{r}} \frac{d}{d\tilde{r}} \left[\frac{\tilde{r} \tilde{\mu} \tilde{p}}{\tilde{\rho}^2} \frac{d\tilde{\rho}}{d\tilde{r}} \right] + (3C K n_o^2) \frac{1}{\tilde{r}} \frac{d}{d\tilde{r}} \left[\frac{\tilde{r} \tilde{\mu}^2}{\tilde{\rho}^2} \frac{d\tilde{\rho}}{d\tilde{r}} \frac{d\tilde{u}_r}{d\tilde{r}} \right] &
\end{aligned}$$

And Ideal Gas:

$$\tilde{p} = \tilde{\rho} \tilde{T} \quad (57)$$

As mentioned above, the ideal gas term can be substituted into the remaining equations, leaving a system of four, which will aid Mathematica's computational time.

6.1 Initial and Boundary Conditions

Determining the initial and boundary conditions is arguably one of the most important processes in solving this system of equations. Inadequate boundary and initial conditions can cause problems ranging from false solutions to failed convergence. Since the desire is to determine the properties at a final time for all radii, the boundary conditions should focus on the behavior of the system at low and high radii at all times.

The properties at far-field radii are straight forward, since all properties have been nondimensionalized. The velocities will diminish to zero and temperature, density, and pressure will return to ambient conditions with a value of one. Additionally, all these derivatives are set to zero, as there would be no change from point-to-point at high radii values. The values for the end boundary condition can be seen below in Table 1.

Property	Value	$\frac{\partial}{\partial r}(\text{Value})$
$\tilde{\rho}$	1	0
\tilde{T}	1	0
\tilde{u}_θ	0	0
\tilde{u}_r	0	0

Table 1: Property values at $\tilde{r} = 10$

Determining low radii values requires a little finesse. Since singularity issues are encountered at a zero radius value, this system can only be accurately solved down to a magnitude of $\tilde{r} = 0.01$. This allows for the development of the viscous layer, without extremely low radii values distorting the properties. In order to choose values at $\tilde{r} = 0.01$, Mandella's Cauchy curve fitting can be utilized.

Mandella's nondimensionalized density, pressure, and temperature are drawn from equations 42, 43, and 44 respectively. Additionally, Mandella's velocity is represented by:

$$u_\theta = \frac{\left(\frac{r}{\Delta r_p}\right)}{1 + \left(\frac{r}{\Delta r_p}\right)^2} \left[\frac{2 \Delta P}{\rho_\infty - \frac{\Delta \rho}{1 + \left(\frac{r}{\Delta r_p}\right)^2}} \right]^{\frac{1}{2}} \quad (58)$$

While Mandella does not explicitly give an equation for radial velocity, the curve fit contains the same structure, only symmetric about the x-axis. Both tangential and radial velocity can be nondimensionalized at $r = 1$ where the boundary of the vortex exists. Density, pressure, and temperature were nondimensionalized at $r = 10$ since far-field values return to one, whereas velocities fade to zero. The final low radii values of all properties can be seen below in Table 2.

Property	Value
$\tilde{\rho}$	0.399
\tilde{T}	0.750
\tilde{u}_θ	1.1529
\tilde{u}_r	-1.1529

Table 2: Property values at $\tilde{r} = 0.01$

With the boundary conditions set, attention is turned towards the initial conditions. The low radii boundary condition was set for a specific radius over all times, whereas the initial conditions will be set for all radii at a specific time, in this case $\tilde{t} = 0$, since $\tilde{t} = \infty$ is the desired outcome.

The system begins at rest, with velocities equal to zero, and temperature and density equal to one (ambient conditions). At $\tilde{t} = 0$ the solid inner core with a radius of 0.01 begins to rotate (this cylinder does two things - provides the driving force behind our system, and eliminates the singularity). Seen below in Figure 15 are the tangential velocity (blue) and density (yellow) initial conditions, with forcing at $\tilde{r} = 0.01$

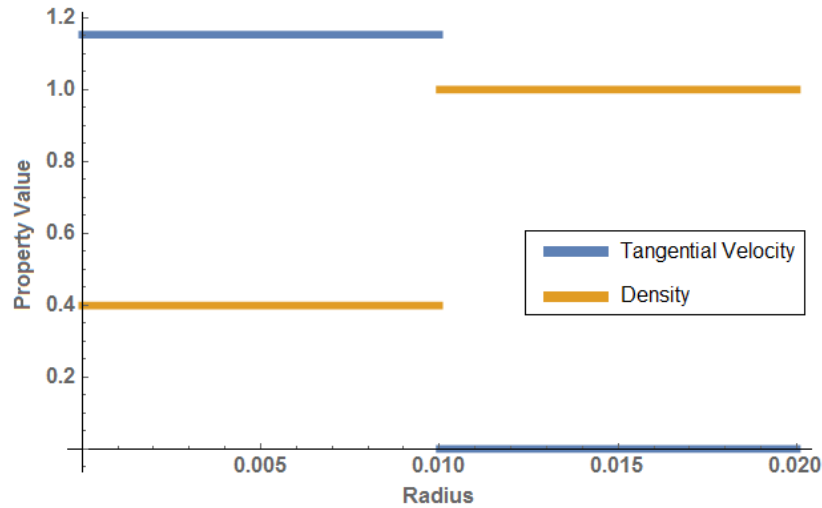


Figure 15: Tangential velocity and density initial conditions

The initial conditions are set up in this way for continuity's sake. The initial conditions must match the boundary conditions at all overlapping edges. Obviously, these piecewise functions create a separate issue. Mathematica cannot use the piecewise function, and instead utilizes a curve-fit, seen below in Figure 16.

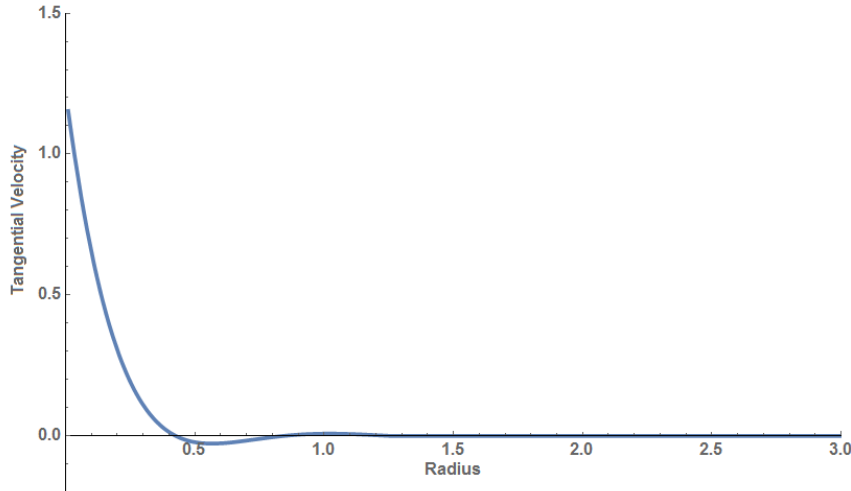


Figure 16: Curve-fit of tangential velocity initial condition ($\tilde{t} = 0$ and $Kn_o = 0.1$)

When allowed to run until $\tilde{t} = 50$, at which time the system stabilizes, we find a velocity profile seen below in Figure 17.

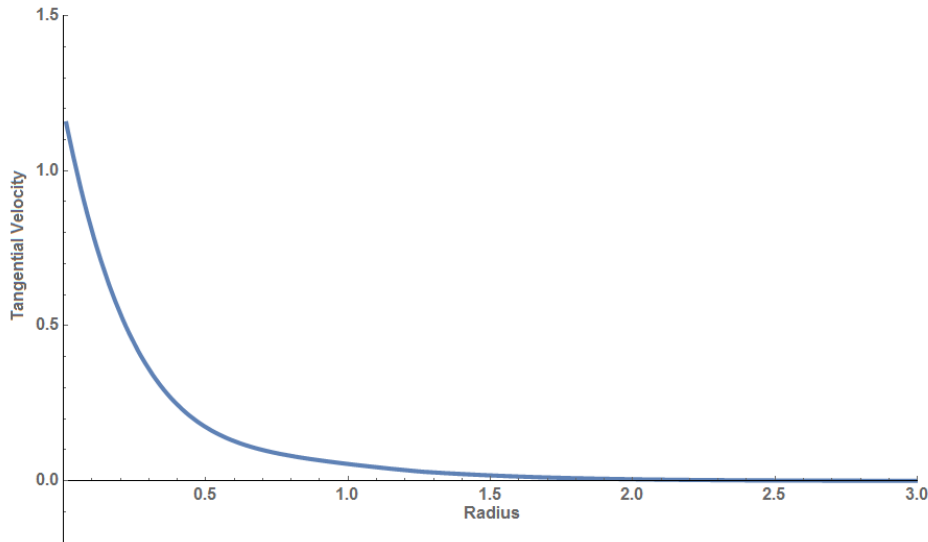


Figure 17: Final tangential velocity at $\tilde{t} = 50$ and $Kn_o = 0.1$

This is an unexpected result, as there is no velocity peak in the viscous layer. Additionally the radial velocity produces no such peak either. However, the remaining properties: temperature, pressure, and density all perform as expected, and are compared to Mandella's curve-fit plots.

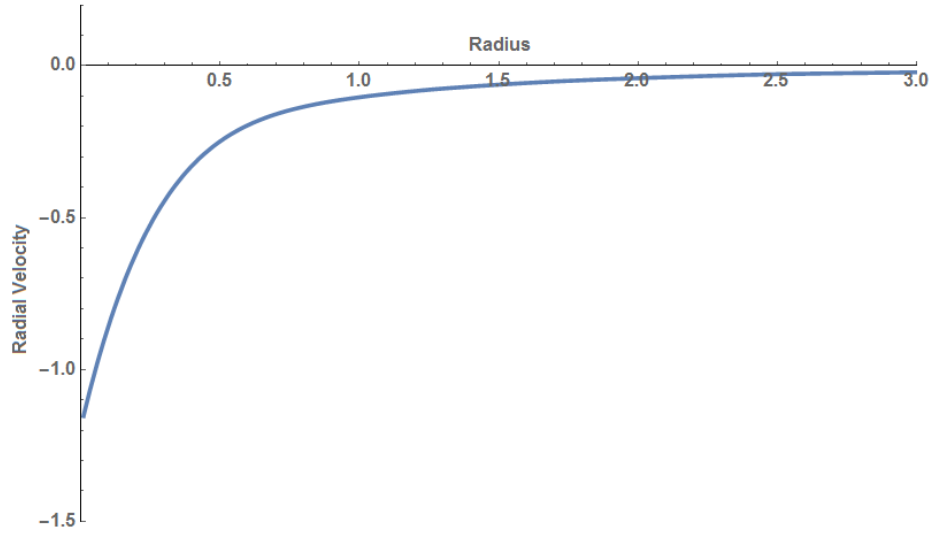


Figure 18: Final radial velocity at $\tilde{t} = 50$ and $Kn_o = 0.1$

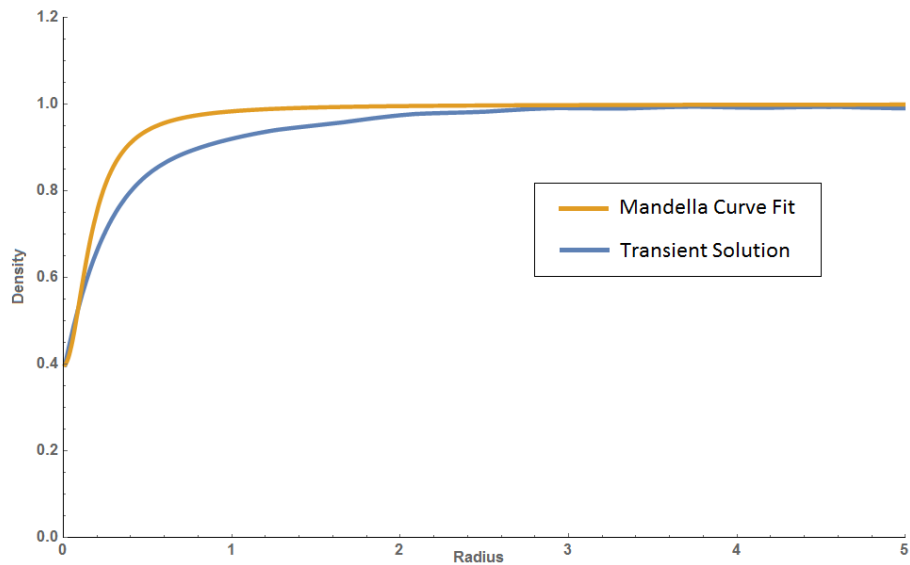


Figure 19: Final density at $\tilde{t} = 50$ and $Kn_o = 0.1$ vs. Mandella at $t = 496\mu s$

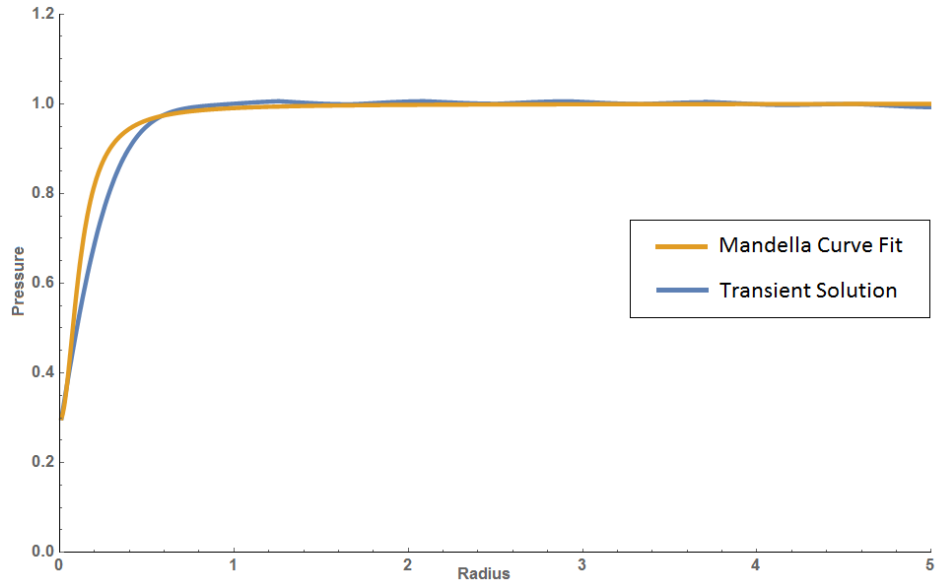


Figure 20: Final pressure at $\tilde{t} = 50$ and $Kn_o = 0.1$ vs. Mandella at $t = 496\mu s$

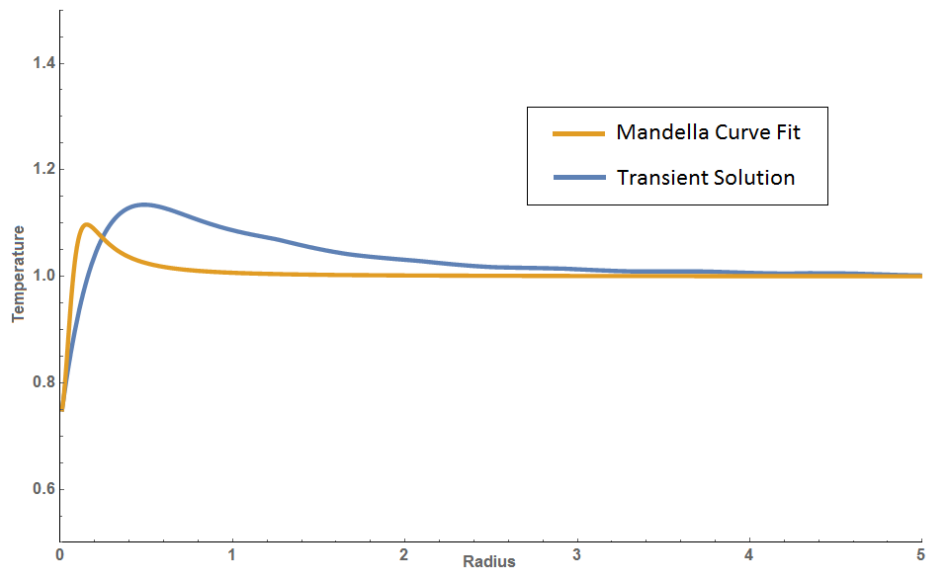


Figure 21: Final Temperature at $\tilde{t} = 50$ and $Kn_o = 0.1$ vs. Mandella at $t = 496\mu s$

It's important to note the time-frame in which these solutions are compared to Mandella's. The dimensionless time of $\tilde{t} = 50$ corresponds to approximately $100\mu s$ or about $1/5$ of the time at which Mandella took his readings. After $\tilde{t} = 50$ the solution begins to break down, hence the shorter time frame. First impressions lead to the belief that a shorter time frame for convergence might produce a result more similar

to Mandella's. The viscous layer appears to be more developed than Mandella's, and that the shorter time frame may bring the layer closer to the core. Upon viewing the convergence series (Figures 22 and 23 below) it can be seen that the layer develops vertically.

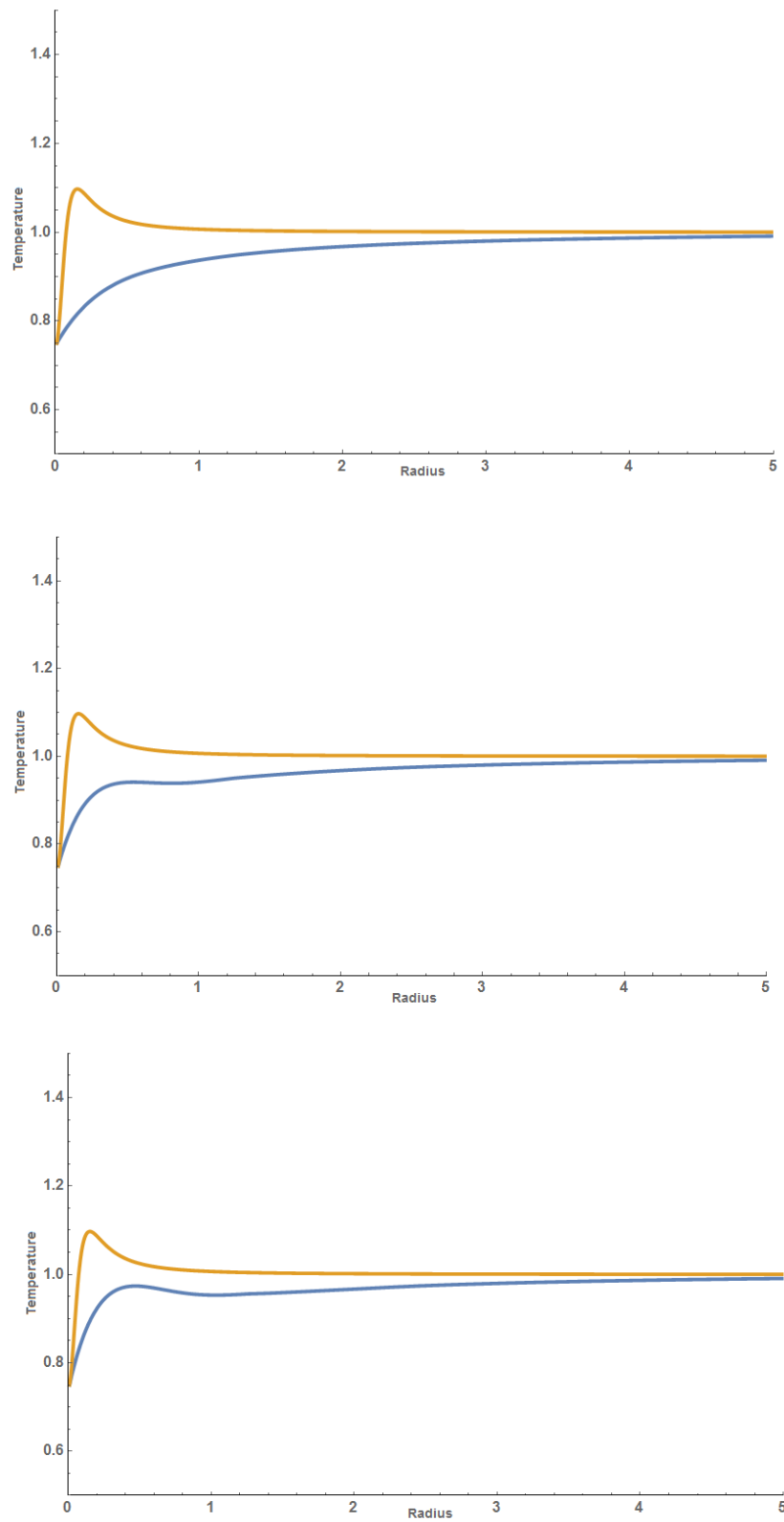


Figure 22: States of convergence of temperature equation (at $\tilde{t} = 0$, $\tilde{t} = 2$, and $\tilde{t} = 4$ respectively) compared to Mandella's $t = 496\mu s$ findings

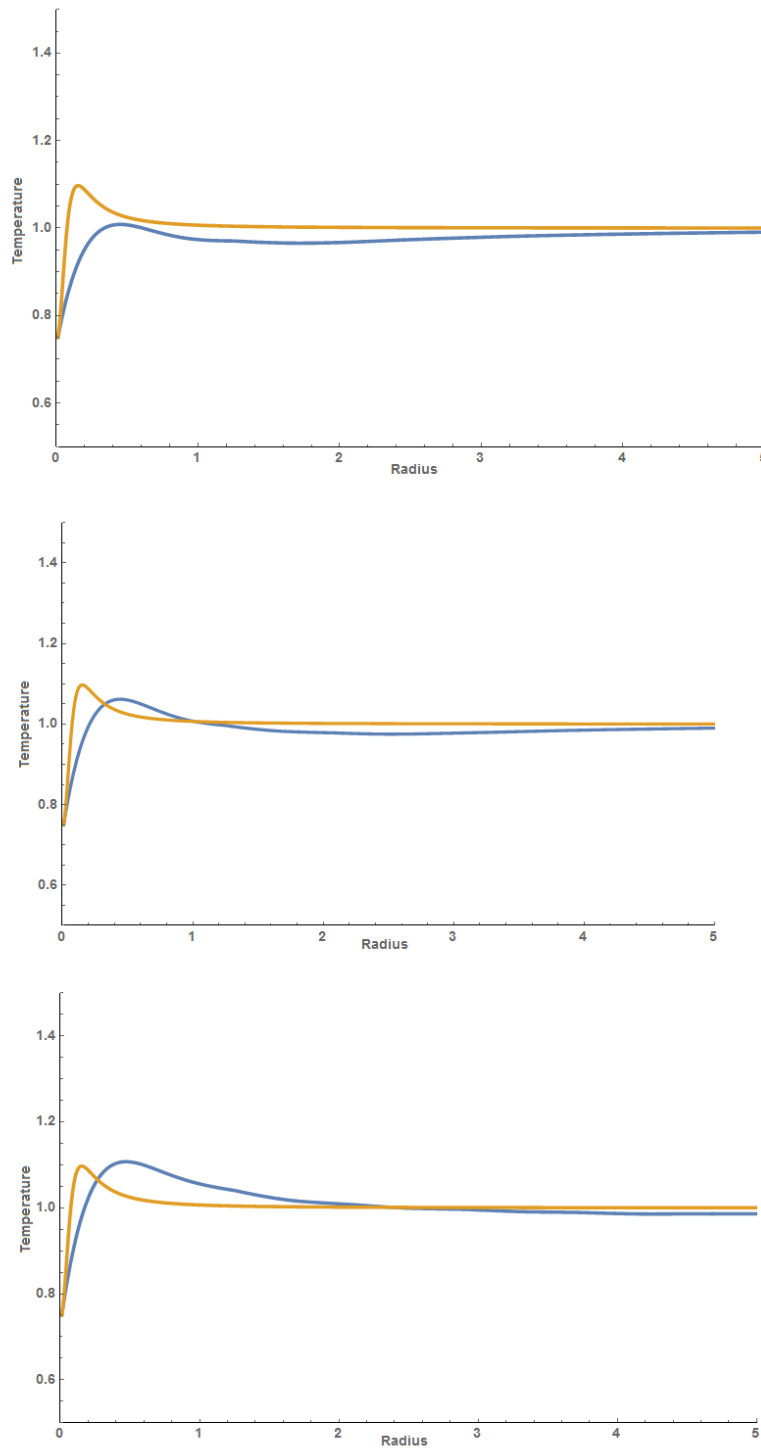


Figure 23: States of convergence of temperature equation (at $\tilde{t} = 7$, $\tilde{t} = 13$, and $\tilde{t} = 27$ respectively) compared to Mandella's $t = 496\mu s$ findings

In addition to how the solution develops across a single Knudsen number, it's important to observe the effects the Knudsen number has on final convergence.

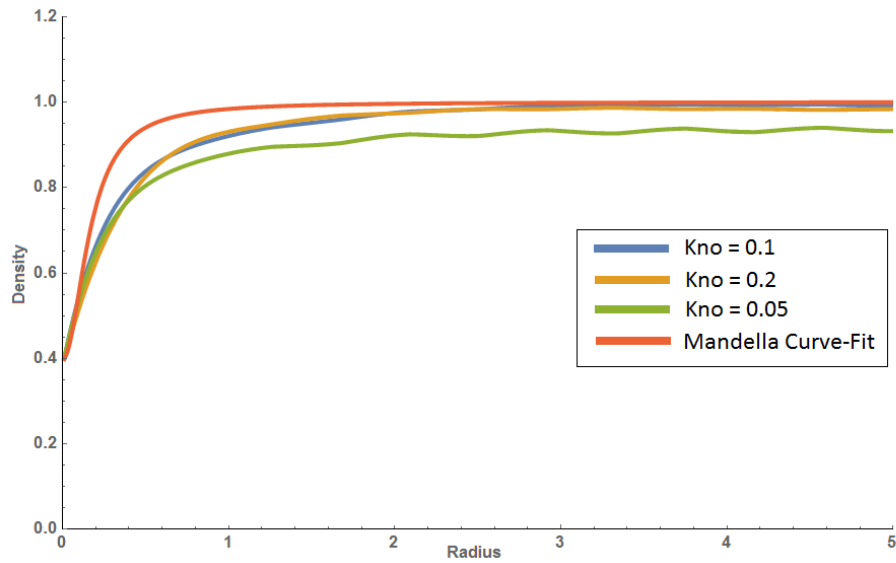


Figure 24: Final density at $\tilde{t} = 50$ and various Knudsen numbers vs. Mandella at $t = 496\mu s$

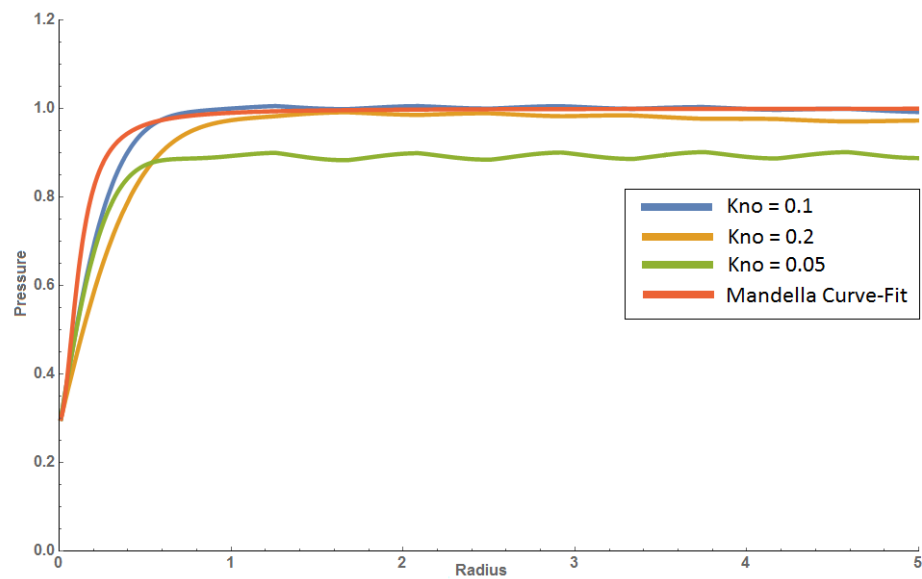


Figure 25: Final pressure at $\tilde{t} = 50$ and various Knudsen numbers vs. Mandella at $t = 496\mu s$

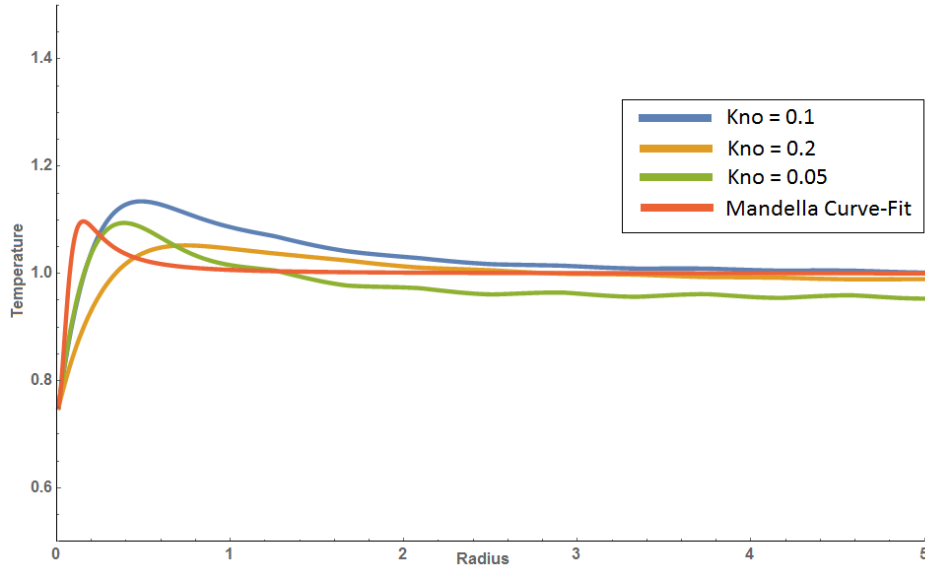


Figure 26: Final Temperature at $\tilde{t} = 50$ and various Knudsen numbers vs. Mandella at $t = 496\mu s$

With only the velocities behaving unexpectedly, revisiting the initial conditions becomes the first option. While the piecewise function may be the most correct, its discontinuities may pose a significant problem. Instead, the initial conditions can be modeled as $\pm 1/(ns \cdot r + A) + B$, where ns adjusts the pitch or steepness of the curves, and the constants A and B allow the curve to move about the axes to meet the desired boundary conditions. While the right side boundary conditions extend to the maximum radius of 10, much of the graph below in Figure 27 has been removed to better illustrate the low radial curvature.

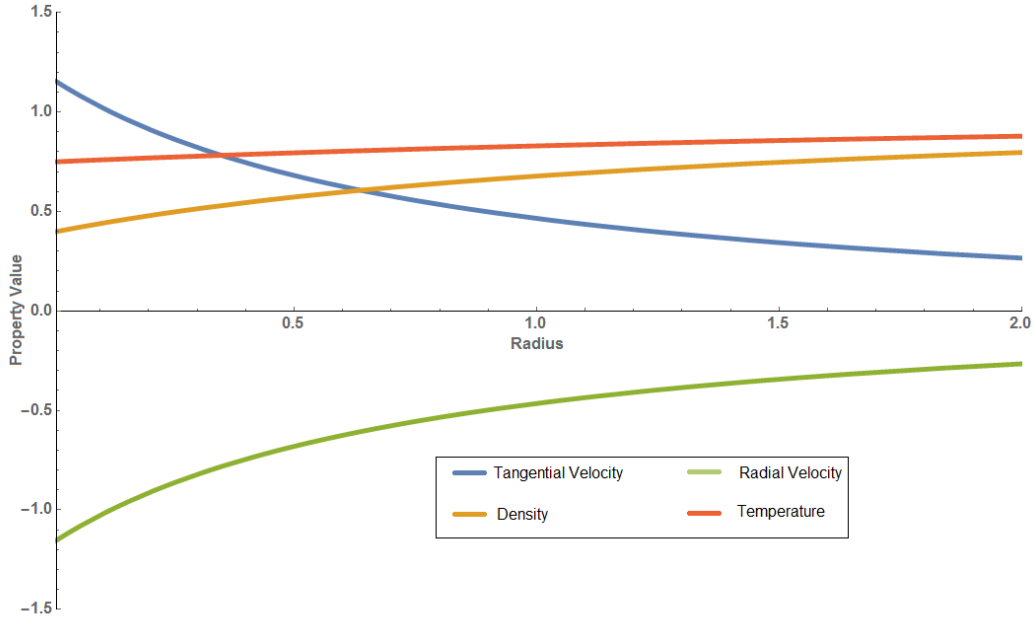


Figure 27: Property initial conditions governed by $\pm 1/(ns \cdot r + A) + B$ with $ns = 1$

These curves are far more gradual, and the hope is that they produce better graphs, as Mathematica does not need to curve fit the piecewise which can cause negative values when none should be present. As expected, this greatly improves both the velocity graphs, seen in Figures 28 and 29 below

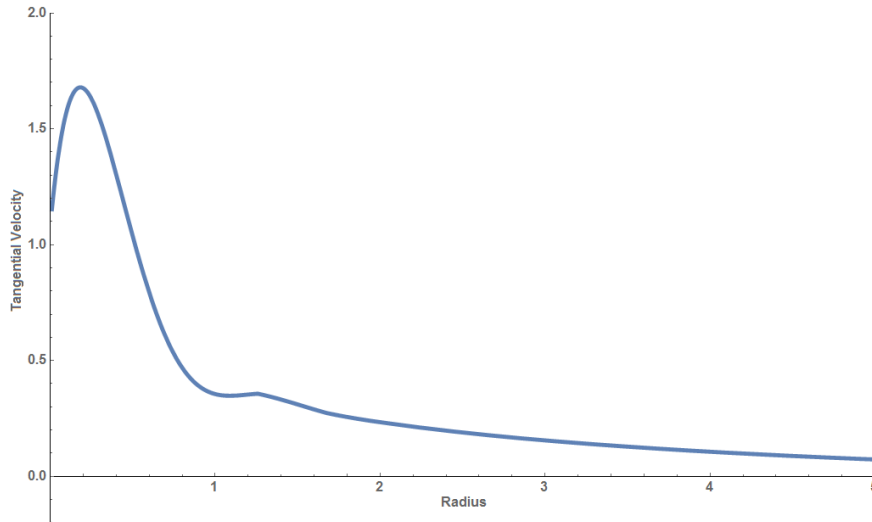


Figure 28: Final tangential velocity at $\tilde{t} = 72$ and $Kn_o = 0.1$

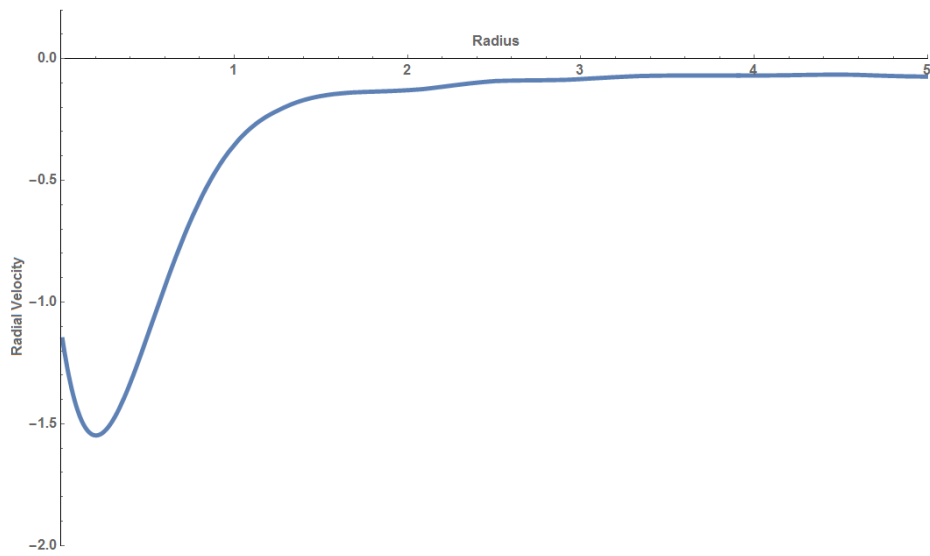


Figure 29: Final radial velocity at $\tilde{t} = 72$ and $Kn_o = 0.1$

While these plots meet expectations, the remaining temperature, pressure, and density remain baffling

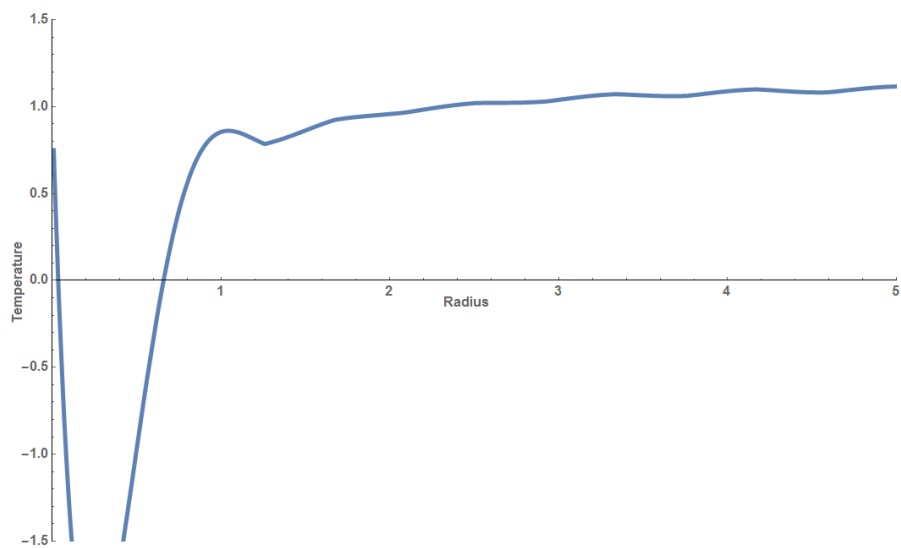
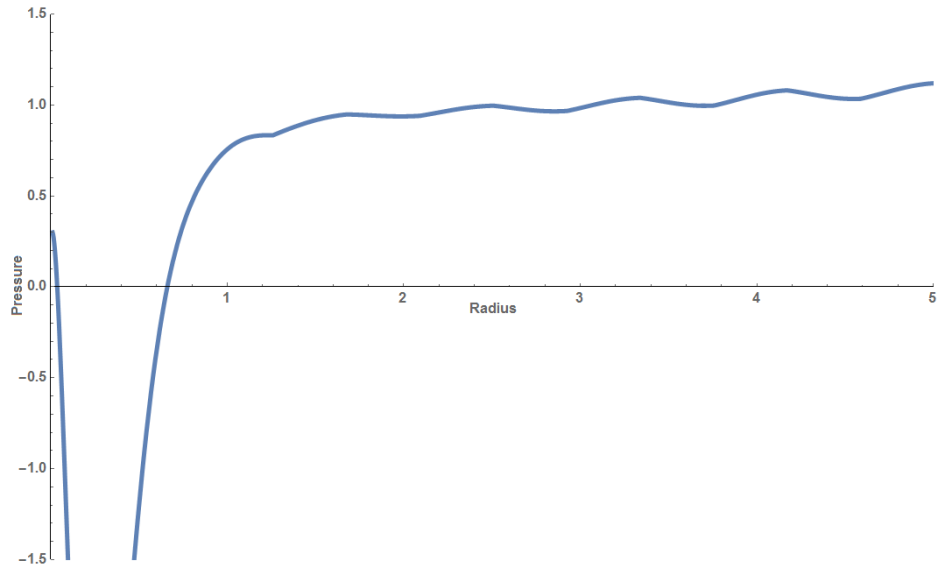
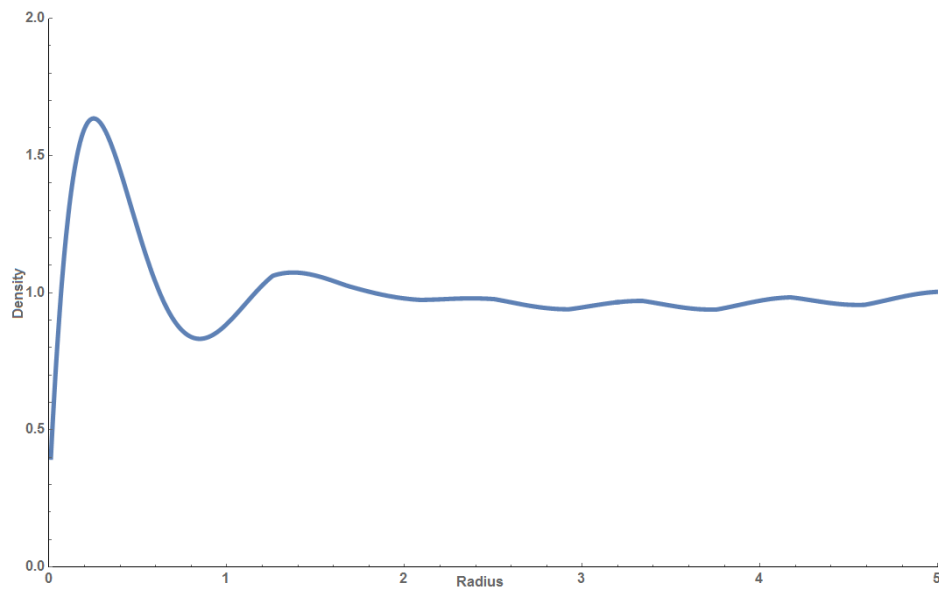


Figure 30: Final temperature at $\tilde{t} = 72$ and $Kn_o = 0.1$

Figure 31: Final pressure at $\tilde{t} = 72$ and $Kn_o = 0.1$ Figure 32: Final density at $\tilde{t} = 72$ and $Kn_o = 0.1$

Again, the effects of the Knudsen number can be observed. It immediately becomes apparent that the problem is seriously ill posed. The velocities begin to fail at increasingly earlier times, making the comparison of their convergence evermore difficult.

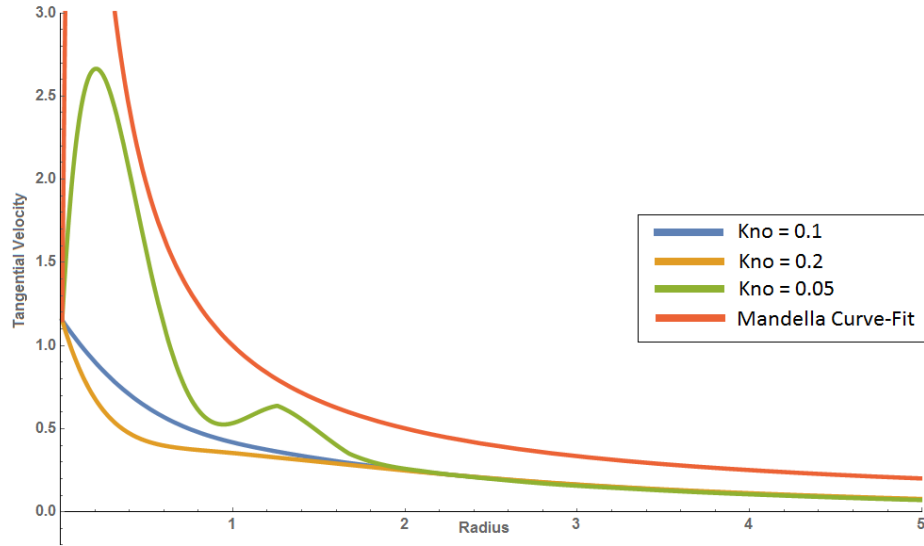


Figure 33: Final tangential velocity at $\tilde{t} = 32$ vs. Mandella at $t = 496\mu s$

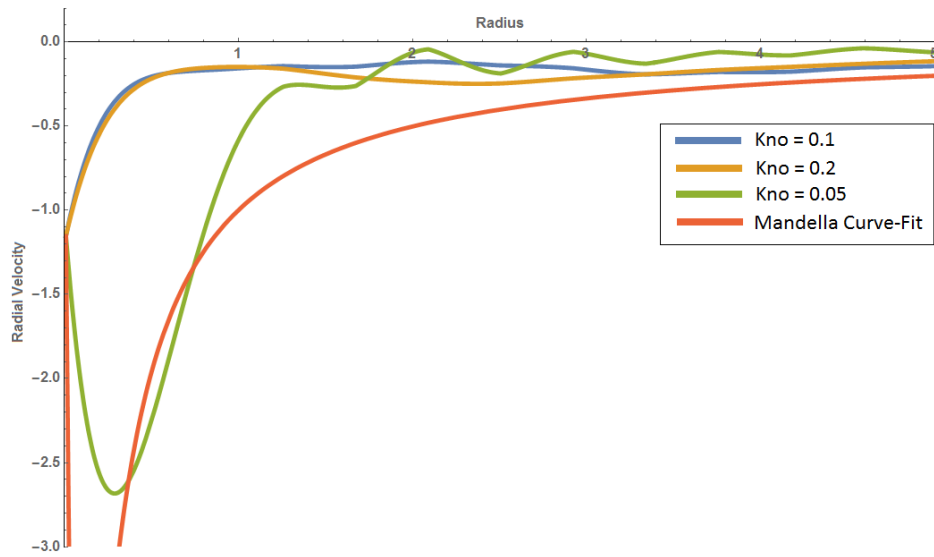


Figure 34: Final radial velocity at $\tilde{t} = 20$ vs. Mandella at $t = 496\mu s$

Unable to approximate Mandella's time scale, the convergence of these equations cannot be trusted. Note that these timescales are $\tilde{t} = 32$ and $\tilde{t} = 20$ respectively. Far lower than the original $Kn_o = 0.1$ and far lower still of Mandella's $t = 496\mu s$.

The next conclusion is the total solution might reside somewhere between in the region of $1 > ns > \infty$, where 1 gives desirable velocities and ∞ (effectively the piecewise function) returns the target temperature curve. It becomes apparent quite

quickly that $ns \rightarrow \infty$ is severely disproportionate. The same effects the piecewise function returns can be achieved to a degree of similarity with values of ns as low as 10. As $ns \rightarrow 1$, all properties remain well behaved, though temperature's viscous layer peak begins to diminish. In fact, the transition appears to occur from $1.0 < ns < 1.1$. Instabilities of this magnitude may in fact be attributed to the derivatives of the initial conditions. Even if this region could be found, the Knudsen number effects are too erratic to predict.

7 Discussion

This thesis has presented numerous competing theories on predicting compressible vortex structures. The Navier-Stokes and Burnett equations have been shown to be inadequate, and while bivelocity has shown promise in recent years, a general solution could not be solved. Multiple initial and boundary conditions were presented, but only a partial solution could be obtained. Discounting pressure - since pressure was shown to be a product of temperature and density - the two velocities matched the expected behavior when given a continuous and gradual boundary condition (at $\tilde{t} = 0$) seen above in Figure 27. However, given a piecewise condition (Figure 15) - or even a continuous but steep boundary conditions - velocities act as if the system were a completely free vortex.

It can also be stated with certainty that the traditional NSF methods for describing vortex motion - or non-continuum flows in general - are inadequate [19, 20, 21] and the proofs provided by this paper on the comparative power of bivelocity to the remaining NSF terms reinforce this idea for the specific vortex case.

7.1 Knudsen Number

This paper was able to demonstrate the importance of the Knudsen number as applied to bivelocity. As the Knudsen number increases, so does the power of the bivelocity term. At approximately $Kn_o = 0.2$ the bivelocity term is on the same order of magnitude as the viscous effects.

7.2 Convergence

The greatest variation to the current system stems from the initial and boundary conditions alone. There is clearly a fine line for convergence, and it may be appropriate to explore additional avenues to ease Mathematica's computations. Several oddities exist - and most likely stem from - the initial and boundary conditions which affect the convergence. Notably, how time dependence affects the development of the

temperature's viscous layer. It was expected that the layer would begin smaller and closer to the core, and as the layer develops, it would spread outward. Interestingly, as convergence data shows, this solution shows the layer developing vertically and not propagating from the core outwards.

7.3 Experimental Validation

Mandella performed his interferogram experiments nearly 30 years ago. While Mandella's data is often cited with respect to compressible vortices, his data is in actuality somewhat chaotic. This paper could not accurately represent Mandella's findings, however in the interest of finding a solution to this problem, increased accuracy could enhance the finding of a solution. Additionally, Mandella presents most data at the $500\mu s$ range, though it would be more beneficial to increase the resolution since this problem can only be solved in transience.

8 Concluding Remarks

Previously, bivelocity has demonstrated its adaptability to various various corners of fluid dynamics. While it maintains advantages over the traditional methods - such as Navier-Stokes - it has yet to be proven for numerous instances of fluid flow, including compressible vortices. This paper successfully derives the appropriate compressible vortex equation sets, and is able to prove the relative importance of bivelocity, but is unable to match past data or expected behavioral patterns completely. The proportionality between the Knudsen number and the power of the bivelocity term shows promising results. Depending on the initial and boundary conditions, the proper viscous layer could be demonstrated to exist - and match Mandella's findings - with theoretical velocity profiles. However, with the appropriate velocity profiles comes a discrepancy in temperature and density. Altering the initial and boundary conditions leads either to the desired velocities, or temperature and density, but not both. Further inspection into initial and boundary condition effects should be examined, and is most likely the best course of action to gain the desired convergence. Because

of the sensitivity to the initial and boundary conditions, this problem is not well posed.

Glaringly absent from this and others' work is an analysis of a third dimension. It is entirely possible that the key to solving this problem lies in the z-direction. Since radial flow is driven towards the core, it could be said that the transient compressibility is not enough to absorb the totality of this term. Since it is known that the fluid moves along the core in the third dimension after leaving the two-dimensional surface, this could potentially alter the convergence of this problem.

9 Appendix A

9.1 Mass Equation

Derivation of the mass equation:

Begin with bivelocity equation governing transport of mass

$$\frac{\partial \rho}{\partial t} + \nabla \cdot (\rho \mathbf{v}) = 0 \quad (59)$$

The velocity vector can be separated into its two fundamental components

$$\mathbf{v} = u_r i_r + u_\theta i_\theta \quad (60)$$

We know if we carry density through, the divergence vector is defined as

$$\nabla \cdot (\rho \mathbf{v}) = \frac{1}{r} \frac{\partial}{\partial r} (\rho r u_r) + \frac{1}{r} \frac{\partial}{\partial \theta} (\rho u_\theta) \quad (61)$$

However, due to the axisymmetric nature of the vortex,

$$\frac{\partial}{\partial \theta} = 0 \quad (62)$$

Such that

$$\nabla \cdot (\rho \mathbf{v}) = \frac{1}{r} \frac{\partial}{\partial r} (\rho r u_r) \quad (63)$$

Since we know that

$$\frac{\partial \rho}{\partial t} + \frac{1}{r} \frac{\partial}{\partial r} (\rho r u_r) = 0 \quad (64)$$

It holds true that

$$\frac{\partial \rho}{\partial t} + u_r \frac{\partial \rho}{\partial r} + \rho \frac{\partial u_r}{\partial r} + \frac{\rho}{r} u_r = 0 \quad (65)$$

9.2 Momentum Equation

Derivation of the momentum equation:

Begin with bivelocity equation governing transport of momentum

$$\rho \frac{D\mathbf{v}_m}{Dt} + \rho \mathbf{v}_m \cdot (\nabla \cdot \mathbf{v}_m) = -\nabla \cdot \mathbf{P} \quad (66)$$

P is a tensor, and can be rewritten as

$$\mathbf{P} = \mathbf{I}p - \mathbf{T} \quad (67)$$

When substituted into Equation 66 we find

$$\rho \frac{D\mathbf{v}_m}{Dt} + \rho \mathbf{v}_m \cdot (\nabla \cdot \mathbf{v}_m) = -\nabla p + \nabla \cdot \mathbf{T} \quad (68)$$

The momentum equation must be broken into two components. The radial and angular momentum equations.

$$\rho \frac{\partial u_r}{\partial t} + \rho (\mathbf{v}_m \cdot \nabla) u_r - \rho \frac{u_\theta^2}{r} = -\frac{dp}{dr} + \nabla \cdot \mathbf{T}|_{rr} \quad (69)$$

$$\rho \frac{\partial u_\theta}{\partial t} + \rho (\mathbf{v}_m \cdot \nabla) u_\theta - \rho \frac{u_r u_\theta}{r} = \nabla \cdot \mathbf{T}|_{r\theta} \quad (70)$$

Note they are almost identical, but the angular momentum equation is missing the pressure term. This is because there is no pressure gradient in the angular direction (axisymmetric).

The viscous stress tensor is defined as

$$\mathbf{T} = 2\mu \overline{\nabla \mathbf{v}_v} \quad (71)$$

Where the volume velocity is defined as

$$\mathbf{v}_v = \mathbf{v}_m + J_v \quad (72)$$

We can expand Equation 71 into two parts

$$\mathbf{T} = 2\mu\overline{\nabla\mathbf{v}_m} + 2\mu\overline{\nabla J_v} \quad (73)$$

The viscous stress tensor can be separated into it's radial and angular directions

$$\mathbf{T}|_{rr} = 2\mu\overline{\nabla\mathbf{v}}|_{rr} + 2\mu\overline{\nabla J_v}|_{rr} \quad (74)$$

$$\mathbf{T}|_{r\theta} = 2\mu\overline{\nabla\mathbf{v}}|_{r\theta} + 2\mu\overline{\nabla J_v}|_{r\theta} \quad (75)$$

Immediately we recognize the lack of an angular diffusive volume flux. So the angular viscous stress tensor can be shortened to

$$\mathbf{T}|_{r\theta} = 2\mu\overline{\nabla\mathbf{v}}|_{r\theta} \quad (76)$$

Here, the overbars in the above equations represent the tensor's symmetric and traceless form. For example,

$$\overline{\mathbf{D}} = \frac{1}{2}(\mathbf{D} + \mathbf{D}^T) - \frac{1}{3}tr(\mathbf{D}) \quad (77)$$

In this case, $tr()$ is the trace and the superscript T is the transpose.

It is important to note that our viscous stress tensor is already traceless, so the last term is not required. When applied to our mass velocity - as seen in Equation 73 - we find

$$\overline{\nabla\mathbf{v}} = \frac{1}{2}\left(\frac{\partial u_i}{\partial x_j} + \frac{\partial u_j}{\partial x_i}\right) \quad (78)$$

Here, the subscripts i and j represent our indices. In this problem, we require both radial and angular components. First, an instance where $i = j = r$ yields

$$\overline{\nabla\mathbf{v}}|_{rr} = \frac{1}{2}\left(\frac{\partial u_r}{\partial r} + \frac{\partial u_r}{\partial r}\right) \quad (79)$$

The radial component of the mass velocity becomes

$$\overline{\nabla \mathbf{v}}|_{rr} = \frac{\partial u_r}{\partial r} \quad (80)$$

In the second instance we have $i = r$ and $j = \theta$. The same Equation 78 yields

$$\overline{\nabla \mathbf{v}}|_{r\theta} = \frac{1}{2} \left(\frac{\partial u_r}{\partial \theta} + \frac{\partial u_\theta}{\partial r} \right) \quad (81)$$

The angular component of the mass velocity becomes

$$\overline{\nabla \mathbf{v}}|_{r\theta} = \frac{1}{2} \frac{\partial u_\theta}{\partial r} \quad (82)$$

To complete the stress tensors, we must calculate $\overline{\nabla J_v}|_r$, which will be incredibly similar to $\overline{\nabla \mathbf{v}}|_r$

$$\overline{\nabla J_v}|_{rr} = \frac{\partial J_v^r}{\partial r} \quad (83)$$

Substituting Equations 80, 82 and 83 into Equations 74 and 76, we find

$$\mathbf{T}|_{rr} = 2\mu \frac{\partial u_r}{\partial r} + 2\mu \frac{\partial J_v^r}{\partial r} \quad (84)$$

$$\mathbf{T}|_{r\theta} = \mu \frac{\partial u_\theta}{\partial r} \quad (85)$$

For these equations to be useful in solving Equations 69 and 70, we must calculate the divergence of them.

$$\nabla \cdot \mathbf{T}|_{rr} = \frac{1}{r} \frac{\partial}{\partial r} \left(r \mu \frac{\partial u_r}{\partial r} \right) - \frac{\mu u_r}{r^2} + \frac{1}{r} \frac{\partial}{\partial r} \left(r \mu \frac{\partial J_v^r}{\partial r} \right) \quad (86)$$

$$\nabla \cdot \mathbf{T}|_{r\theta} = \frac{1}{r} \frac{\partial}{\partial r} \left(r \mu \frac{\partial u_\theta}{\partial r} \right) - \frac{\mu u_\theta}{r^2} \quad (87)$$

Using the above derived equations, the right hand sides of Equations 69 and 70 looks like

$$\rho \frac{\partial u_r}{\partial t} + \rho (\mathbf{v} \cdot \nabla) u_r - \rho \frac{u_\theta^2}{r} = -\frac{dp}{dr} + \frac{1}{r} \frac{\partial}{\partial r} (r \mu \frac{\partial u_r}{\partial r}) - \frac{\mu u_r}{r^2} + \frac{1}{r} \frac{\partial}{\partial r} (r \mu \frac{\partial J_v^r}{\partial r}) \quad (88)$$

$$\rho \frac{\partial u_\theta}{\partial t} + \rho (\mathbf{v} \cdot \nabla) u_\theta + \rho \frac{u_r u_\theta}{r} = \frac{1}{r} \frac{\partial}{\partial r} (r \mu \frac{\partial u_\theta}{\partial r}) - \frac{\mu u_\theta}{r^2} \quad (89)$$

The last step in completing the radial and angular momentum equations is simplifying $(\mathbf{v} \cdot \nabla)$, which is defined as

$$(\mathbf{v} \cdot \nabla) = \frac{\partial}{\partial t} + u_r \frac{\partial}{\partial r} + \frac{u_\theta}{r} \frac{\partial}{\partial \theta} + u_z \frac{\partial}{\partial z} \quad (90)$$

Since we've defined our vortex as two-dimensional and axisymmetric, $\frac{\partial}{\partial \theta} = 0$ and $\frac{\partial}{\partial z} = 0$. Multiplying this by the radial and angular components yields

$$\rho \frac{\partial u_r}{\partial t} + \rho u_r \frac{\partial u_r}{\partial r} - \rho \frac{u_\theta^2}{r} = -\frac{dp}{dr} + \frac{1}{r} \frac{\partial}{\partial r} (r \mu \frac{\partial u_r}{\partial r}) - \frac{\mu u_r}{r^2} + \frac{1}{r} \frac{\partial}{\partial r} (r \mu \frac{\partial J_v^r}{\partial r}) \quad (91)$$

$$\rho \frac{\partial u_\theta}{\partial t} + \rho u_r \frac{\partial u_\theta}{\partial r} + \rho \frac{u_r u_\theta}{r} = \frac{1}{r} \frac{\partial}{\partial r} (r \mu \frac{\partial u_\theta}{\partial r}) - \frac{\mu u_\theta}{r^2} \quad (92)$$

Next, we want to clean up these expressions. It is more helpful to have the equations expressed as functions of u_r , u_θ , ρ , p and T . This requires removing J_v^r , which can be defined as

$$J_v = \frac{C}{Pr} \frac{\mu}{\rho} \nabla \ln(\rho) \quad (93)$$

And since

$$\nabla \ln(\rho) = \frac{1}{\rho} \frac{d\rho}{dr} \quad (94)$$

And since J_v is only dependent on the radial direction, we find

$$J_v^r = \frac{C}{Pr} \frac{\mu}{\rho^2} \frac{d\rho}{dr} \quad (95)$$

It is important to remember our fluid properties (like μ , k , γ , etc) are not constant. Substituting J_v^r back into Equation 91, we find our finalized momentum equations can be expressed as

$$\rho \frac{\partial u_r}{\partial t} + \rho u_r \frac{\partial u_r}{\partial r} - \left(\rho \frac{u_\theta^2}{r} \right) = -\frac{dp}{dr} + \frac{1}{r} \frac{\partial}{\partial r} (r \mu \frac{\partial u_r}{\partial r}) - \frac{\mu u_r}{r^2} + \frac{1}{r} \frac{\partial}{\partial r} (r \mu \frac{\partial}{\partial r} (\frac{C}{Pr} \frac{\mu}{\rho^2} \frac{d\rho}{dr})) \quad (96)$$

$$\rho \frac{\partial u_\theta}{\partial t} + \rho u_r \frac{\partial u_\theta}{\partial r} + \left(\rho \frac{u_r u_\theta}{r} \right) = \frac{1}{r} \frac{\partial}{\partial r} (r \mu \frac{\partial u_\theta}{\partial r}) - \frac{\mu u_\theta}{r^2} \quad (97)$$

9.3 Energy Equation

Derivation of the energy equation:

Begin with bivelocity equation governing transport of energy

$$\rho \frac{D\hat{u}}{Dt} + \rho \mathbf{v} \cdot \nabla \hat{e} = -\nabla \cdot \mathbf{J}_e \quad (98)$$

Knowing that diffusive energy flux is dependent on internal energy flux as well as pressure and volume velocity, we can write

$$\mathbf{J}_e = J_u + \mathbf{P} \cdot \mathbf{v}_v \quad (99)$$

Where internal energy flux is dependent on the gradient of temperature and the thermal conductivity ratio

$$J_u = -k' \nabla T \quad (100)$$

Where the thermal conductivity ratio is defined as

$$k' = \frac{k}{\gamma} \quad (101)$$

γ is defined as the ratio of specific heats

$$\gamma = \frac{\hat{c}_p}{\hat{c}_v} \quad (102)$$

Each specific heat can be expressed as a function of the ideal gas constant R such that γ becomes a constant

$$\hat{c}_p = \frac{5}{2} R \quad \text{and} \quad \hat{c}_v = \frac{3}{2} R \quad (103)$$

$$\gamma = \frac{5}{3} \quad (104)$$

So finally

$$k' = \frac{3}{5} k \quad (105)$$

Ultimately, we can express energy flux as

$$J_e = -k' \nabla T + (\mathbf{P} \cdot \mathbf{v}) + (\mathbf{P} \cdot J_v) \quad (106)$$

First, we redefine the gradient of temperature

$$\nabla T = \left(\frac{\partial T}{\partial r}\right) i_r + \left(\frac{1}{r} \frac{\partial T}{\partial \theta}\right) i_\theta \quad (107)$$

Since the system is axisymmetric,

$$\nabla T = \left(\frac{\partial T}{\partial r}\right) i_r \quad (108)$$

The second and third terms of the right hand side of Equation 106 require a little more detail since \mathbf{P} is a tensor and \mathbf{v} and J_v are vectors. If we break this down and look at the indices, we see

$$(\mathbf{P} \cdot \mathbf{v}) = \mathbf{P}_{ij} \mathbf{v}_j \quad (109)$$

In observing the radial and angular directions, we find

$$(\mathbf{P} \cdot \mathbf{v})|_r = \mathbf{P}_{rr} u_r + \mathbf{P}_{r\theta} u_\theta \quad (110)$$

$$(\mathbf{P} \cdot \mathbf{v})|_\theta = \mathbf{P}_{\theta r} u_r + \mathbf{P}_{\theta\theta} u_\theta \quad (111)$$

Since the pressure matrix is symmetric, $\mathbf{P}_{\theta r} = \mathbf{P}_{r\theta}$.

The process is similar for J_v . But since J_v^θ , does not exist, the equations become

$$(\mathbf{P} \cdot J_v)|_r = \mathbf{P}_{rr} J_v^r + \mathbf{P}_{r\theta} J_v^\theta = \mathbf{P}_{rr} J_v^r \quad (112)$$

$$(\mathbf{P} \cdot \mathbf{J}_v)|_\theta = \mathbf{P}_{\theta r} J_v^r + \mathbf{P}_{\theta\theta} J_v^\theta = \mathbf{P}_{\theta r} J_v^r \quad (113)$$

Substituting back into Equation 101, we find the radial and angular components of J_e to be

$$J_e^r = \left(-k' \frac{\partial T}{\partial r}\right) + (\mathbf{P}_{rr} u_r + \mathbf{P}_{r\theta} u_\theta) + (\mathbf{P}_{rr} J_v^r) \quad (114)$$

$$J_e^\theta = (\mathbf{P}_{r\theta} u_r + \mathbf{P}_{\theta\theta} u_\theta) + (\mathbf{P}_{r\theta} J_v^r) \quad (115)$$

To continue the evaluation of Equation 98, we must take the divergence of J_e

$$\nabla \cdot \mathbf{J}_e = \frac{1}{r} \frac{\partial}{\partial r} (r J_e^r) + \frac{1}{r} \frac{\partial}{\partial \theta} (J_e^\theta) \quad (116)$$

Which loses the second term due to its axisymmetric nature

$$\nabla \cdot \mathbf{J}_e = \frac{1}{r} \frac{\partial}{\partial r} (r J_e^r) \quad (117)$$

J_e^r from Equation 114 can be plugged into Equation 117 to find

$$\nabla \cdot \mathbf{J}_e = \frac{1}{r} \frac{\partial}{\partial r} \left(r \left((-k' \frac{\partial T}{\partial r}) + (\mathbf{P}_{rr} u_r + \mathbf{P}_{r\theta} u_\theta) + (\mathbf{P}_{rr} J_v^r) \right) \right) \quad (118)$$

Which can be separated to

$$\nabla \cdot \mathbf{J}_e = -\frac{1}{r} \frac{\partial}{\partial r} \left(k' r \frac{\partial T}{\partial r} \right) + \frac{1}{r} \frac{\partial}{\partial r} (r (\mathbf{P}_{rr} u_r + \mathbf{P}_{r\theta} u_\theta)) + \frac{1}{r} \frac{\partial}{\partial r} (r (\mathbf{P}_{rr} J_v^r)) \quad (119)$$

Equation 98 now becomes

$$\rho \frac{D\hat{u}}{Dt} + \rho \mathbf{v} \cdot \nabla \hat{e} = \frac{1}{r} \frac{\partial}{\partial r} \left(k' r \frac{\partial T}{\partial r} \right) - \frac{1}{r} \frac{\partial}{\partial r} (r (\mathbf{P}_{rr} u_r + \mathbf{P}_{r\theta} u_\theta)) - \frac{1}{r} \frac{\partial}{\partial r} (r (\mathbf{P}_{rr} J_v^r)) \quad (120)$$

Because of mass conservation, the right hand side can be rewritten as

$$\rho \mathbf{v} \cdot \nabla \hat{e} = \nabla \cdot (\rho \mathbf{v} \hat{e}) \quad (121)$$

Noting the axisymmetric nature, the gradient of energy \hat{e} is

$$\nabla \hat{e} = \left(\frac{\partial \hat{e}}{\partial r}\right) i_r + \left(\frac{\partial \hat{e}}{\partial \theta}\right) i_\theta = \frac{\partial \hat{e}}{\partial r} \quad (122)$$

Thus the energy equation can be written as

$$\rho \frac{D\hat{e}}{Dt} + \rho u_r \frac{\partial \hat{e}}{\partial r} = \frac{1}{r} \frac{\partial}{\partial r} (k' r \frac{\partial T}{\partial r}) - \frac{1}{r} \frac{\partial}{\partial r} (r (\mathbf{P}_{rr} u_r + \mathbf{P}_{r\theta} u_\theta)) - \frac{1}{r} \frac{\partial}{\partial r} (r (\mathbf{P}_{rr} J_v^r)) \quad (123)$$

Similar to the momentum equations, we want to simplify terms. The energy of the system \hat{e} can be written as

$$\hat{e} = \mathbf{U} + \frac{\mathbf{V}^2}{2} \quad (124)$$

Where the magnitude of the mass velocity vector is defined as

$$\mathbf{V} = (u_r^2 + u_\theta^2)^{1/2} \quad (125)$$

The internal energy \mathbf{U} is defined as

$$\mathbf{U} = C_v T = \frac{3}{2} RT \quad (126)$$

And our energy equation now becomes

$$\hat{e} = \frac{3}{2} RT + \frac{\mathbf{V}^2}{2} \quad (127)$$

The pressure tensors can be expanded to

$$\mathbf{P}_{rr} = \mathbf{I}p - \mathbf{T}_{rr} \quad (128)$$

$$\mathbf{P}_{r\theta} = \mathbf{I}p - \mathbf{T}_{r\theta} \quad (129)$$

And where

$$\mathbf{T}_{rr} = 2\mu e_{rr} = 2\mu \frac{\partial u_r}{\partial r} \quad (130)$$

$$\mathbf{T}_{r\theta} = 2\mu e_{r\theta} = r\mu \frac{\partial}{\partial r} \left(\frac{u_\theta}{r} \right) \quad (131)$$

Our last term to be defined is J_v^r , which was already defined in the previous section as Equation 95

$$J_v^r = \frac{C}{Pr} \gamma \frac{1}{\rho} \frac{d\rho}{dr} \quad (132)$$

Substituting the above derived into Equation 123, we find

$$\begin{aligned} \rho R \frac{\partial T}{\partial t} + \rho u_r \frac{\partial}{\partial r} \left(\frac{3}{2} RT + \frac{\mathbf{V}^2}{2} \right) &= \frac{1}{r} \frac{\partial}{\partial r} \left(k' r \frac{\partial T}{\partial r} \right) - \frac{1}{r} \frac{\partial}{\partial r} \left(r \left((p - 2\mu \frac{\partial u_r}{\partial r}) u_r \right. \right. \\ &\quad \left. \left. + (p - r\mu \frac{\partial}{\partial r} \left(\frac{u_\theta}{r} \right)) u_\theta \right) \right) - \frac{1}{r} \frac{\partial}{\partial r} \left(r \left((p - 2\mu \frac{\partial u_r}{\partial r}) \left(\frac{C}{Pr} \frac{\mu}{\rho^2} \frac{d\rho}{dr} \right) \right) \right) \end{aligned} \quad (133)$$

9.4 Ideal Gas

Our list of unknown variables includes u_r , u_θ , T , ρ and p . With one more equation required, we can relate density, temperature and pressure using the Ideal Gas Law

$$p = \rho R T \quad (134)$$

9.5 Nondimensionalization

For convenience, we will nondimensionalize our equations using the parameters below:

$$\tilde{u}_r = \frac{u_r}{\sqrt{R T_o}} \quad (135) \quad \tilde{u}_\theta = \frac{u_\theta}{\sqrt{R T_o}} \quad (138) \quad \tilde{T} = \frac{T}{T_o} \quad (141)$$

$$\tilde{r} = \frac{r}{r_o} \quad (136) \quad \tilde{p} = \frac{p}{p_o} \quad (139) \quad \tilde{\mu} = \frac{\mu}{\mu_o} \quad (142)$$

$$\tilde{\rho} = \frac{\rho}{\rho_o} \quad (137) \quad \tilde{k} = \frac{k}{\mu_o \hat{c}_p} \quad (140) \quad \tilde{t} = \frac{t}{r_o^2 \rho_o 10^{-2} \mu_o^{-1}} \quad (143)$$

It's important to note that since our gas is modeled as Maxwellian and monatomic, thermal conductivity and dynamic viscosity are proportional to temperature [13].

$$\tilde{\mu} = \tilde{T} \quad (144) \quad \tilde{k} = \frac{3}{2} \tilde{T} \quad (145)$$

9.5.1 Mass

Starting with the mass equation (Equation 65)

$$\frac{\partial \rho}{\partial t} + u_r \frac{\partial \rho}{\partial r} + \rho \frac{\partial u_r}{\partial r} + \frac{\rho}{r} u_r = 0 \quad (146)$$

Substituting in our parameters from above yields

$$\frac{100 \rho_o \mu_o}{r_o^2 \rho_o} \left[\frac{\partial \tilde{\rho}}{\partial \tilde{t}} \right] + \frac{\rho_o \sqrt{R T_o}}{r_o} \left[\tilde{u}_r \frac{\partial \tilde{\rho}}{\partial \tilde{r}} + \tilde{\rho} \frac{\partial \tilde{u}_r}{\partial \tilde{r}} + \frac{\tilde{\rho}}{\tilde{r}} \tilde{u}_r \right] = 0 \quad (147)$$

We can divide through by the coefficient of the first term to yield

$$100 \frac{\partial \tilde{\rho}}{\partial \tilde{t}} + \frac{\rho_o r_o \sqrt{RT_o}}{\mu_o} \left[\tilde{u}_r \frac{\partial \tilde{\rho}}{\partial \tilde{r}} + \tilde{\rho} \frac{\partial \tilde{u}_r}{\partial \tilde{r}} + \frac{\tilde{\rho}}{\tilde{r}} \tilde{u}_r \right] = 0 \quad (148)$$

Where the parameter $\frac{\rho_o r_o \sqrt{RT_o}}{\mu_o}$ can be simplified to the inverse of the Knudsen Number Kn_o

$$100 \frac{\partial \tilde{\rho}}{\partial \tilde{t}} + \frac{1}{Kn_o} \left[\tilde{u}_r \frac{\partial \tilde{\rho}}{\partial \tilde{r}} + \tilde{\rho} \frac{\partial \tilde{u}_r}{\partial \tilde{r}} + \frac{\tilde{\rho}}{\tilde{r}} \tilde{u}_r \right] = 0 \quad (149)$$

9.5.2 Radial Momentum

Next, taking the radial momentum equation:

$$\rho \frac{\partial u_r}{\partial t} + \rho u_r \frac{\partial u_r}{\partial r} - \left(\rho \frac{u_\theta^2}{r} \right) = -\frac{dp}{dr} + \frac{1}{r} \frac{\partial}{\partial r} \left(r \mu \frac{\partial u_r}{\partial r} \right) - \frac{\mu u_r}{r^2} + \frac{1}{r} \frac{\partial}{\partial r} \left(r \mu \frac{\partial}{\partial r} \left(\frac{C}{Pr} \frac{\mu}{\rho^2} \frac{\partial \rho}{\partial r} \right) \right) \quad (150)$$

Substituting in our parameters from above and simplifying yields

$$\begin{aligned} \left(\frac{100 \mu_o \sqrt{RT_o}}{r_o^2} \right) \tilde{\rho} \frac{\partial \tilde{u}_r}{\partial \tilde{t}} + \left(\frac{\rho_o RT_o}{r_o} \right) \tilde{\rho} \tilde{u}_r \frac{\partial \tilde{u}_r}{\partial \tilde{r}} - \left(\frac{\rho_o RT_o}{r_o} \right) \frac{\tilde{\rho} \tilde{u}_\theta^2}{\tilde{r}} = \left(\frac{-p_o}{r_o} \right) \frac{\partial \tilde{p}}{\partial \tilde{r}} \\ + \left(\frac{\mu_o \sqrt{RT_o}}{r_o^2} \right) \frac{1}{\tilde{r}} \frac{\partial}{\partial \tilde{r}} \left[\tilde{r} \tilde{\mu} \frac{\partial \tilde{u}_r}{\partial \tilde{r}} \right] - \left(\frac{\mu_o \sqrt{RT_o}}{r_o^2} \right) \frac{\tilde{\mu} \tilde{u}_r}{\tilde{r}^2} \\ + \left(\frac{C \mu_o^2}{Pr \rho_o r_o^3} \right) \frac{1}{\tilde{r}} \frac{\partial}{\partial \tilde{r}} \left[\tilde{r} \tilde{\mu} \frac{\partial}{\partial \tilde{r}} \left(\frac{\tilde{\mu}}{\tilde{\rho}^2} \frac{\partial \tilde{\rho}}{\partial \tilde{r}} \right) \right] \end{aligned} \quad (151)$$

Note that the pressure term houses a reference pressure. We can replace this with $\rho_o RT_o$ from the ideal gas equation. Once that substitution has been made, the coefficient of the pressure term matches the coefficients on the left side of the equality. Multiplying by $\frac{r_o}{\rho_o RT_o}$ will eliminate these coefficients and yield:

$$\begin{aligned} \left(\frac{100 \mu_o}{r_o \rho_o \sqrt{RT_o}} \right) \tilde{\rho} \frac{\partial \tilde{u}_r}{\partial \tilde{t}} + \tilde{\rho} \tilde{u}_r \frac{\partial \tilde{u}_r}{\partial \tilde{r}} - \frac{\tilde{\rho} \tilde{u}_\theta^2}{\tilde{r}} = \\ - \frac{\partial \tilde{p}}{\partial \tilde{r}} + \left(\frac{\mu_o}{\sqrt{RT_o} \rho_o r_o} \right) \frac{1}{\tilde{r}} \frac{\partial}{\partial \tilde{r}} \left[\tilde{r} \tilde{\mu} \frac{\partial \tilde{u}_r}{\partial \tilde{r}} \right] - \left(\frac{\mu_o}{\sqrt{RT_o} \rho_o r_o} \right) \frac{\tilde{\mu} \tilde{u}_r}{\tilde{r}^2} \\ + \left(\frac{C \mu_o^2}{Pr RT_o \rho_o^2 r_o^2} \right) \frac{1}{\tilde{r}} \frac{\partial}{\partial \tilde{r}} \left[\tilde{r} \tilde{\mu} \frac{\partial}{\partial \tilde{r}} \left(\frac{\tilde{\mu}}{\tilde{\rho}^2} \frac{\partial \tilde{\rho}}{\partial \tilde{r}} \right) \right] \end{aligned} \quad (152)$$

Remembering that the Knudson number is defined as:

$$Kn_o = \frac{\mu_o}{\rho_o r_o \sqrt{RT_o}} \quad (153)$$

We can express all three of our coefficients in terms of the Knudson number.

$$\begin{aligned}
100 Kn_o \tilde{\rho} \frac{\partial \tilde{u}_r}{\partial \tilde{t}} + \tilde{\rho} \tilde{u}_r \frac{\partial \tilde{u}_r}{\partial \tilde{r}} - \frac{\tilde{\rho} \tilde{u}_\theta^2}{\tilde{r}} = -\frac{\partial \tilde{p}}{\partial \tilde{r}} + \left(Kn_o \right) \frac{1}{\tilde{r}} \frac{\partial}{\partial \tilde{r}} \left[\tilde{r} \tilde{\mu} \frac{\partial \tilde{u}_r}{\partial \tilde{r}} \right] \\
- \left(Kn_o \right) \frac{\tilde{\mu} \tilde{u}_r}{\tilde{r}^2} + \left(\frac{C Kn_o^2}{Pr} \right) \frac{1}{\tilde{r}} \frac{\partial}{\partial \tilde{r}} \left[\tilde{r} \tilde{\mu} \frac{\partial}{\partial \tilde{r}} \left(\frac{\tilde{\mu}}{\tilde{\rho}^2} \frac{\partial \tilde{\rho}}{\partial \tilde{r}} \right) \right]
\end{aligned} \tag{154}$$

Additionally, the Prandtl number is defined as:

$$Pr = \frac{\nu}{\alpha} = \frac{\mu/\rho}{k/\rho \hat{c}_p} = \hat{c}_p \frac{\mu}{k} \tag{155}$$

Notice Equations 144 and 145 which defined $\tilde{\mu}$ and \tilde{k} . Nondimensionalizing the Prandtl number, and applying these two equations gives

$$Pr = \hat{c}_p \frac{\tilde{\mu} \mu_o}{\tilde{k} \mu_o \hat{c}_p} = \frac{\tilde{\mu}}{\tilde{k}} \tag{156} \qquad Pr = \frac{\tilde{\mu}}{\tilde{k}} = \frac{\tilde{\mu}}{\frac{3}{2} \tilde{\mu}} = \frac{2}{3} \tag{157}$$

replacing the Prandtl number and utilizing the Knudson number, our Radial Momentum equation becomes:

$$\begin{aligned}
100 Kn_o \tilde{\rho} \frac{\partial \tilde{u}_r}{\partial \tilde{t}} + \tilde{\rho} \tilde{u}_r \frac{\partial \tilde{u}_r}{\partial \tilde{r}} - \frac{\tilde{\rho} \tilde{u}_\theta^2}{\tilde{r}} = -\frac{\partial \tilde{p}}{\partial \tilde{r}} + Kn_o \frac{1}{\tilde{r}} \frac{\partial}{\partial \tilde{r}} \left[\tilde{r} \tilde{\mu} \frac{\partial \tilde{u}_r}{\partial \tilde{r}} \right] \\
- Kn_o \frac{\tilde{\mu} \tilde{u}_r}{\tilde{r}^2} + \left(\frac{3 C Kn_o^2}{2} \right) \frac{1}{\tilde{r}} \frac{\partial}{\partial \tilde{r}} \left[\tilde{r} \tilde{\mu} \frac{\partial}{\partial \tilde{r}} \left(\frac{\tilde{\mu}}{\tilde{\rho}^2} \frac{\partial \tilde{\rho}}{\partial \tilde{r}} \right) \right]
\end{aligned} \tag{158}$$

While this is now a reduced and usable form of our conservation equation, Matlab is unable to utilize this form. The nested derivatives must be removed.

$$\begin{aligned}
100 Kn_o \tilde{\rho} \frac{\partial \tilde{u}_r}{\partial \tilde{t}} + \tilde{\rho} \tilde{u}_r \frac{\partial \tilde{u}_r}{\partial \tilde{r}} - \frac{\tilde{\rho} \tilde{u}_\theta^2}{\tilde{r}} = -\frac{\partial \tilde{p}}{\partial \tilde{r}} + Kn_o \left[\frac{\partial \tilde{\mu}}{\partial \tilde{r}} \frac{\partial \tilde{u}_r}{\partial \tilde{r}} + \tilde{\mu} \left(\frac{\partial^2 \tilde{u}_r}{\partial \tilde{r}^2} + \frac{1}{\tilde{r}} \frac{\partial \tilde{u}_r}{\partial \tilde{r}} \right) - \frac{\tilde{\mu} \tilde{u}_\theta^2}{\tilde{r}^2} \right] \\
+ \left(\frac{3 C Kn_o^2}{2} \right) \frac{1}{\tilde{\rho}^2} \left[\tilde{\mu} \frac{\partial^2 \tilde{\mu}}{\partial \tilde{r}^2} \frac{\partial \tilde{\rho}}{\partial \tilde{r}} + 3 \tilde{\mu} \frac{\partial \tilde{\mu}}{\partial \tilde{r}} \frac{\partial^2 \tilde{\rho}}{\partial \tilde{r}^2} + \left(\frac{\partial \tilde{\mu}}{\partial \tilde{r}} - 2 \tilde{\mu} \frac{\partial \tilde{\rho}}{\partial \tilde{r}} + \tilde{\mu} - \frac{4 \tilde{\mu}}{\tilde{\rho}} \frac{\partial \tilde{\rho}}{\partial \tilde{r}} \right) \frac{\partial \tilde{\mu}}{\partial \tilde{r}} \frac{\partial \tilde{\rho}}{\partial \tilde{r}} \right. \\
\left. + \frac{\tilde{\mu}^2}{\tilde{r}} \frac{d^2 \tilde{\rho}}{d \tilde{r}^2} - \frac{6 \tilde{\mu}^2}{\tilde{\rho}} \frac{\partial \tilde{\rho}}{\partial \tilde{r}} \frac{d^2 \tilde{\rho}}{d \tilde{r}^2} + \frac{6 \tilde{\mu}^2}{\tilde{\rho}^2} \left(\frac{\partial \tilde{\rho}}{\partial \tilde{r}} \right)^3 - \frac{2 \tilde{\mu}^2}{\tilde{\rho}} \left(\frac{\partial \tilde{\rho}}{\partial \tilde{r}} \right)^2 + \tilde{\mu} \frac{\partial^3 \tilde{\rho}}{\partial \tilde{r}^3} \right]
\end{aligned} \tag{159}$$

This form can now be used in Matlab, but notice only the first line remains when bivelocity compressibility is ignored ($C = 0$)

9.5.3 Angular Momentum

The original angular momentum is

$$\rho \frac{\partial u_\theta}{\partial t} + \rho u_r \frac{\partial u_\theta}{\partial r} + \left(\rho \frac{u_r u_\theta}{r} \right) = \frac{1}{r} \frac{\partial}{\partial r} \left(r \mu \frac{\partial u_\theta}{\partial r} \right) - \frac{\mu u_\theta}{r^2} \quad (160)$$

Nondimensionalizing angular momentum is simpler and yields

$$\begin{aligned} \left(\frac{100 \mu_o \sqrt{RT_o}}{r_o^2} \right) \tilde{\rho} \frac{\partial \tilde{u}_\theta}{\partial \tilde{t}} + \left(\frac{\rho_o RT_o}{r_o} \right) \tilde{\rho} \tilde{u}_r \frac{\partial \tilde{u}_\theta}{\partial \tilde{r}} + \left(\frac{\rho_o RT_o}{r_o} \right) \frac{\tilde{\rho} \tilde{u}_\theta \tilde{u}_r}{\tilde{r}} = \\ \left(\frac{\mu_o \sqrt{RT_o}}{r_o^2} \right) \frac{1}{\tilde{r}} \frac{\partial}{\partial \tilde{r}} \left[\tilde{r} \tilde{\mu} \frac{\partial \tilde{u}_\theta}{\partial \tilde{r}} \right] - \left(\frac{\mu_o \sqrt{RT_o}}{r_o^2} \right) \frac{\tilde{\mu} \tilde{u}_\theta}{\tilde{r}^2} \end{aligned} \quad (161)$$

Multiplying by $\frac{r_o}{\rho_o RT_o}$ will remove most of the coefficients from the left hand side of the equation, and allow us to make substitutions in the remaining areas.

$$\begin{aligned} \left(\frac{100 \mu_o}{r_o \rho_o \sqrt{RT_o}} \right) \tilde{\rho} \frac{\partial \tilde{u}_\theta}{\partial \tilde{t}} + \tilde{\rho} \tilde{u}_r \frac{\partial \tilde{u}_\theta}{\partial \tilde{r}} + \frac{\tilde{\rho} \tilde{u}_\theta \tilde{u}_r}{\tilde{r}} = \\ \left(\frac{\mu_o}{r_o \rho_o \sqrt{RT_o}} \right) \frac{1}{\tilde{r}} \frac{\partial}{\partial \tilde{r}} \left[\tilde{r} \tilde{\mu} \frac{\partial \tilde{u}_\theta}{\partial \tilde{r}} \right] - \left(\frac{\mu_o}{r_o \rho_o \sqrt{RT_o}} \right) \frac{\tilde{\mu} \tilde{u}_\theta}{\tilde{r}^2} \end{aligned} \quad (162)$$

Again, we can quickly identify the Knudsen numbers and make the substitutions to obtain our final equation.

$$100 Kn_o \tilde{\rho} \frac{\partial \tilde{u}_\theta}{\partial \tilde{t}} + \tilde{\rho} \tilde{u}_r \frac{\partial \tilde{u}_\theta}{\partial \tilde{r}} + \frac{\tilde{\rho} \tilde{u}_\theta \tilde{u}_r}{\tilde{r}} = \frac{Kn_o}{\tilde{r}} \frac{\partial}{\partial \tilde{r}} \left[\tilde{r} \tilde{\mu} \frac{\partial \tilde{u}_\theta}{\partial \tilde{r}} \right] - Kn_o \frac{\tilde{\mu} \tilde{u}_\theta}{\tilde{r}^2} \quad (163)$$

However, similar to radial momentum, angular momentum needs to be rearranged into a form MatLab can utilize, which means removing the nested derivatives. The expanded form becomes:

$$100 Kn_o \tilde{\rho} \frac{\partial \tilde{u}_\theta}{\partial \tilde{t}} + \tilde{\rho} \tilde{u}_r \frac{\partial \tilde{u}_\theta}{\partial \tilde{r}} + \frac{\tilde{\rho} \tilde{u}_\theta \tilde{u}_r}{\tilde{r}} = Kn_o \left[\frac{\partial \tilde{\mu}}{\partial \tilde{r}} \frac{\partial \tilde{u}_\theta}{\partial \tilde{r}} + \tilde{\mu} \frac{\partial^2 \tilde{u}_\theta}{\partial \tilde{r}^2} + \frac{\tilde{\mu}}{\tilde{r}} \frac{\partial \tilde{u}_\theta}{\partial \tilde{r}} \right] - Kn_o \frac{\tilde{\mu} \tilde{u}_\theta}{\tilde{r}^2} \quad (164)$$

9.5.4 Energy

Next, we start with our energy equation

$$\begin{aligned} \rho R \frac{\partial T}{\partial t} + \rho u_r \frac{\partial}{\partial r} \left(\frac{3}{2} RT + \frac{\mathbf{V}^2}{2} \right) &= \frac{1}{r} \frac{\partial}{\partial r} \left(k' r \frac{\partial T}{\partial r} \right) - \frac{1}{r} \frac{\partial}{\partial r} \left(r \left((p - 2\mu \frac{\partial u_r}{\partial r}) u_r \right. \right. \\ &\quad \left. \left. + (p - r\mu \frac{\partial}{\partial r} \left(\frac{u_\theta}{r} \right)) u_\theta \right) \right) - \frac{1}{r} \frac{\partial}{\partial r} \left(r \left((p - 2\mu \frac{\partial u_r}{\partial r}) \left(\frac{C}{Pr} \frac{\mu}{\rho^2} \frac{\partial \rho}{\partial r} \right) \right) \right) \end{aligned} \quad (165)$$

First, expanding the equation will help with nondimensionalizing

$$\begin{aligned} \rho R \frac{\partial T}{\partial t} + \rho u_r \left[\frac{3R}{2} \frac{\partial T}{\partial r} + \frac{1}{2} \frac{\partial u_r^2}{\partial r} + \frac{1}{2} \frac{\partial u_\theta^2}{\partial r} \right] &= \frac{1}{r} \frac{\partial}{\partial r} \left(k' r \frac{\partial T}{\partial r} \right) \\ &\quad - \frac{1}{r} \frac{\partial}{\partial r} \left[r u_r p + r u_\theta p - 2r u_r \mu \frac{\partial u_r}{\partial r} - r^2 u_\theta \mu \frac{\partial}{\partial r} \left(\frac{u_\theta}{r} \right) \right] \\ &\quad - \frac{C}{r Pr} \left[\frac{\partial}{\partial r} \left(\frac{r \mu p}{\rho^2} \frac{\partial \rho}{\partial r} \right) - 2 \frac{\partial}{\partial r} \left(\frac{r \mu^2}{\rho^2} \frac{\partial \rho}{\partial r} \frac{\partial u_r}{\partial r} \right) \right] \end{aligned} \quad (166)$$

Expanding the 2nd and 3rd lines such that we have 2 terms on the left and 5 terms on the right will also be beneficial.

$$\begin{aligned} \rho R \frac{\partial T}{\partial t} + \rho u_r \left[\frac{3R}{2} \frac{\partial T}{\partial r} + \frac{1}{2} \frac{\partial u_r^2}{\partial r} + \frac{1}{2} \frac{\partial u_\theta^2}{\partial r} \right] &= \frac{1}{r} \frac{\partial}{\partial r} \left(k' r \frac{\partial T}{\partial r} \right) \\ &\quad - \frac{1}{r} \frac{\partial}{\partial r} [r p (u_r + u_\theta)] + \frac{1}{r} \frac{\partial}{\partial r} \left[2r u_r \mu \frac{\partial u_r}{\partial r} + r^2 u_\theta \mu \frac{\partial}{\partial r} \left(\frac{u_\theta}{r} \right) \right] \\ &\quad - \frac{C}{r Pr} \frac{\partial}{\partial r} \left[\frac{r \mu p}{\rho^2} \frac{\partial \rho}{\partial r} \right] + \frac{2C}{r Pr} \frac{\partial}{\partial r} \left[\frac{r \mu^2}{\rho^2} \frac{\partial \rho}{\partial r} \frac{\partial u_r}{\partial r} \right] \end{aligned} \quad (167)$$

All of our terms will be straightforward to nondimensionalize, with the exception of k' . Using Equation 105 we can replace k'

$$\begin{aligned} \rho R \frac{\partial T}{\partial t} + \rho u_r \left[\frac{3R}{2} \frac{\partial T}{\partial r} + \frac{1}{2} \frac{\partial u_r^2}{\partial r} + \frac{1}{2} \frac{\partial u_\theta^2}{\partial r} \right] &= \frac{1}{r} \frac{\partial}{\partial r} \left(\frac{3}{5} k r \frac{\partial T}{\partial r} \right) \\ &\quad - \frac{1}{r} \frac{\partial}{\partial r} [r p (u_r + u_\theta)] + \frac{1}{r} \frac{\partial}{\partial r} \left[2r u_r \mu \frac{\partial u_r}{\partial r} + r^2 u_\theta \mu \frac{\partial}{\partial r} \left(\frac{u_\theta}{r} \right) \right] \\ &\quad - \frac{C}{r Pr} \frac{\partial}{\partial r} \left[\frac{r \mu p}{\rho^2} \frac{\partial \rho}{\partial r} \right] + \frac{2C}{r Pr} \frac{\partial}{\partial r} \left[\frac{r \mu^2}{\rho^2} \frac{\partial \rho}{\partial r} \frac{\partial u_r}{\partial r} \right] \end{aligned} \quad (168)$$

Nondimensionalizing, our equation becomes

$$\begin{aligned}
& \frac{100 \mu_o R T_o}{r_o^2} \left(\tilde{\rho} \frac{\partial \tilde{T}}{\partial \tilde{t}} \right) + \frac{1}{2} \frac{\tilde{\rho} \rho_o \tilde{u}_r}{r_o} (R T_o)^{3/2} \left[3 \frac{d\tilde{T}}{d\tilde{r}} + \frac{d\tilde{u}_r^2}{d\tilde{r}} + \frac{d\tilde{u}_\theta^2}{d\tilde{r}} \right] = \\
& \frac{1}{\tilde{r} r_o^2} \frac{d}{d\tilde{r}} \left(\frac{3}{5} \tilde{k} \mu_o \hat{c}_p \tilde{r} r_o \frac{T_o}{r_o} \frac{d\tilde{T}}{d\tilde{r}} \right) - \frac{1}{\tilde{r} r_o^2} \frac{d}{d\tilde{r}} \left[\tilde{r} r_o \tilde{p} p_o \sqrt{R T_o} (\tilde{u}_r + \tilde{u}_\theta) \right] \\
& + \frac{1}{\tilde{r} r_o^2} \frac{d}{d\tilde{r}} \left[2 \tilde{r} r_o \tilde{\mu} \mu_o \tilde{u}_r \frac{R T_o}{r_o} \frac{d\tilde{u}_r}{d\tilde{r}} + \tilde{r}^2 r_o^2 \tilde{\mu} \mu_o \tilde{u}_\theta \frac{R T_o}{r_o^2} \frac{d}{d\tilde{r}} \left(\frac{\tilde{u}_\theta}{\tilde{r}} \right) \right] \\
& - \frac{C}{\tilde{r} r_o^2 Pr} \frac{d}{d\tilde{r}} \left[\frac{\tilde{r} r_o \tilde{\mu} \mu_o \tilde{p} p_o}{\tilde{\rho}^2 \rho_o^2} \frac{d\tilde{\rho}}{d\tilde{r}} \right] + \frac{2C}{\tilde{r} r_o^2 Pr} \frac{d}{d\tilde{r}} \left[\frac{\tilde{r} r_o \tilde{\mu}^2 \mu_o^2 \rho_o \sqrt{R T_o}}{\tilde{\rho}^2 \rho_o^2} \frac{d\tilde{\rho}}{d\tilde{r}} \frac{d\tilde{u}_r}{d\tilde{r}} \right]
\end{aligned} \tag{169}$$

With some preliminary simplification, we find

$$\begin{aligned}
& \frac{100 \mu_o R T_o}{r_o^2} \left(\tilde{\rho} \frac{\partial \tilde{T}}{\partial \tilde{t}} \right) + \left(\frac{1}{2} \frac{\rho_o}{r_o} (R T_o)^{3/2} \right) (\tilde{\rho} \tilde{u}_r) \left[3 \frac{d\tilde{T}}{d\tilde{r}} + \frac{d\tilde{u}_r^2}{d\tilde{r}} + \frac{d\tilde{u}_\theta^2}{d\tilde{r}} \right] = \\
& \left(\frac{3 \mu_o \hat{c}_p T_o}{5 r_o^2} \right) \frac{1}{\tilde{r}} \frac{d}{d\tilde{r}} \left[\tilde{k} \tilde{r} \frac{d\tilde{T}}{d\tilde{r}} \right] - \left(\frac{p_o \sqrt{R T_o}}{r_o} \right) \frac{1}{\tilde{r}} \frac{d}{d\tilde{r}} \left[\tilde{r} \tilde{p} (\tilde{u}_r + (\tilde{u}_\theta)) \right] \\
& + \left(\frac{\mu_o R T_o}{r_o^2} \right) \frac{1}{\tilde{r}} \frac{d}{d\tilde{r}} \left[2 \tilde{r} \tilde{\mu} \tilde{u}_r \frac{d\tilde{u}_r}{d\tilde{r}} + \tilde{r}^2 \tilde{\mu} \tilde{u}_\theta \frac{d}{d\tilde{r}} \left(\frac{\tilde{u}_\theta}{\tilde{r}} \right) \right] \\
& - \left(\frac{C \mu_o p_o}{r_o^2 \rho_o Pr} \right) \frac{1}{\tilde{r}} \frac{d}{d\tilde{r}} \left[\frac{\tilde{r} \tilde{\mu} \tilde{p}}{\tilde{\rho}^2} \frac{d\tilde{\rho}}{d\tilde{r}} \right] + \left(\frac{2C \mu_o^2 \sqrt{R T_o}}{r_o^3 \rho_o Pr} \right) \frac{1}{\tilde{r}} \frac{d}{d\tilde{r}} \left[\frac{\tilde{r} \tilde{\mu}^2}{\tilde{\rho}^2} \frac{d\tilde{\rho}}{d\tilde{r}} \frac{d\tilde{u}_r}{d\tilde{r}} \right]
\end{aligned} \tag{170}$$

We can immediately remove \tilde{k} and replace it with $\frac{3}{2} \tilde{T}$. Our next simplification comes from dividing both sides by p_o

$$\begin{aligned}
& \frac{100 \mu_o R T_o}{r_o^2 p_o} \left(\tilde{\rho} \frac{\partial \tilde{T}}{\partial \tilde{t}} \right) + \left(\frac{1}{2} \frac{\rho_o}{p_o r_o} (R T_o)^{3/2} \right) (\tilde{\rho} \tilde{u}_r) \left[3 \frac{d\tilde{T}}{d\tilde{r}} + \frac{d\tilde{u}_r^2}{d\tilde{r}} + \frac{d\tilde{u}_\theta^2}{d\tilde{r}} \right] = \\
& \left(\frac{9 \mu_o \hat{c}_p T_o}{10 p_o r_o^2} \right) \frac{1}{\tilde{r}} \frac{d}{d\tilde{r}} \left[\tilde{T} \tilde{r} \frac{d\tilde{T}}{d\tilde{r}} \right] - \left(\frac{\sqrt{R T_o}}{r_o} \right) \frac{1}{\tilde{r}} \frac{d}{d\tilde{r}} \left[\tilde{r} \tilde{p} (\tilde{u}_r + (\tilde{u}_\theta)) \right] \\
& + \left(\frac{\mu_o R T_o}{p_o r_o^2} \right) \frac{1}{\tilde{r}} \frac{d}{d\tilde{r}} \left[2 \tilde{r} \tilde{\mu} \tilde{u}_r \frac{d\tilde{u}_r}{d\tilde{r}} + \tilde{r}^2 \tilde{\mu} \tilde{u}_\theta \frac{d}{d\tilde{r}} \left(\frac{\tilde{u}_\theta}{\tilde{r}} \right) \right] \\
& - \left(\frac{C \mu_o}{r_o^2 \rho_o Pr} \right) \frac{1}{\tilde{r}} \frac{d}{d\tilde{r}} \left[\frac{\tilde{r} \tilde{\mu} \tilde{p}}{\tilde{\rho}^2} \frac{d\tilde{\rho}}{d\tilde{r}} \right] + \left(\frac{2C \mu_o^2 \sqrt{R T_o}}{p_o r_o^3 \rho_o Pr} \right) \frac{1}{\tilde{r}} \frac{d}{d\tilde{r}} \left[\frac{\tilde{r} \tilde{\mu}^2}{\tilde{\rho}^2} \frac{d\tilde{\rho}}{d\tilde{r}} \frac{d\tilde{u}_r}{d\tilde{r}} \right]
\end{aligned} \tag{171}$$

We can see on the left hand side, that the density and an $R T_o$ can be replaced by pressure using the ideal gas law.

$$\begin{aligned}
\frac{100 \mu_o}{r_o^2 \rho_o} \left(\tilde{\rho} \frac{\partial \tilde{T}}{\partial \tilde{t}} \right) + \left(\frac{1}{2} \frac{\sqrt{RT_o}}{r_o} \right) (\tilde{\rho} \tilde{u}_r) \left[3 \frac{d\tilde{T}}{d\tilde{r}} + \frac{d\tilde{u}_r^2}{d\tilde{r}} + \frac{d\tilde{u}_\theta^2}{d\tilde{r}} \right] = \\
\left(\frac{9 \mu_o \hat{c}_p T_o}{10 p_o r_o^2} \right) \frac{1}{\tilde{r}} \frac{d}{d\tilde{r}} \left[\tilde{r} \tilde{T} \frac{d\tilde{T}}{d\tilde{r}} \right] - \left(\frac{\sqrt{RT_o}}{r_o} \right) \frac{1}{\tilde{r}} \frac{d}{d\tilde{r}} \left[\tilde{r} \tilde{p} (\tilde{u}_r + (\tilde{u}_\theta)) \right] \\
+ \left(\frac{\mu_o RT_o}{p_o r_o^2} \right) \frac{1}{\tilde{r}} \frac{d}{d\tilde{r}} \left[2 \tilde{r} \tilde{\mu} \tilde{u}_r \frac{d\tilde{u}_r}{d\tilde{r}} + \tilde{r}^2 \tilde{\mu} \tilde{u}_\theta \frac{d}{d\tilde{r}} \left(\frac{\tilde{u}_\theta}{\tilde{r}} \right) \right] \\
- \left(\frac{C \mu_o}{r_o^2 \rho_o Pr} \right) \frac{1}{\tilde{r}} \frac{d}{d\tilde{r}} \left[\frac{\tilde{r} \tilde{\mu} \tilde{p}}{\tilde{\rho}^2} \frac{d\tilde{\rho}}{d\tilde{r}} \right] + \left(\frac{2 C \mu_o^2 \sqrt{RT_o}}{p_o r_o^3 \rho_o Pr} \right) \frac{1}{\tilde{r}} \frac{d}{d\tilde{r}} \left[\frac{\tilde{r} \tilde{\mu}^2}{\tilde{\rho}^2} \frac{d\tilde{\rho}}{d\tilde{r}} \frac{d\tilde{u}_r}{d\tilde{r}} \right]
\end{aligned} \tag{172}$$

Divide both sides by $\sqrt{RT_o}$

$$\begin{aligned}
\frac{100 \mu_o}{r_o^2 \rho_o \sqrt{RT_o}} \left(\tilde{\rho} \frac{\partial \tilde{T}}{\partial \tilde{t}} \right) + \left(\frac{1}{2} \frac{1}{r_o} \right) (\tilde{\rho} \tilde{u}_r) \left[3 \frac{d\tilde{T}}{d\tilde{r}} + \frac{d\tilde{u}_r^2}{d\tilde{r}} + \frac{d\tilde{u}_\theta^2}{d\tilde{r}} \right] = \\
\left(\frac{9 \mu_o \hat{c}_p T_o}{10 p_o r_o^2 \sqrt{RT_o}} \right) \frac{1}{\tilde{r}} \frac{d}{d\tilde{r}} \left[\tilde{r} \tilde{T} \frac{d\tilde{T}}{d\tilde{r}} \right] - \left(\frac{1}{r_o} \right) \frac{1}{\tilde{r}} \frac{d}{d\tilde{r}} \left[\tilde{r} \tilde{p} (\tilde{u}_r + (\tilde{u}_\theta)) \right] \\
+ \left(\frac{\mu_o \sqrt{RT_o}}{p_o r_o^2} \right) \frac{1}{\tilde{r}} \frac{d}{d\tilde{r}} \left[2 \tilde{r} \tilde{\mu} \tilde{u}_r \frac{d\tilde{u}_r}{d\tilde{r}} + \tilde{r}^2 \tilde{\mu} \tilde{u}_\theta \frac{d}{d\tilde{r}} \left(\frac{\tilde{u}_\theta}{\tilde{r}} \right) \right] \\
- \left(\frac{C \mu_o}{r_o^2 \rho_o Pr \sqrt{RT_o}} \right) \frac{1}{\tilde{r}} \frac{d}{d\tilde{r}} \left[\frac{\tilde{r} \tilde{\mu} \tilde{p}}{\tilde{\rho}^2} \frac{d\tilde{\rho}}{d\tilde{r}} \right] + \left(\frac{2 C \mu_o^2}{p_o r_o^3 \rho_o Pr} \right) \frac{1}{\tilde{r}} \frac{d}{d\tilde{r}} \left[\frac{\tilde{r} \tilde{\mu}^2}{\tilde{\rho}^2} \frac{d\tilde{\rho}}{d\tilde{r}} \frac{d\tilde{u}_r}{d\tilde{r}} \right]
\end{aligned} \tag{173}$$

Knudson number in the 1st and 6th terms, and multiply both sides by r_o

$$\begin{aligned}
100 Kn_o \tilde{\rho} \frac{\partial \tilde{T}}{\partial \tilde{t}} + \frac{1}{2} (\tilde{\rho} \tilde{u}_r) \left[3 \frac{d\tilde{T}}{d\tilde{r}} + \frac{d\tilde{u}_r^2}{d\tilde{r}} + \frac{d\tilde{u}_\theta^2}{d\tilde{r}} \right] = \left(\frac{9 \mu_o \hat{c}_p T_o}{10 p_o r_o \sqrt{RT_o}} \right) \frac{1}{\tilde{r}} \frac{d}{d\tilde{r}} \left[\tilde{r} \tilde{T} \frac{d\tilde{T}}{d\tilde{r}} \right] \\
- \frac{1}{\tilde{r}} \frac{d}{d\tilde{r}} \left[\tilde{r} \tilde{p} (\tilde{u}_r + (\tilde{u}_\theta)) \right] + \left(\frac{\mu_o \sqrt{RT_o}}{p_o r_o} \right) \frac{1}{\tilde{r}} \frac{d}{d\tilde{r}} \left[2 \tilde{r} \tilde{\mu} \tilde{u}_r \frac{d\tilde{u}_r}{d\tilde{r}} + \tilde{r}^2 \tilde{\mu} \tilde{u}_\theta \frac{d}{d\tilde{r}} \left(\frac{\tilde{u}_\theta}{\tilde{r}} \right) \right] \\
- \left(\frac{C}{Pr} Kn_o \right) \frac{1}{\tilde{r}} \frac{d}{d\tilde{r}} \left[\frac{\tilde{r} \tilde{\mu} \tilde{p}}{\tilde{\rho}^2} \frac{d\tilde{\rho}}{d\tilde{r}} \right] + \left(\frac{2 C \mu_o^2}{p_o r_o^2 \rho_o Pr} \right) \frac{1}{\tilde{r}} \frac{d}{d\tilde{r}} \left[\frac{\tilde{r} \tilde{\mu}^2}{\tilde{\rho}^2} \frac{d\tilde{\rho}}{d\tilde{r}} \frac{d\tilde{u}_r}{d\tilde{r}} \right]
\end{aligned} \tag{174}$$

Next, the remaining pressure terms can be replaced with $\rho_o RT_o$ thanks to the ideal gas law

$$\begin{aligned}
100 Kn_o \tilde{\rho} \frac{\partial \tilde{T}}{\partial \tilde{t}} + \frac{1}{2} (\tilde{\rho} \tilde{u}_r) \left[3 \frac{d\tilde{T}}{d\tilde{r}} + \frac{d\tilde{u}_r^2}{d\tilde{r}} + \frac{d\tilde{u}_\theta^2}{d\tilde{r}} \right] &= \left(\frac{9 \mu_o \hat{c}_p T_o}{10 \rho_o R T_o r_o \sqrt{R T_o}} \right) \frac{1}{\tilde{r}} \frac{d}{d\tilde{r}} \left[\tilde{r} \tilde{T} \frac{d\tilde{T}}{d\tilde{r}} \right] \\
&- \frac{1}{\tilde{r}} \frac{d}{d\tilde{r}} \left[\tilde{r} \tilde{p} (\tilde{u}_r + \tilde{u}_\theta) \right] + \left(\frac{\mu_o \sqrt{R T_o}}{\rho_o R T_o r_o} \right) \frac{1}{\tilde{r}} \frac{d}{d\tilde{r}} \left[2 \tilde{r} \tilde{\mu} \tilde{u}_r \frac{d\tilde{u}_r}{d\tilde{r}} + \tilde{r}^2 \tilde{\mu} \tilde{u}_\theta \frac{d}{d\tilde{r}} \left(\frac{\tilde{u}_\theta}{\tilde{r}} \right) \right] \\
&- \left(\frac{C}{Pr} Kn_o \right) \frac{1}{\tilde{r}} \frac{d}{d\tilde{r}} \left[\frac{\tilde{r} \tilde{\mu} \tilde{p}}{\tilde{\rho}^2} \frac{d\tilde{\rho}}{d\tilde{r}} \right] + \left(\frac{2C \mu_o^2}{\rho_o R T_o r_o^2 \rho_o Pr} \right) \frac{1}{\tilde{r}} \frac{d}{d\tilde{r}} \left[\frac{\tilde{r} \tilde{\mu}^2}{\tilde{\rho}^2} \frac{d\tilde{\rho}}{d\tilde{r}} \frac{d\tilde{u}_r}{d\tilde{r}} \right]
\end{aligned} \tag{175}$$

There are Knudson numbers in the 3rd and 5th terms and two in the 7th term

$$\begin{aligned}
100 Kn_o \tilde{\rho} \frac{\partial \tilde{T}}{\partial \tilde{t}} + \frac{1}{2} (\tilde{\rho} \tilde{u}_r) \left[3 \frac{d\tilde{T}}{d\tilde{r}} + \frac{d\tilde{u}_r^2}{d\tilde{r}} + \frac{d\tilde{u}_\theta^2}{d\tilde{r}} \right] &= \left(\frac{9 \hat{c}_p T_o}{10 R T_o} Kn_o \right) \frac{1}{\tilde{r}} \frac{d}{d\tilde{r}} \left[\tilde{r} \tilde{T} \frac{d\tilde{T}}{d\tilde{r}} \right] \\
&- \frac{1}{\tilde{r}} \frac{d}{d\tilde{r}} \left[\tilde{r} \tilde{p} (\tilde{u}_r + \tilde{u}_\theta) \right] + (Kn_o) \frac{1}{\tilde{r}} \frac{d}{d\tilde{r}} \left[2 \tilde{r} \tilde{\mu} \tilde{u}_r \frac{d\tilde{u}_r}{d\tilde{r}} + \tilde{r}^2 \tilde{\mu} \tilde{u}_\theta \frac{d}{d\tilde{r}} \left(\frac{\tilde{u}_\theta}{\tilde{r}} \right) \right] \\
&- \left(\frac{C}{Pr} Kn_o \right) \frac{1}{\tilde{r}} \frac{d}{d\tilde{r}} \left[\frac{\tilde{r} \tilde{\mu} \tilde{p}}{\tilde{\rho}^2} \frac{d\tilde{\rho}}{d\tilde{r}} \right] + \left(\frac{2C}{Pr} Kn_o^2 \right) \frac{1}{\tilde{r}} \frac{d}{d\tilde{r}} \left[\frac{\tilde{r} \tilde{\mu}^2}{\tilde{\rho}^2} \frac{d\tilde{\rho}}{d\tilde{r}} \frac{d\tilde{u}_r}{d\tilde{r}} \right]
\end{aligned} \tag{176}$$

Notice that the rest of the third term (other than the Knudson number) reduces, since \hat{c}_p is a function of R

$$\begin{aligned}
100 Kn_o \tilde{\rho} \frac{\partial \tilde{T}}{\partial \tilde{t}} + \frac{1}{2} (\tilde{\rho} \tilde{u}_r) \left[3 \frac{d\tilde{T}}{d\tilde{r}} + \frac{d\tilde{u}_r^2}{d\tilde{r}} + \frac{d\tilde{u}_\theta^2}{d\tilde{r}} \right] &= \left(\frac{45}{20} Kn_o \right) \frac{1}{\tilde{r}} \frac{d}{d\tilde{r}} \left[\tilde{r} \tilde{T} \frac{d\tilde{T}}{d\tilde{r}} \right] \\
&- \frac{1}{\tilde{r}} \frac{d}{d\tilde{r}} \left[\tilde{r} \tilde{p} (\tilde{u}_r + \tilde{u}_\theta) \right] + (Kn_o) \frac{1}{\tilde{r}} \frac{d}{d\tilde{r}} \left[2 \tilde{r} \tilde{\mu} \tilde{u}_r \frac{d\tilde{u}_r}{d\tilde{r}} + \tilde{r}^2 \tilde{\mu} \tilde{u}_\theta \frac{d}{d\tilde{r}} \left(\frac{\tilde{u}_\theta}{\tilde{r}} \right) \right] \\
&- \left(\frac{C}{Pr} Kn_o \right) \frac{1}{\tilde{r}} \frac{d}{d\tilde{r}} \left[\frac{\tilde{r} \tilde{\mu} \tilde{p}}{\tilde{\rho}^2} \frac{d\tilde{\rho}}{d\tilde{r}} \right] + \left(\frac{2C}{Pr} Kn_o^2 \right) \frac{1}{\tilde{r}} \frac{d}{d\tilde{r}} \left[\frac{\tilde{r} \tilde{\mu}^2}{\tilde{\rho}^2} \frac{d\tilde{\rho}}{d\tilde{r}} \frac{d\tilde{u}_r}{d\tilde{r}} \right]
\end{aligned} \tag{177}$$

As demonstrated in the momentum section, the Prandtl number can be replaced with $\frac{2}{3}$, giving a final energy equation as:

$$\begin{aligned}
100 Kn_o \tilde{\rho} \frac{\partial \tilde{T}}{\partial \tilde{t}} + \frac{1}{2} (\tilde{\rho} \tilde{u}_r) \left[3 \frac{\partial \tilde{T}}{\partial \tilde{r}} + \frac{\partial \tilde{u}_r^2}{\partial \tilde{r}} + \frac{\partial \tilde{u}_\theta^2}{\partial \tilde{r}} \right] &= \left(\frac{45}{20} Kn_o \right) \frac{1}{\tilde{r}} \frac{\partial}{\partial \tilde{r}} \left[\tilde{r} \tilde{T} \frac{\partial \tilde{T}}{\partial \tilde{r}} \right] \\
&- \frac{1}{\tilde{r}} \frac{\partial}{\partial \tilde{r}} \left[\tilde{r} \tilde{p} (\tilde{u}_r + \tilde{u}_\theta) \right] + (Kn_o) \frac{1}{\tilde{r}} \frac{\partial}{\partial \tilde{r}} \left[2 \tilde{r} \tilde{\mu} \tilde{u}_r \frac{\partial \tilde{u}_r}{\partial \tilde{r}} + \tilde{r}^2 \tilde{\mu} \tilde{u}_\theta \frac{\partial}{\partial \tilde{r}} \left(\frac{\tilde{u}_\theta}{\tilde{r}} \right) \right] \\
&- \left(\frac{3C}{2} Kn_o \right) \frac{1}{\tilde{r}} \frac{\partial}{\partial \tilde{r}} \left[\frac{\tilde{r} \tilde{\mu} \tilde{p}}{\tilde{\rho}^2} \frac{\partial \tilde{\rho}}{\partial \tilde{r}} \right] + \left(3C Kn_o^2 \right) \frac{1}{\tilde{r}} \frac{\partial}{\partial \tilde{r}} \left[\frac{\tilde{r} \tilde{\mu}^2}{\tilde{\rho}^2} \frac{\partial \tilde{\rho}}{\partial \tilde{r}} \frac{\partial \tilde{u}_r}{\partial \tilde{r}} \right]
\end{aligned} \tag{178}$$

Lastly, the nested derivatives must again be removed in order to implement this equation into MatLab. This expansion greatly increases the equation's size, but is necessary. Conservation of energy becomes:

$$\begin{aligned}
100 Kn_o \tilde{\rho} \frac{\partial \tilde{T}}{\partial \tilde{t}} + \frac{1}{2} (\tilde{\rho} \tilde{u}_r) \left[3 \frac{\partial \tilde{T}}{\partial \tilde{r}} + \frac{\partial \tilde{u}_r^2}{\partial \tilde{r}} + \frac{\partial \tilde{u}_\theta^2}{\partial \tilde{r}} \right] = \\
\left(\frac{45 Kn_o}{20 \tilde{r}} \right) \left[\tilde{r} \tilde{T} \frac{\partial^2 \tilde{T}}{\partial \tilde{r}^2} + \tilde{r} \left(\frac{\partial \tilde{T}}{\partial \tilde{r}} \right)^2 + \tilde{T} \frac{\partial \tilde{T}}{\partial \tilde{r}} \right] \\
- \frac{1}{\tilde{r}} \left[\tilde{r} \frac{\partial \tilde{\rho}}{\partial \tilde{r}} (\tilde{u}_r + \tilde{u}_\theta) + \tilde{\rho} (\tilde{r} \frac{\partial \tilde{u}_r}{\partial \tilde{r}} + \tilde{u}_r + \tilde{r} \frac{\partial \tilde{u}_\theta}{\partial \tilde{r}} + \tilde{u}_\theta) \right] \\
+ \frac{Kn_o}{\tilde{r}} \left[2 \tilde{r} \tilde{u}_r \frac{\partial \tilde{\mu}}{\partial \tilde{r}} \frac{\partial \tilde{u}_r}{\partial \tilde{r}} + \tilde{u}_\theta \left(\tilde{r} \frac{\partial \tilde{\mu}}{\partial \tilde{r}} \frac{\partial \tilde{u}_\theta}{\partial \tilde{r}} + \tilde{\mu} \left(\tilde{r} \frac{\partial^2 \tilde{u}_\theta}{\partial \tilde{r}^2} - \frac{\partial \tilde{u}_\theta}{\partial \tilde{r}} \right) \right) \right. \\
\left. - \tilde{u}_\theta^2 \frac{\partial \tilde{\mu}}{\partial \tilde{r}} + \tilde{\mu} \left(\tilde{r} \left(2 \left(\frac{\partial \tilde{u}_r}{\partial \tilde{r}} \right)^2 + \left(\frac{\partial \tilde{u}_\theta}{\partial \tilde{r}} \right)^2 \right) + 2 \tilde{u}_r \left(\tilde{r} \frac{\partial^2 \tilde{u}_r}{\partial \tilde{r}^2} + \frac{\partial \tilde{u}_r}{\partial \tilde{r}} \right) \right) \right] \\
- \frac{3 C Kn_o}{2 \tilde{r} \tilde{\rho}^3} \left[\tilde{\rho} \left(\tilde{r} \tilde{p} \frac{\partial \tilde{\mu}}{\partial \tilde{r}} \frac{\partial \tilde{p}}{\partial \tilde{r}} + \tilde{\mu} \left(\tilde{r} \left(\frac{\partial \tilde{p}}{\partial \tilde{r}} \right)^2 + \tilde{p} \left(\tilde{r} \frac{\partial^2 \tilde{p}}{\partial \tilde{r}^2} + \frac{\partial \tilde{p}}{\partial \tilde{r}} \right) \right) \right) - 2 \tilde{r} \tilde{\mu} \tilde{p} \frac{\partial \tilde{\rho}}{\partial \tilde{r}} \frac{\partial \tilde{p}}{\partial \tilde{r}} \right] \\
+ \left(\frac{3 C Kn_o^2 \tilde{\mu}}{\tilde{r} \tilde{\rho}^3} \right) \left[\tilde{\rho} \left(2 \tilde{r} \frac{\partial \tilde{\rho}}{\partial \tilde{r}} \frac{\partial \tilde{\mu}}{\partial \tilde{r}} \frac{\partial \tilde{u}_r}{\partial \tilde{r}} + \tilde{\mu} \left(\tilde{r} \frac{\partial^2 \tilde{\rho}}{\partial \tilde{r}^2} \frac{\partial \tilde{u}_r}{\partial \tilde{r}} + \frac{\partial \tilde{\rho}}{\partial \tilde{r}} \left(\tilde{r} \frac{\partial^2 \tilde{u}_r}{\partial \tilde{r}^2} + \frac{\partial \tilde{u}_r}{\partial \tilde{r}} \right) \right) \right) \right. \\
\left. - 2 \tilde{r} \tilde{\mu} \frac{\partial \tilde{u}_r}{\partial \tilde{r}} \left(\frac{\partial \tilde{\rho}}{\partial \tilde{r}} \right)^2 \right]
\end{aligned} \tag{179}$$

9.5.5 Ideal Gas

Lastly, the ideal gas equation

$$p = \rho R T \quad (180)$$

It is also known that it can be written in terms of reference parameters only.

$$p_o = \rho_o R T_o \quad (181)$$

Dividing the two, yields

$$\frac{p}{p_o} = \frac{\rho}{\rho_o} \frac{T}{T_o} \quad (182)$$

Where each parameter can be replaced by its nondimensional form

$$\tilde{p} = \tilde{\rho} \tilde{T} \quad (183)$$

10 Bibliography

References

- [1] Brenner, H., 2012, "Beyond Navier-Stokes," *International Journal of Engineering Science*, 54pp. 67.
- [2] Mandella, M. J., 1987, "Experimental and Analytical Studies of Compressible Vortices."
- [3] Caradonna, F. X., and Isom, M. P., 1972, "Subsonic and Transonic Potential Flow Over Helicopter Rotor Blades," *American Institute of Aeronautics and Astronautics*, 10(12) pp. 1606.
- [4] Coloni, T., Lele, S. K., and Moin, P., 1991, "The Free Compressible Viscous Vortex," *Journal of Fluid Mechanics*, 230pp. 45.
- [5] Mandella, M., Moon, Y. J., and Bershad, D., 1986, "Quantitative Study of Shock Generated Compressible Vortex Flows," *Shock Waves and Shock Tubes*, D. Bershad and R. Hanson, eds. Stanford University Press, pp. 471.
- [6] White, F.M., 2011, "Fluid Mechanics," McGraw Hill, New York, NY, pp. 235-236.
- [7] Amiri-Jaghargh, A., Roohi, E., Niazmand, H., 2013, "DSMC Simulation of Low Knudsen Micro/Nanoflows using Small Number of Particles Per Cells," *Journal of Heat Transfer*, 135(10).
- [8] Kundu, P.K., Cohen, I.M., and Dowling, D.R., 2012, "Fluid Mechanics," Elsevier, Boston, pp. 891.
- [9] Choudhuri, A.R., 1998, "The Physics of Fluids and Plasmas: An Introduction for Astrophysicists," Cambridge University Press, Cambridge, UK, pp. 427.
- [10] Dadzie, S. K., and Brenner, H., 2012, "Predicting Enhanced Mass Flow Rates in Gas Microchannels using Nonkinetic Models," *Physical Review*, 86.

-
- [11] Burnett, D., 1935, "The Distribution of Velocities in a Slightly Non-Uniform Gas," *Proceeding of the London Mathematical Society*, 39(1).
- [12] Agarwal, R. K., and Yun, K., 2002, "Burnett Equations for Similation of Transitional Flows," *Applied Mechanics Reviews*, 55(3).
- [13] Walls, P., 2013, "Bivelocity Hydrodynamics of Micro-Channel Couette Flow" .
- [14] Aboelkassem, Y., Vatistas, G. H., Esmail, N., 2005, "Viscous dissipation of Rankine vortex profile in zero meridional flow" *Acta Mech Sinica*, 21: 550-556
- [15] Taylor, G. I., 1918 "On The Dissipation of Eddies." Ed. G. K. Batchelor. *The Scientific Papers of G.I. Taylor: Meterology, Oceanography and Turbulent Flow*. Vol. 2. Cambridge: 96-101.
- [16] White, F.M., 2006, "Viscous Fluid Flow," McGraw Hill, New York, NY, pp. 27, Chapter 1.
- [17] Ellenrieder, K., and Cantwell, J., 2000, "Self-similar, slightly compressible, free vortex," *Journal of Fluid Mechanics*, 423, pp. 293-315
- [18] Bagai, A., and Leishman J. G., 1993, "Flow Visualization of Compressible Vortex Structures Using Density Gradient Techniques." *Experiments in Fluids* 15: 431-42.
- [19] Brenner, H., 2013, "Proposal of a Critical Test of the Navier-Stokes-Fourier Paradigm for Compressible Fluid Continua," *Physical Review*, 87.
- [20] Brenner, H., 2013, "Steady-state heat conduction in a gas undergoing rigid-body rotation. Comparison of Navier-Stokes-Fourier and bivelocity paradigms," *International Journal of Engineering Science*, 713, pp. 29-45.
- [21] Brenner, H., 2011, "Steady-state heat conduction in quiescent fluids: Incompleteness of the Navier-Stokes-Fourier equations," *Physica A*, 390, pp. 3216-3244.

-
- [22] Brenner, H., and Bielenberg, J. R., 2005, "A Continuum Approach to Phoretic Motions: Thermophoresis," *Physica A: Statistical Mechanics and its Applications*, 355(2-4) pp. 251.
- [23] Walls, P., Abedian, B., and Brenner, H., 2014, "Bivelocity Gas Dynamics of Mirco-Channel Couette Flow," *International Journal of Engineering Science*, 79, pp. 21.
- [24] Brenner, H., "Kinematics of volume transport". *Physica A: Statistical Mechanics and its Applications*, 349(12):11 59, 2005.
- [25] Greenshields, C., and Reese, J. M., 2006, "The structure of shock waves as a test of Brenner's modifications to the Navier-Stokes equations," *Journal of Fluid Mechanics*, 580, pp. 407-429
- [26] Maxwell, J. C.. 1879, "On stresses in rarified gases arising from inequalities of temperature". *Philosophical Transactions of the Royal Society of London*, 170, 231256.
- [27] H. Xue, H. M. Ji, and C. Shu, *International Journal of Heat and Mass Transfer* 44, 4139 (2001).